ALUMINA CERAMIC MEMBRANE INCORPORATED WITH GRAPHENE OXIDE FRAMEWORKS FOR PROTEIN RECOVERY

NOOR FAUZIYAH BT ISHAK

FACULTY OF ENGINEERING
UNIVERSITY OF MALAYA
KUALA LUMPUR

2020

ALUMINA CERAMIC MEMBRANE INCORPORATED WITH GRAPHENE OXIDE FRAMEWORKS FOR PROTEIN RECOVERY

NOOR FAUZIYAH BT ISHAK

THESIS SUBMITTED IN FULFILMENT OF THE REQUIREMENTS FOR THE DEGREE OF DOCTOR OF PHILOSOPHY (PHD)

FACULTY OF ENGINEERING
UNIVERSITY OF MALAYA
KUALA LUMPUR

2020

UNIVERSITY OF MALAYA

ORIGINAL LITERARY WORK DECLARATION

Name of Candidate: NOOR FAUZIYAH BT ISHAK

Matric No: KHA140025

Name of Degree: PHILOSOPHY OF DOCTORATE

Title of Thesis: ALUMINA CERAMIC MEMBRANE INCORPORATED WITH GRAPHENE OXIDE FRAMEWORKS FOR PROTEIN RECOVERY

Field of Study: SEPARATION AND PURIFICATION

I do solemnly and sincerely declare that:

(1) I am the sole author/writer of this Work;
(2) This Work is original;
(3) Any use of any work in which copyright exists was done by way of fair dealing and for permitted purposes and any excerpt or extract from, or reference to or reproduction of any copyright work has been disclosed expressly and sufficiently and the title of the Work and its authorship have been acknowledged in this Work;
(4) I do not have any actual knowledge nor do I ought reasonably to know that the making of this work constitutes an infringement of any copyright work;
(5) I hereby assign all and every rights in the copyright to this Work to the University of Malaya ("UM"), who henceforth shall be owner of the copyright in this Work and that any reproduction or use in any form or by any means whatsoever is prohibited without the written consent of UM having been first had and obtained;
(6) I am fully aware that if in the course of making this Work I have infringed any copyright whether intentionally or otherwise, I may be subject to legal action or any other action as may be determined by UM.

Candidate's Signature Date:

Subscribed and solemnly declared before,

Witness's Signature Date:

Name:

Designation:

ALUMINA CERAMIC MEMBRANE INCORPORATED WITH GRAPHENE OXIDE FRAMEWORKS FOR PROTEIN RECOVERY

ABSTRACT

Alumina ceramic membrane is undergoing rapid development and innovation for protein recovery process. However, the limitation of this membrane type is membrane fouling due to the deposition and adsorption of proteins on the surface and pore walls of the membranes. It is crucial to minimize membrane fouling by reducing interactions between protein and the membrane surface via surface modification technique. Thus, the main objective of this research is to develop an alumina membrane with enhanced antifouling property for protein recovery process. An alumina dope consisting of 57 wt.% alumina loading was used to fabricate two alumina membrane configurations; which are flat-sheet alumina (FSA) and hollow fibre alumina (HFA) membranes, via phase-inversion and sintering method. The FSA membrane was prepared through parametric study by optimizing the fabrication parameters which are the blade gap and sintering temperature. With the use of a blade gap of 1 mm and sintering temperature of 1500°C, it was possible to produce an FSA membrane with the highest flexure strength of 697 MPa and a pure water flux (PWF) of 1716 L/m^2.h and peak diameter for pore size distribution of 0.14μm. Meanwhile, the HFA membrane prepared for this study has a PWF of 242.63 ± 24 L/m^2.h, flexure strength of 156 ± 25MPa, contact angle of 29 ± 6°, surface roughness of 59.69nm and peak diameter for pore size distribution of 0.182μm. For the performance of protein recovery, FSA and HFA membranes have a low value of 35 ± 5% and 63.58 ± 0.5% respectively. In addition, the flux recovery rates (FRR) for FSA and HFA membranes were 25.32% and 63.37% respectively. Next, the surface of these membranes was further modified using graphene oxide frameworks

(GOFs) as modifier agents to form a selective layer on alumina support. Three different concentrations of GOF(EDA) film was prepared for FSA membrane, and the lowest GO concentration of 5ppm which was 5GOF(EDA)/FSA composite membrane, had the highest PWF of 38.6 ± 1.1L/m^2.h. It also had a BSA recovery of 55 ± 6% at FRR of 46 ± 3% and the membrane pore size of 0.12 μm. In contrast, the HFA membrane had three composite membranes with different diamine monomers which are ethylenediamine (EDA), butylenediamide (BDA) and phenylenediamine (PDA). Among the composite membranes, the GOF(BDA)/HFA exhibited the highest PWF of 10 ± 0.6 L/m^2.h and flexure strength of 197.58 ± 12 MPa. For protein recovery, this composite membrane also exhibited the highest recovery rate among other modified membranes which are 98.40, 98.32, 95.82 and 95.65% for bovine serum albumin (BSA), egg albumin (EA), trypsin (TR) dan lysozyme (LSZ) protein respectively. Furthermore, the FRR and Rt result also suggest that GOF(BDA)/HFA composite membrane had better antifouling properties as it has the highest FRR and lowest total fouling ratio (Rt) of 94.86 % and 21.70 %, respectively for a total of 72h filtration time. As a conclusion, both surfaces modified with FSA and HFA membrane using GOF exhibited better performance in protein recovery application due to antifouling properties.

Keywords: alumina membrane, graphene oxide frameworks, flat-sheet, hollow fibre, protein recovery

MEMBRAN SERAMIK ALUMINA DIGABUNGKAN DENGAN KERANGKA GRAPHENE OXIDE UNTUK PEMULIHAN PROTEIN

ABSTRAK

Membran seramik alumina menjalani perkembangan yang pesat dan inovasi untuk proses pemulihan protein. Walaubagaimanapun, kekangan dalam penggunaan membran ini ialah kekotoran membran yang disebabkan oleh pemendapan dan penjerapan protein ke atas permukaan dan dinding liang membran. Ini penting untuk mengurangkan kekotoran membran dengan menghalang interaksi di antara protein dan permukaan membran melalui teknik pengubahsuaian permukaan. Oleh itu, objektif utama kajian ini adalah menghasilkan membran alumina dengan meningkatkan ciri penyahan kotoran untuk digunakan dalam proses pemulihan protein. 57 wt.% kandungan alumina dalam larutan alumina telah digunakan untuk menghasilkan dua bentuk membran alumina, iaitu alumina lembaran-rata (FSA) dan alumina serat berongga (HFA) melalui proses fasa penyongsangan dan pembakaran. Membran FSA telah dihasilkan melalui kajian parametrik untuk mengoptimumkan parameter pembentukan iaitu jarak bilah dan suhu pembakaran. Jarak bilah sebanyak 1 mm dan suhu pembakaran pada 1500°C telah berjaya menghasilkan membran FSA yang mempunyai kekuatan lentur yang paling tinggi iaitu 697MPa dan fluk air tulen (PWF) sebanyak 1716L/m^2.h dan juga mempunyai taburan saiz liang dengan puncak diameter pada 0.14μm. Manakala, membran HFA mempunyai PWF sebanyak 242.63 ± 24L/m^2.h, kekuatan lentur sebanyak 156 ± 25MPa, sudut kenalan sebanyak 29 ± 6°, dan kekasaran permukaan sebanyak 59.69nm dan nilai puncak diameter untuk taburan saiz liang ialah 0.182 μm. Prestasi untuk pemulihan protein, membran FSA and HFA mempunyai nilai yang rendah iaitu sebanyak 35 ± 5% dan 63.58 ± 0.5%. Tambahan pula, nilai kadar

pemulihan flux (FRR) untuk FSA dan HFA membran adalah sebanyak 25.32% dan 63.37%. Kemudian, kedua-dua permukaan membran alumina ini diteruskan dengan pengubahsuaian menggunakan *graphene oxide frameworks* (GOFs) sebagai ejen pengubahsuai untuk membentuk satu lapisan pemilihan di atas membran alumina. Tiga jenis lapisan GOF(EDA) yang berlainan kepekatan telah disediakan untuk FSA membrane, dan kepekatan yang paling rendah iaitu 5ppm menghasilkan membran komposit 5GOF(EDA)/FSA mempunyai nilai PWF yang paling tinggi iaitu 38.6 ± 1.1 $L/m^2.h$. Ia juga mempunyai pemulihan BSA sebanyak 55 ± 6% pada nilai FRR sebanyak 46 ± 3% dan saiz liang adalah 0.12 μm. Bertentangan dengan itu, membran HFA mempunyai tiga membran komposit yang berlainan jenis monomer diamine iaitu *ethylenediamine* (EDA), *butylenediamide* (BDA) and *phenylenediamine* (PDA). Dikalangan membran komposit ini, membran GOF(BDA)/HFA telah menghasilkan nilai PWF yang tertinggi sebanyak 10 ± $0.6L/m^2.h$ dan kekuatan lentur sebanyak 197.58 ± 12MPa. Untuk kajian pemulihan protein, membran komposit GOF(BDA)/HFA ini juga telah menghasilkan kadar pemulihan yang tertinggi iaitu sebanyak 98.40, 98.32, 95.82 dan 95.65 % untuk *bovine serum albumin* (BSA), *egg albumin* (EA), *trypsin* (TR) dan *lysozyme* (LSZ). Tambahan pula, nilai FRR dan nisbah jumlah kekotoran (Rt) juga mencadangkan membran komposit ini mempunyai antikotoran yang terbaik kerana mempunyai nilai FRR yang tingi iaitu sebanyak 94.86% dan nilai jumlah nisbah kekotoran (Rt) yang terendah iaitu sebanyak dan 21.70 % untuk pemulihan selama 72h. Sebagai kesimpulan, kedua-dua membran FSA dan HFA yang telah diubahsuai permukaan dengan menggunakan GOF dapat menghasilkan peningkatan dalam proses pemulihan protein kerana mempunyai ciri nyah-kotoran.

Kata kunci: membran alumina, kerangka graphene oxide, lembaran-rata, serat berongga, pemulihan protein

ACKNOWLEDGEMENTS

First and foremost, a great thankful to Allah S.W.T for blessing me, giving me an opportunity, good health, strength and make my life easier until I completed my PhD journey.

I wholeheartedly want to express my gratitude to my supervisor Dr. Nur Awanis binti Hashim and Assoc. Prof. Dr. Mohd Hafiz Dzarfan bin Othman. Their support and understanding, both academically and personally, have made this long journey less difficult and more satisfying. Both my experimental skills and theoretical knowledge have been significantly enriched during our discussion and interaction.

I also want to thank all of my friends in UM and UTM, who not only offered me academic assistance during my research and study but also, helped me in my personal life. I am grateful to all my colleagues from the same research group, who often gave me great advice and assisted me in various experiments, and my office mates in particle lab, who often dampened my worries and stress.

In addition, I cannot possibly fully express my appreciation for the unconditional understanding, caring, love and support of my family members. Especially to my mother and father, they always stood by me and encouraged me all the time. I feel really happy to have you as a parent. Not forgot to my lovely husband and my little cute baby, thanks for existing in my life for moral support at the end of my PhD journey.

Last but not least, I would like to thanks to my sponsorship. This research was funded by the Ministry of Higher Education, Malaysia and University of Mara Technology (UiTM) for Ph.D. study bursary.

TABLE OF CONTENTS

LIST OF FIGURES

LIST OF TABLES

LIST OF SYMBOLS AND ABBREVIATIONS

3D	:	Three-dimension
Al_2O	:	Alumina
BDA	:	Butylenediamide
BET	:	Brunauer Emmet Teller
BSA	:	Bovine serum albumin
C	:	Carbon
CA	:	Contact angle
CO_2	:	Carbon dioxide
DLS	:	Dynamic light scattering
DSC	:	Differential scanning calorimetry
EA	:	Egg albumin
EDA	:	Ethylenediamine
EDX	:	Energy dispersive X-ray
FESEM	:	Field emission scanning electron microscopy
FRR	:	Flux recovery rate
FSA	:	Flat-sheet alumina
FTIR	:	Fourier transform infrared
GO	:	Graphene oxide
GOF	:	Graphene oxide framework
GPC	:	Gel permeation chromatography
H_2O_2	:	Hydrogen peroxide
H_2SO_4	:	Sulphuric acid
H_3PO_4	:	Phosphoric acid
HCl	:	Hydrogen chloride

HFA	:	Hollow fibre alumina
HNO_3	:	Acid nitric
$KMnO_4$	:	Potassium permanganate
LSZ	:	Lysozyme
MC	:	Membrane chromatography
MF	:	Microfiltration
N	:	Nitrogen
Na	:	Sodium
NaOH	:	Sodium hydroxide
NF	:	Nanofiltration
NMP	:	*N*-methyl-2-pyrrolidone
NPT	:	National pipe thread
O	:	Oxygen
OH	:	Hydroxyl
PDA	:	Phenylenediamine
PDD	:	Pressure driven deposition
PEG	:	Poly-ethylene glycol
PESf	:	Polyethersulfone
PSD	:	Particle size distribution
PWF	:	Pure water flux
Ra	:	Average surface roughness
Rir	:	Irreversible fouling ratio
Rr	:	Reversible fouling ratio
Rt	:	Total fouling ratio
SEM	:	Scanning electron microscopy
SiO_2	:	Silica

TGA	:	Thermogravimetric analysis
TiO_2	:	Titania
TR	:	Trypsin
UF	:	Ultrafiltration
VD	:	Vacuum deposition
XPS	:	X-ray photoelectron spectroscopy
XRD	:	X-ray powder diffraction
ZP	:	Zeta potential
ZrO_2	:	Zirconia

CHAPTER 1: INTRODUCTION

1.1 Research background

In biotechnology industries such as in the fish, dairy, agricultural and pharmaceutical industries were widely discovered for their wastewaters management. The wastewaters from the downstream process in these industries contain a high amount of proteins (Ravindran & Jaiswal, 2016), they should not be discharged without suitable treatment in order to allow the recovery of high value by-products. The utilization of by-products is a significant opportunity for the biotechnology industry, as it can potentially generate additional revenue as well as reduce disposal costs (Arvanitoyannis & Kassaveti, 2008). For example, a plant of 100 ton fish/h capacity generates 10 – 40 m^3/h effluent with a protein load of 0.5 – 20 g/l (Afonso, Ferrer, & Bórquez, 2004). Protein from this wastewater can be used as an animal feed supplement and serve as a substitute for common sources of protein in soybean meal and commercial fishmeal (Arvanitoyannis & Kassaveti, 2008; Benhabiles et al., 2013). Thus, these proteins should be recovered as high value by-product in order to prevent the environmental effects caused by their disposal.

Generally, protein is a biomacromolecule which is an essential material in biotechnology process, and to extend its application, the protein is required to be purified and recovered. Membrane technology is an alternative application for protein recovery processes, in particular microfiltration (MF), ultrafiltration (UF) and nanofiltration (NF) (Chew, Aroua, & Hussain, 2017; Chew, Aroua, Hussain, & Ismail, 2016; Rashidi et al., 2015). The membrane technology has been acknowledged as the most significant process owing to low energy consumption, environment friendly nature

and simple operation requirements (Q. Li, Bi, Lin, Bian, & Wang, 2013) for protein bio-separation application.

Membrane technology is also effective in removing particulates, bacteria, and pyrogens, as well as in recovering valuable ingredients. For example, membrane technology is used in the processing of wastewater stream for protein recovery process. The recovered protein is expected to retain its quality and functionality because the non-thermal membrane operation prevents protein from undergoing thermal denaturation (Lo, Cao, Argin-Soysal, Wang, & Hahm, 2005). Protein recovery is widely implemented in downstream process in dairy (P. Kumar et al., 2013), pharmaceutical (Yang & Yen, 2013) and food processing (B. Li et al., 2012) industries. The purpose of the protein recovery is to enhance protein purity and stability as well as concentration (Arunima Saxena, Bijay P. Tripathi, Mahendra Kumar, & Vinod K. Shahi, 2009).

A great deal of attention has been paid to MF and UF for protein recovery due to lower operation cost and higher output purity. Furthermore, UF provides size exclusion effects (generally proteins have effective particle sizes between about 2 to 15 nm). The UF is considered as a high selectivity technique having potential usage in high resolution protein recovery processes (Rabiller-Baudry, Chaufer, Lucas, & Michel, 2001). Moreover, UF has largely replaced gel permeation chromatography (GPC) for concentration and biofiltration type of applications. Meanwhile, MF has found increasingly greater use in the biopharmaceutical industry for sterilization of therapeutic proteins prior to formulation due to some apparent advantages over other competing techniques (Álvarez et al., 2014). It is widely used for the initial yield of therapeutic proteins from mammalian, yeast and bacterial cell cultures over other competing processes such as centrifugation and bed chromatography (Biron, Bortoluz, Zeni, Bergmann, & Santos, 2016; Hassan, Ennouri, Lafforgue, Schmitz, & Ayadi, 2013).

However, the drawbacks of membrane application in protein recovery is challenged by membrane fouling phenomenon (Su, Lu, Cui, & Thomas, 2000). Membrane fouling is very complex in nature due to its dependency on a large number of parameters. One of the crucial parameters is protein-membrane interactions that occur during protein recovery processes which lead to membrane fouling. Generally, the adsorption and deposition of proteins on the membrane surfaces occurs via van derWaals forces, electrostatic attraction, hydrogen bonding and hydrophobic interactions (Raja Ghosh, Wan, Cui, & Hale, 2003; Mendret, Hatat-Fraile, Rivallin, & Brosillon, 2013; P. Wang, Tan, Kang, & Neoh, 2002). The protein-membrane interaction not only has significant affect to fouling, but also reduces purity and stability of the protein (Yeu, Lunn, Rangel, & Shantz, 2009). It also demands frequent chemical cleaning for the membrane which in turn shortens the usage life of the membrane (D'Souza & Mawson, 2005; Popović, Djurić, Milanović, Tekić, & Lukić, 2010). Consequently, the effectiveness of these membrane applications would strongly be dependent on the selection of membrane properties. Therefore, the desired membrane properties in this requirement are high selectivity and good surface character.

A good membrane surface characteristic refers to the antifouling and antibacterial capability (Mahesh Kumar & Roy, 2008; Arunima Saxena et al., 2009). In earlier decades, poly-ethylene glycol (PEG) was used as surface modifier on alumina Anopore^{TM} membranes via grafting technique to improve surface hydrophilicity (Yeu et al., 2009). This approach led to a significant reduction in membrane fouling. Generally, membrane fouling can be reduced by improving the preparation methods and modifying the membrane's surface in order to decrease the interactions between proteins and the membrane surface (S. Zhou et al., 2013). In order to advance the use of a membrane for protein recovery, it is necessary to understand the fabrication and their surface modification methods. Therefore, to achieve good performance of protein recovery

process, alumina membrane as a ceramic membrane was selected in this study and the alumina membrane was made to go through surface modification using graphene oxide frameworks (GOFs) to enhance antifouling properties.

1.2 Problem statement

As mentioned, the key issue in the application of protein recovery process using membrane technology is the protein-membrane interactions which significantly affect fouling phenomena, resolution and protein stability, and result in the reduction of the membrane performance. Protein is known as a biological foulant can absorb at smoother surface or deposit onto the membrane via convection (A. Saxena, B. P. Tripathi, M. Kumar, & V. K. Shahi, 2009). Moreover, proteins can denature or aggregate, and this would lead to more complex deposition onto the membrane (C. Wang, Yang, & Zhang, 2010). Therefore, it can be difficult to characterize the fouling method due to multiple possible mechanisms leading to fouling. Thus, this problem is given great of attention by academicians and researchers who attempt to address the problem by developing ways for membrane surface modification to avoid the protein fouling in protein recovery application.

The main purpose of surface modification is to decrease further the effective pore size, and change the wettability property of the surface (Tang & Li, 2013), which would result in a decline of the fouling effect during the protein recovery process (S. Zhou et al., 2014). Currently, the study on the modification of alumina membrane is significant, particularly with its focus on the modifier material selection and the development of modification methods. Recently, graphene oxide (GO) as a carbon-based material has obtained a great attention due to its special properties of antifouling properties (Alam et al., 2018; J. Lee et al., 2013; Zinadini, Zinatizadeh, Rahimi, Vatanpour, & Zangeneh, 2014). GO has a high hydroxyl group and a high negativity

charge, which could enhance the hydrophilicity character and electrostatic repulsion on the membrane surface, thus preventing the protein from depositing onto the membrane surface. In addition, GO is a nanoparticle which could improve the selectivity of membrane surface by reducing and narrowing down the pore size distribution (J. Lee et al., 2013).

We hypothesize that GO, as a modifier material could reduce protein fouling due to the improvement of modified alumina surface properties. However, there is a lack of study on adhesion strength that could cause the modified layer on membrane surface to peel off. Therefore, the implementation of linker agents between GO and membrane surface is a decent alternative in order to increase their adhesion strength. This research intends to provide a detailed evaluation study and highlight the practical solutions through surface modification technique by adding diamine linker groups into GO suspension, to form promising GOFs for both flat sheet and hollow fibre configurations. This modification technique is anticipated to provide new insights into the protein recovery applications using a robust ceramic alumina membrane.

1.3 Scope of study

The present study focused on the preparation of alumina dope for fabrication of ceramic membrane in the form of flat sheet and hollow fibre configurations. Then, both configurations of alumina membranes were incorporated with GOFs as selective layer on composite alumina membranes. The GOFs were prepared using diamine monomers functionalization as a cross-linker in GO suspension. These modified membranes are also known as GOFs/Alumina composite membranes, and the introduction of these modified membranes is a novel implementation in protein recovery process. Figure 1.1 shows the general flow chart for the whole study with four specific scopes which are preparation of alumina dope, fabrication of alumina membrane, incorporation of GOFs

on alumina surface and characterization and performance of the modified membranes for protein recovery.

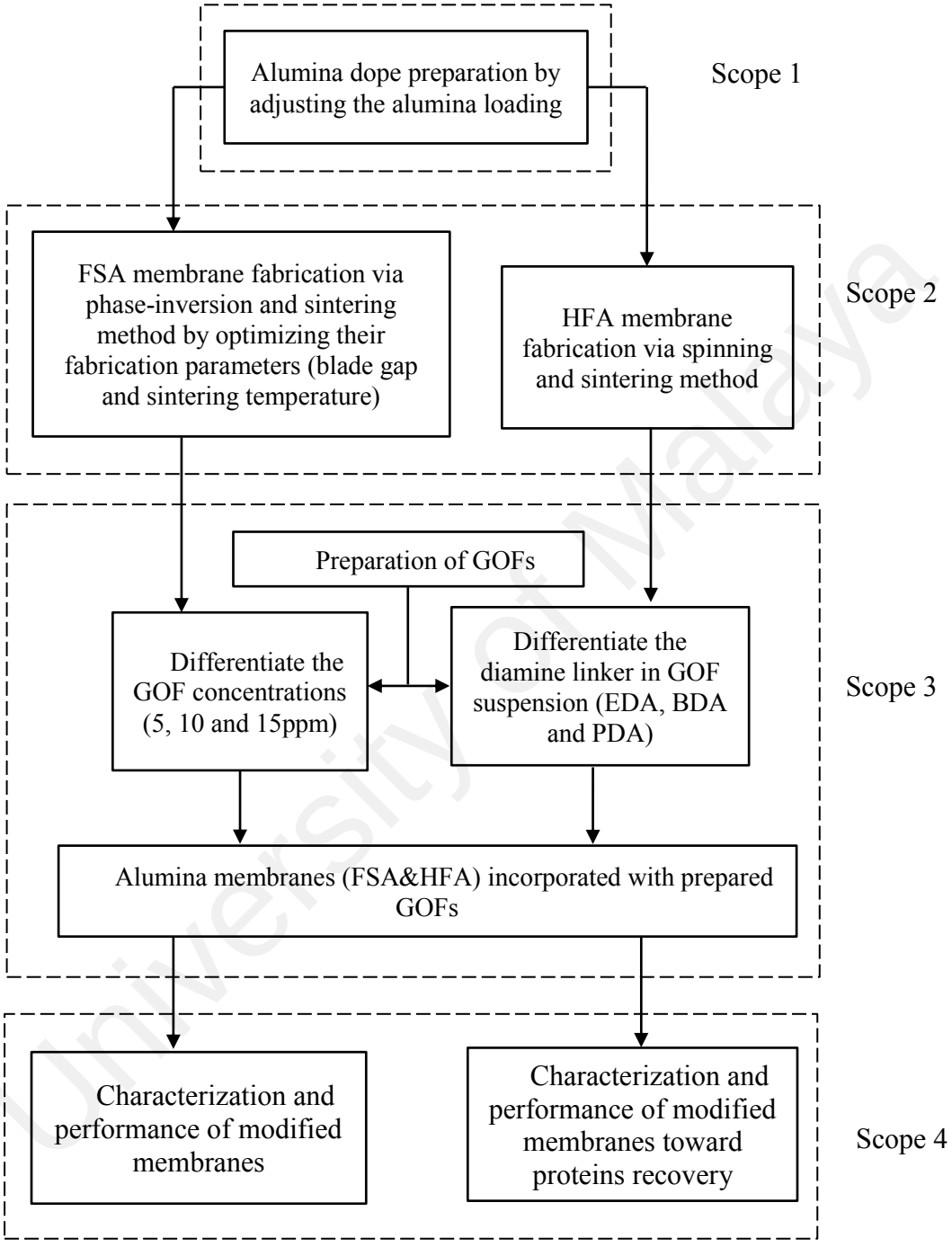

Figure 1.1: General flow chart for the whole study with the specific scope

From the figure, the first step is alumina dope preparation using certain particle size distribution of alumina powders, which are achievable by adjusting alumina loading. The second step is the fabrication of flat-sheet alumina (FSA) membranes by optimizing

the fabrication parameters which are the blade gap in casting step and sintering temperature. For the FSA membrane, three different GOF concentrations were used (5, 10 and 15ppm) as a selective layer via pressure driven deposition (PDD) method. The next step is the fabrication of hollow fibre alumina (HFA) membrane owing to their advance configuration toward membrane technology application. The HFA membrane was incorporated with GOFs via vacuum deposition (VD) method using different diamine monomers which are ethylenediamine (EDA), butylenediamide (BDA) and phenylenediamine (PDA). All the modified membranes had their properties characterized and their performance analysed. Last but not least, the composite membranes were tested for antifouling properties using certain proteins with different molecular weight. As a conclusion, the scope of the study completely covered ceramic dope preparation until the application of modified membranes in protein recovery due to antifouling study.

1.4 Aim and objectives

The aim of this study is to produce alumina composite membrane with antifouling property for protein recovery process. The process begins with the preparation of alumina dope to fabricate alumina membrane with certain properties. Then, the prepared alumina membranes were incorporated with GOFs to prepare alumina composite membranes. In order to achieve the aim of this study, four specific objectives need to be highlighted which are alumina dope preparation, membrane fabrication, incorporation of GOFs as selective layer and performance study of composite alumina membranes. The specific objectives of this research are as follow:

1) To investigate the effect of preparation condition of alumina dope by adjusting alumina loading as a main component on ceramic membrane fabrication.

2) To fabricate two type of alumina membrane configurations which are flat sheet and hollow fibre via phase inversion and sintering method.
3) To examine the effect of incorporation of GOFs as selective layer using PDD and VD method on flat sheet and hollow fibre alumina membranes, respectively.
4) To evaluate the performance of protein recovery and antifouling properties of the modified membranes in terms of morphology structure, chemical and mechanical properties such as wettability and flexure strength.

1.5 Research significance

This study is of significance to the research of biotechnology downstream industries which involves protein recovery process using membrane technology. The introduction of GOFs as a selective layer on alumina membrane was to form a composite membrane. The alumina composite membrane was improved the protein recovery by enhancing recovery rate and reducing protein deposition on the composite surface. The results obtained in the study also provide the properties of composite membranes, which lead to the requirement in membrane technology application for protein recovery process.

1.6 Thesis outline

This thesis is presented in the conventional style format which consists of five chapters. First two chapters provide a general introduction and literature review on the research study. The following three chapters address materials and experimental works, results and discussions, and finally the conclusion and recommendations. The introduction part provides an introduction of research study on fabrication and incorporation of GOF on alumina membrane for protein recovery process. The scopes of study, problem statement, aim and objectives and significant of this research study was also presented.

Meanwhile, at literature review part was given information on general fundamental and research outcome from previous study that related on fabrication methods and surface modification techniques of alumina membrane, recent development of GO as modifier agent in order to form a desire composite membrane for protein recovery study were described. All this information was gathered to produce the overall literature review. Then, material and method part presents the materials used in this research which is to prepare alumina dope such as alumina powder as a main component, binder, dispersant and solvent. Meanwhile, for the GO and GOFs were used to prepare selective layer material. The methodology of experimental works also explained in detail in this chapter including the analysis was used to characterize and perform the membrane toward protein recovery application.

Next chapter was result and discussion which presents the whole finding in this research which divided into four parts as referring to four specific objectives of the research. The first finding refers to preparation of alumina dope by adjusting alumina loading to optimize its preparation of alumina membrane. In addition, the preparation method of GO and GOF synthesis using simplified Hummer's method and diamine-functionalization, respectively was also discovered. The second discovery is the fabrication of FSA and HFA membrane via phase-inversion and sintering method. The third finding is incorporation of GOF by grafting technique via PDD and VD methods. The prepared modified membranes were characterised for morphology structure, chemical and mechanical properties, and perform their capability on water permeation study. All these characterizations and performance study was used for examined the last finding which is to apply them for protein recovery process. And the final chapter was elucidating all summary findings of this research work and conclusions have been highlighted. Recommendations for future studies relevant to this research have also been suggested.

CHAPTER 2: LITERATURE REVIEW

2.1 Introduction

A membrane is defined as a selective barrier that allows certain molecules or ions to pass through by combining sieving and diffusion mechanism. Membranes also can be classified based on its materials, i.e. polymeric (organic) and ceramic (inorganic) (Tavolaro & Drioli, 1999). It can be further categorised based on its permeability and structure, in which membrane permeability is defined as permeable, semi-permeable and impermeable (M. Zawrah, Khattab, Girgis, El Shereefy, & Sawan, 2014) while membrane structure is defined to be either porous or dense. Currently, polymeric membranes are the leading membrane type in industrial applications. Meanwhile, ceramic membranes are mainly used in special cases where the application of polymeric membranes is deemed unsuitable and inapplicable. Polymeric membrane suffers from several problems such as proclivity to bio-fouling, low fluxes, low mechanical strength and restricted chemical and thermal stability (Ng, Mohammad, Leo, & Hilal, 2013). As a result, ceramic membranes have been seen as the best candidate to replace polymeric membranes in harsh condition applications due to their capability of working in acidic or basic conditions (Mahesh Kumar & Roy, 2008).

Ceramic membrane is made from inorganic materials, generally metal oxides and non-oxides. Widely used metal oxide materials are alumina (Al_2O_3) (Patel, Baig, & Laoui, 2011), titania (TiO_2) (Jingxian, Dongliang, Weisensel, & Greil, 2004), silica (SiO_2) (Duran, Sato, Hotta, & Watari, 2007) and zirconia (ZrO_2) (C. C. Wei, Chen, Liu, & Li, 2008), while non-oxide materials (Eom, Kim, & Raju, 2013) refer to silicon carbide and silicon nitride. Generally, ceramic membranes have great mechanical strength as well as high thermal and chemical stability (Tang & Li, 2013; Van

Heetvelde et al., 2013) For most of the applications, alumina is used due to economical material (Elaine Fung & Wang, 2013) and enable the use of high trans-membrane pressures and reverse cleaning due to their incompressible structure (Kikkinides, Stoitsas, Zaspalis, & Burganos, 2004). Meanwhile, covalent bonding of the membranes allows the use of strong chemicals due to less sensitivity to re-hydroxylation during the cleaning procedure (Rezaei Hosseinabadi et al., 2014; S. Zhou et al., 2013). Even more impressive, hydrophilic characteristics that are naturally found in alumina due to the presence of hydroxyl (OH) groups encourage the adsorption of water and can avoid micro-organisms foulant to grow on the alumina surface (Mahesh Kumar & Roy, 2008; Rezaei Hosseinabadi et al., 2014).

A number of studies have explored the fabrication of alumina membranes in different configurations such as flat-sheet, tubular, and hollow fibres. The alumina membrane also used as a support in composite membranes (Barma & Mandal, 2014; Poletto, da Silva Biron, Zeni, Bergmann, & dos Santos, 2013; Qin, Peng, Lv, & Wu, 2014). The structure of a membrane can be further modified to enhance permeability and separation factors. Modification of a membrane can be applied to the internal pore surface or on to the top of the membrane to prevent the adsorption of protein which causes fouling (S. Zhou et al., 2013). Efforts have been made to improve the membrane surface using a few modification techniques.

There are very limited reviews that describe the surface modification of alumina membrane, while membrane surface modification is an important issue that should be addressed to enhance the efficiency of protein recovery. This review mainly focuses on the progress of alumina membrane towards surface modification and its effects on hydrophilicity enhancement and fouling reduction. The discussion provides insights into its potential applications in the field of protein recovery. The crucial part of the review

focuses on new findings about modifier materials, especially graphene-derivatives which offer high hydrophilic characteristics. Thus, this review will provide an extensive reference for researchers working on the recent development of graphene derivative-alumina composites.

2.2 Overview of alumina membranes

2.2.1 Characteristics of alumina membranes

Alumina or also known as aluminium oxide is the most common ceramic material used in membrane fabrication owing to properties such as high surface area, resistance to organic solvents, narrow particle size distributions, high density and low fabrication cost (Sarkar, Bandyopadhyay, Larbot, & Cerneaux, 2012; Treccani, Yvonne Klein, Meder, Pardun, & Rezwan, 2013). Table 2.1 shows the mechanical and thermal properties of alumina as a ceramic material in membrane fabrication. Moreover, alumina is the most economical ceramic membrane material with regards to its chemical stability in strong acid solvent (Elaine Fung & Wang, 2013) in comparison with common stainless steel 316. All these characteristics combined with its abundance have made alumina an attractive ceramic material. The selections of raw material powders as well as particle size are important in determining the properties of membrane structure. Commercial alumina ceramics are commonly made of alumina powders with a particle size in the range of 20-40 μm (Qi, Fan, Xing, & Winnubst, 2010).

Physical properties such as pore size and pore size distribution of membrane are the key matters in separation performance (F. Li, Yang, Fan, Xing, & Wang, 2012). Indeed, particle size distribution is an important material characteristic in the preparation of an asymmetric membrane because it is directly related to pore size and porosity (De Angelis & de Cortalezzi, 2013). In order to achieve a good asymmetric structure, different particle sizes alumina is used in fabrication. Kingsbury and Li (2009)

developed asymmetric hollow fibres using alumina of three different particle sizes (B. F. K. Kingsbury & K. Li, 2009). The different particle sizes are fine, medium and coarse, which easily fill in all the spaces of the specimen including tiny spaces, gaps and interior pores. This arrangement leads to a decrease in porosity with an increase in densification, corrosion resistance and asymmetric ceramic membrane strength (Q. Wang et al., 2014). In practice, membranes need to be highly permeable, corrosive resistant, have a narrow pore size distribution and perfect surface quality without defects. Thus, among metal oxide materials, alumina is the most promising option in the preparation of ceramic membranes due to its small amount of shrinkage during sintering (H. B. Lim, Cho, & Kim, 2012).

Table 2.1: Mechanical and thermal properties of alumina

Mechanical properties	
Tensile Strength (MPa)	117 – 173
Bending Strength (MPa)	307 - 413
Modulus of Elasticity (E) X 10^8 (MPa)	21.27 – 26.8
Compressive Strength (MPa)	1600 - 3733
Modulus of Ridity (G) X 10^8 (MPa)	8.67 – 11.3
Hardness on the Mohs scale	9
Thermal properties	
Melting point (°C)	2051 ± 9.7
Thermal coefficient at 200 -1000 °C ($°C^{-1}$)	8.80 x 10^{-6}
Boiling point (°C)	353000

Reported by Auerkari et. al., (2011) (Auerkari, 1996; Vasanth, Uppaluri, & Pugazhenthi, 2011).

2.2.2 Structure of alumina membranes

Ceramic membranes consist of several thin layers with an overall thickness of between a few nanometres up to a few microns (Qi et al., 2010). Alumina membrane applications mostly utilise a porous structure. Porous membranes are widely used in industries that involve solid-liquid and solid-gas separation. This is primarily due to

their high structural durability, easy cleaning, low energy consumption and controllable microstructure (Abbad Brahim, Azeddine Lounis, Sylvie Condom, & K Taibi, 2013; Sahnoun & Baklouti, 2013). Porous membrane comprises of a 3-dimensional interconnected network of either symmetric or asymmetric structure (Ohji, 2013) as presented in Figure 2.1. Symmetric structure refers to pores that are equally sized throughout the membrane while asymmetric structure refers to pore size that gradually decreases towards the surface where separation occurs. Processes of porous membranes are based on the size exclusion of matter in which rejected substances have sizes bigger than the pores of the membranes (B. Wang et al., 2009).

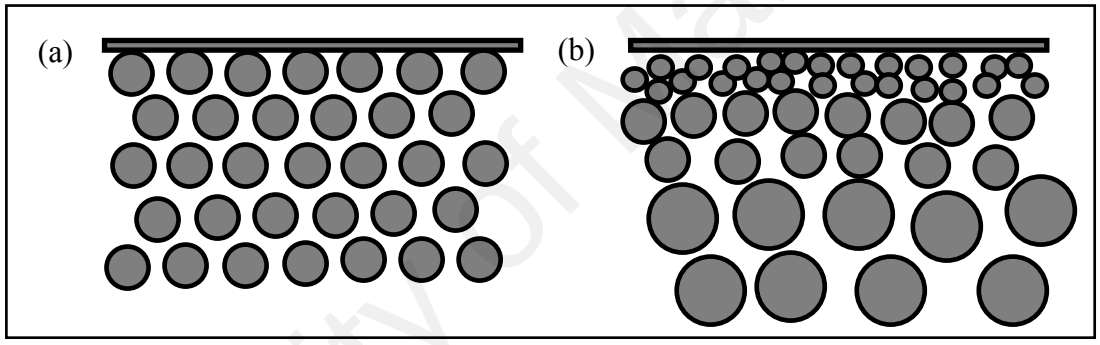

Figure 2.1: Schematic structure of (a) symmetric and (b) asymmetric ceramic membranes

Pressure driven membrane processes, that is MF, UF and NF as shown in Figure 2.2 are widely used in protein separation application. MF membranes have pore sizes in the range of 0.05 to 10 μm, which make them able to retain cells and cell debris while allowing proteins to permeate (van Reis & Zydney, 2007). Meanwhile, UF membranes have pore sizes of 1 - 100 nm, making them highly desirable for protein separation (Arunima Saxena et al., 2009). Furthermore, their application is also focused on protein concentration such as protein recovery from blood plasma (Manjumol, Shajesh, Baiju, & Warrier, 2011) and whey proteins in the dairy industry (Galanakis, Chasiotis, Botsaris, & Gekas, 2014). On the other hand, NF have pore sizes of 0.5 - 5 nm that are used to separate solutes based on particle charge and size (Arunima Saxena et al., 2009).

Thus, NF ceramic membranes can be applied in the separation of viruses from the blood stream (van Reis & Zydney, 2007).

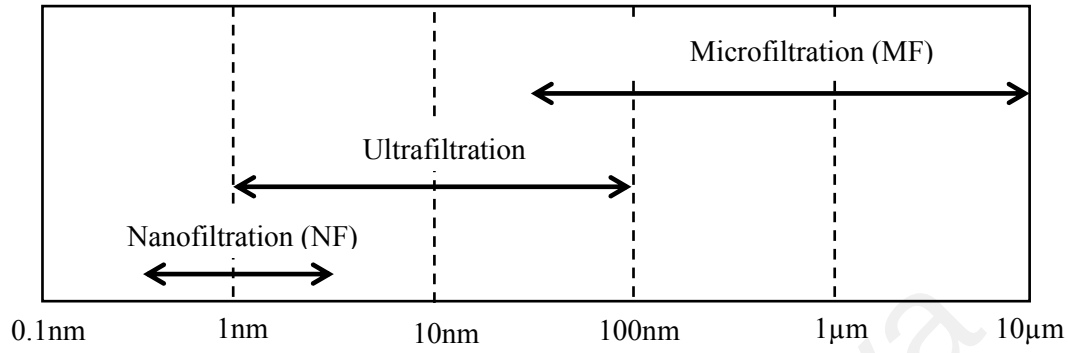

Figure 2.2: Average pore size of the membrane used in pressure driven processes

2.3 Configurations of alumina membrane

There is wide variety of available membrane configuration, depending on the chosen of formation technique in the fabrication process. Alumina membranes come in two main types of element configurations, which are flat and cylindrical membranes (M. Lee, Wu, Wang, & Li, 2014; Seal, Chattopadhyay, Das Sharma, Sen, & Maiti, 2004). The choice of the membrane configuration depends largely on the application, such as the required operating parameters and feed conditions. Different configurations are offer different packing density, possible application and price as well (Le, Cabaltica, & Bui, 2014).

Flat alumina membranes divided into disc or plate-sheet form as shown in Figure 2.3 (a). The packing density of this membrane configuration is generally low and hence they are limited to use in small scale industrial and laboratory applications. However, these membranes are easy to handle in maintenance service such as cleaning process and replace the modules when it's packed. Meanwhile, the cylindrical alumina membranes consist of tubular and hollow fibre configurations as shown in Figure 2.3 (b) and (c), respectively. Generally, tubular membrane has larger diameter size of

between 10 – 25 mm, whereas hollow fibre membrane has lower diameter size in the range of 4- 0.5 mm (B. F. K. Kingsbury & K. Li, 2009; Manjumol et al., 2011). The flow system also different for these two configurations; where the tubular membranes run inside-out system while the hollow fibre run out-inside system.

Due to larger diameter size, the tubular alumina membranes are more suitable for the separation of feeds that have large volume of suspended solids as well as more easily to cleaned mechanically, and high cross-flow velocities to control fouling. To further improve the packing density of the tubular membranes, the membrane fabricated as multi-channel tubes, called monoliths, with surface area to volume ratio of up to 782 m^2/m^3 (M. Lee, Wang, Wu, & Li, 2015). In contrast, the hollow fibre alumina membranes has lower diameter size, which is compact modules with high effective membrane surface areas can be achieved (M. Lee, Wang, & Li, 2016). In addition, they require lower trans-membrane pressures to drive permeate flow due to the thinner membrane, and its cleaning method such as backwashing and forward flushing.

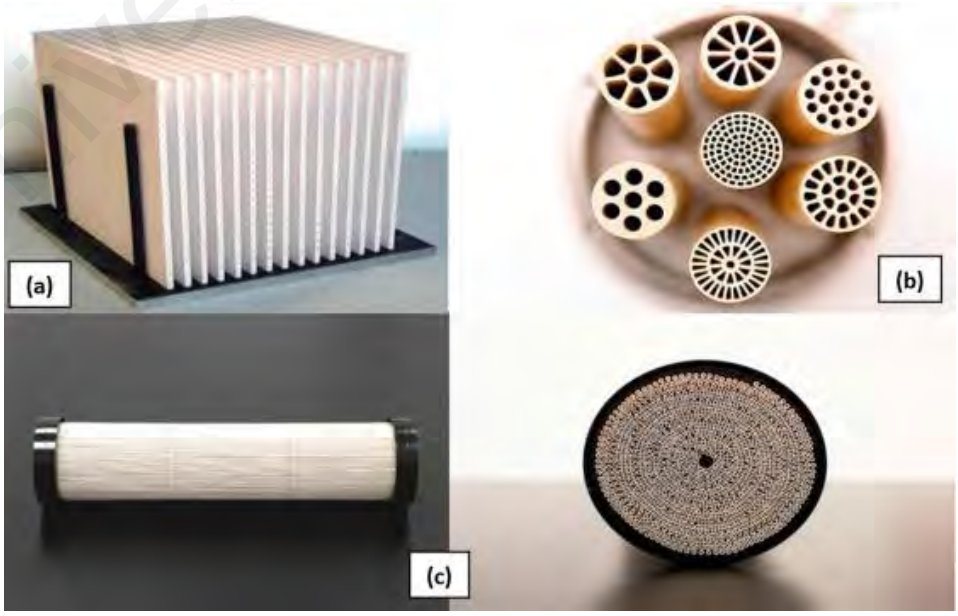

Figure 2.3: Ceramic membranes at different configurations as reported by Samaei et al., (2018) (Samaei, Gato-Trinidad, & Altaee, 2018)

2.4 Fabrication methods of alumina membranes

In the last three decades, the fabrication of alumina membranes for new processes and applications has undergone rapid growth in food processing, biotechnology and wastewater treatment (Barredo-Damas, Alcaina-Miranda, Iborra-Clar, & Mendoza-Roca, 2012; Cheow, Ting, Tan, & Toh, 2008; Qi et al., 2010; H. Zhang, Zhong, & Xing, 2013). Usually, alumina membranes are fabricated as a multi-layered structure (Sarkar et al., 2012) with gradual changes in pore size and thickness from one layer to the other. The applications of alumina membrane have placed it in the limelight of biotechnology due to its efficiency in protein separation and purification and the fact that it fits a certain size range from the fabrication method selection (Arunima Saxena et al., 2009).

The fabrication method of membranes depends on the type of configuration needed in specific application. The most common fabrication processes are extrusion, tape casting, dip and spin coating. Extrusion and tape casting methods are used for support or MF fabrication and dip and spin coating are used for UF and NF modification on alumina membranes. MF and UF of alumina membranes have found widespread industrial application while NF is still mainly a subject of academic research. In this review, the preparation of alumina membranes from research works has been well explained. Several techniques can be employed to fabricate alumina membrane such as slip casting (Levanen & Mantyla, 2002), extrusion (Issaoui, Bouaziz, & Fourati, 2013) powder pressing (Elaine Fung & Wang, 2013) and vapour phase deposition (Elam, Routkevitch, Mardilovich, & George, 2003; Song et al., 2016) and such extra. Special attention has been paid to the phase-inversion technique of the ceramic membrane fabrication due to their asymmetric structure formation which possible to many applications.

2.4.1 Slip casting

Slip casting is a method commonly used in membrane preparation due to its simplicity and reproducibility. The step takes a long time compared with other preparation methods and produces only symmetric membrane structures. Start with dope suspension preparation, then the dope is either allowed to sedimentation on top of a porous support or porous mould while solvent is settle down by capillary action, resulting a solid precursor (de F. Souza & Mansur, 2004). The remaining unsolidified dope is then poured away and the mould is removed, while the solidified precursor is then sinter at elevated temperature. A benefit of this method is that the tube that results is nearly perfect spherical in shape which enables sealing during module preparation (da Silva, Bernardin, & Hotza, 2014). In order to achieve a small membrane pore size, particles in the dope should be small enough, but it is takes longer casting times and difficulty in controlling membrane thickness.

2.4.2 Sol-gel technique

Sol-gel process has been used for preparation of porous alumina ceramic membrane for biotechnology, pharmaceutical industry, treatment of wastewater and nuclear industry application (Prabhakaran, Ojha, Gokhale, & Sharma, 2009). According to Ahmad et al., the sol-gel process is the most practical method among other methods used to prepare inorganic membranes (Ahmad, Idrus, & Othman, 2005). The benefits of this method are obtaining uniform pore size, high purity product at low temperature and some additives can be added. Homogeneity and high mechanical strength of the solid precursor offer great advantages for fabrication parts with nanometre pore sizes of 3-6 nm (M. F. Zawrah, Khattab, Girgis, El Shereefy, & Abo Sawan, 2014). However, the disadvantage of this technique is the formation of cracks during drying of the gels (Xie, Ma, & Huang, 2003). Furthermore, the sol-gel technique requires expensive metal alkoxides as raw materials and involves multistep coating and sintering processes (B.

Wang et al., 2009). Due to this, the sol-gel technique needs intensive energy and, thus the produced membranes are very expensive.

Sols are primary state of colloid in films are produced through coating the surface with some special technique followed by evaporating the solvent or called hydrolysis (N. Das & Maiti, 2009). The coating is generally made by dip and spins coating and must be carried out at the sol stage. In sol-gel technique the consolidating of dispersion medium is required where monomers in the suspension are polymeric or gelation of a polymer is induced at high temperatures (Gaucher, Jaouen, Legentilhomme, & Comiti, 2003). Consolidation could be induced by applying heat, adjusting pH or changing the ionic strength of the suspension. The Figure 2.4 shows the main steps of sol-gel process. In this process, the inorganic network is prepared as a colloidal suspension (sol) and finally, during the formation process of gel, the liquid phase is removed from it. The polymeric gel formed as three-dimensional structure which causes the porous in membrane. After shrinkage during drying, it will form a solid precursor.

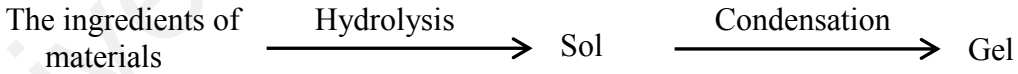

Figure 2.4: Schematic of general steps of sol-gel process (B. Wang, Wu, Livingston, & Li, 2009)

Polymeric binders are often added to the sol to prevent cracking in the drying process and burned out during sintering (Xie et al., 2003). The problem in using polymeric dispersants and organic modifiers were the prolonged initial heating, preferably very slow rates and the retention of organic species in solid precursor limiting green densities (Ananthakumar, Raja, & Warrier, 2000). Therefore, this leads to the formation of hair-

like cracks in a sintered product and produce microstructural defects that finally affect the mechanical performance of the product. Prabhakaran et al., (2009) were used soluble urea-formaldehyde oligomers formed in the initial stages of polymerization act as steric stabilizer for alumina particle in the suspension (Prabhakaran et al., 2009). The urea-formaldehyde polymer used as gelling agent acts as template for pores that could achieve porosity of more than 70% from dope of alumina loading 23 vol%. However, the average pore size of membrane substrate in the range of 0.48-0.56 μm (Prabhakaran, Priya, Gokhale, & Sharma, 2007). The porosity and pore size of membrane substrate was decrease with decreased the polymer concentration. Das and Maiti (2009) was prepared alumina MF membrane by tape-casting process and used this MF membrane as substrate, thin UF layer was prepared from boehmite sol by spin-coating method (N. Das & Maiti, 2009).

2.4.3 Tape casting

Tape casting is used for making thin, flat and dense ceramics (da Silva et al., 2014). This method is fabrication technique with a low cost that can produce extensively and homogenously microstructure membrane (Mukherjee, Maiti, Das Sharma, Basu, & Maiti, 2001), but in limited of the membrane thickness were obtained. Basically, tape casting consists of ceramic powder as the functional phase, solvent, and the additives such are anti-foaming, dispersing agent, surfactant, binder and plasticizer (Seal et al., 2004). The solid precursor is formed from dope as a result of the relative movement between doctor blade and a support. Generally, the casting speed varies from 0.1 to 1.5 m/min (M. a. P. Albano & Garrido, 2005). The viscosity of dope must be well controlled to facilitate the flowability of the slip through the doctor blade. Rheological behaviour is important characteristic for successfully tape casting method (Seal et al., 2004).

After casting, the solid precursor is dried and removed from the support, which is very easily handled because of its plastic characteristics. Next steps were followed by drying and sintering to remove organics compound from the solid precursor. If required, the shaping could be done in between drying and sintering. The thickness of ceramic membrane by using tape cast technique is typically in the range of 20 μm to a few millimetres (Pećanac et al., 2013). Fang et al., (2013) was prepared the porous ceramics that involves the use of hydrolysable pore formers such as starch, polymers and graphite (Hong Fang et al., 2013). During sintering, these substances are burned out from ceramic precursor by leaving pores in the final ceramics. Thus, the large porosity and shape of the pore formers are determined. Usually, the method was used in electronic application such an electrolyte or the anode for solid oxide fuel cells (Snijkers, de Wilde, Mullens, & Luyten, 2004).

Tape casting system may be classified according to the type of solvent used which organic and water based systems (M. P. Albano & Garrido, 2008). Generally, organic solvent is used due to low boiling points and prevent the ceramic powder from hydration. Meanwhile, water solvent is slow evaporation and agglomeration due to hydrogen bonding. Water-based casting processes that use water and natural products as solvent and binders in order to replace any toxic constituents. The typical examples for organic solvent-soluble and water-soluble binders are polyvinyl butyral (PVB) (Bose & Das, 2013) and methyl cellulose (Jana, Purkait, & Mohanty, 2011) respectively. Generally, solvent based tape casting considers a better choice compared to water based but it has less environmental concern.

2.4.4 Extrusion

Extrusion is a common method for the production of ceramic tubes and monolith structures by forced a dope ceramic through a die (Ghouil et al., 2015). The rheological property of the dope is utmost importance to effective the extrusion. The dope must be homogenous and exhibit plastic properties to form a rigid solid of precursor through the extrusion process, however above a certain yield stress the deformation of precursor may occur (Jana, Purkait, & Mohanty, 2010). In practice, an extremely viscous of dope ceramic is needed to extrude under high pressure through a die. The pressure, shear and temperature were used within extrusion apparatus to flow the dope and produce a solid precursor as tube form. As usual, the last part is sintering process in order to form a ceramic membrane by removing the binder or any additives at elevated temperature. Although the methods are well established it is only possible to prepare a limited range of structures and typically successive layers must be applied to either the inner or outer surfaces of the support using techniques such as sol-gel processing or chemical vapour deposition in order to generate the asymmetric structures that are required to achieve acceptable levels of flux and selectivity.

2.4.5 Spinning

Spinning process is achieved via tube-in-orifice spinnerets method with two or more extrude layers. These spinnerets can deliver simultaneous extrusions of the ceramic dope suspension, bore liquid, and any other components in separate layers at certain thicknesses (M. Lee et al., 2016). Typically, dual layer spinneret was used for spinning of single-layered ceramic hollow fibre. The two separated streams were extruded simultaneously through the spinneret, and once they leave the spinneret, they come into contact with one another, as well as with the external coagulation bath, whereby solvent and non- solvent exchange and phase inversion occurs (M. Lee et al., 2014). These spinnerets also can be designed to simultaneously extrude multiple layers or multiple

channels and can be specifically tailored for a wide range of hollow fibres. Although the process of spinning ceramic hollow fibre membranes is similar to the spinning of polymeric ones (Awanis Hashim, Liu, Moghareh Abed, & Li, 2012), some rules and optimisation of the polymeric spinning system cannot be applied directly to the ceramic spinning process, due to the significantly different composition of the spinning dope ceramic.

The presence of a large amount of ceramic particles also changes the mechanisms behind the formation of the different membrane structures. Basically, two type of structures was develop within the observation of membrane cross-section structure; sponge sponge-like denser structures, and micro-channels, which can be closed or open (B. F. Kingsbury & K. Li, 2009). The positioning and dimensions of these different structures can be regulated mainly by changing the parameters during the spinning process. Thus, in order to implement the desired membrane structure, some parameters should be chosen carefully, and the list as below:

a) Spinning dope suspension viscosity
b) Fibre extrusion rate
c) Internal coagulant composition
d) Internal coagulant flow rate
e) External coagulant composition
f) Air-gap between spinneret and coagulant bath

Although the existence of many parameters that affect the fibre properties can make fibre preparation difficult to predict, if a good level of understanding of the fibre formation process is achieved then the presence of many parameters allows for a high level of control over the fibre structure.

2.4.6 Phase inversion

The phase inversion is a simple and effective method for preparation of porous ceramic and originally was developed for polymer membranes preparation (C. C. Wei et al., 2008). The term phase inversion refers to the transformation of polymer or ceramic dope suspension from liquid to solid state (S. Liu, Li, & Hughes, 2003). Precipitation of polymer/ceramic occurs during immersion in water (non-solvent) via the exchange of the organic solvent with water. Water is often used as a non-solvent but organic solvents such as methanol can be used as well. In order to view the environmental point, water the most used as non-solvent. During this immersion-precipitation process, polymer solution was phase-separates into a polymer-rich and polymer-lean phase (S. Liu et al., 2003). Polymer-rich is former functioning as a binder for the ceramic dope suspension, while polymer-lean is pore-former. The as-formed solid precursor of hollow fibres is converted into ceramic hollow fibres by sintering at high temperatures.

Last few decades, phase inversion phenomenon has been explored for preparation of porous ceramic especially for flat sheet and hollow fibre geometry. For flat-sheet and hollow fibre, the tape casting and spinning method were used respectively and combine with phase inversion, results large finger like pores after removal of the polymer lean phase through a sintering step (Bai et al., 2014). The formation of finger like macrovoids in ceramic is caused by diffusion flows of solvent from the polymer solution surrounding the nuclei (C. C. Wei et al., 2008). Fang et al., (2013) was implemented the tape casting with phase inversion to prepare porous alumina membrane with high desired flexibility and mechanical strength of solid precursor, which can be easily handled (Hong Fang et al., 2013). Therefore, no cracking and wrapping occurred during sintering and flat alumina ceramic was successfully obtained.

2.4.7 Sintering step

Sintering process is the last stage in the ceramic membrane fabrication. Sintering process released carbon dioxide (CO_2) gas and produced the porous structure with high porosity in the ceramic membrane (Sahnoun & Baklouti, 2013). Sintering temperature and holding time have significant effects on the ultimate membrane porosity, which increases with time as well as temperature (N. Das & Maiti, 2009). High sintering temperature and large particle size in dope suspension were chosen to avoid defect formation of the prepared membrane (Levanen & Mantyla, 2002). The large particle size could reduce the densification rate, while the small particle size favours the defect formation and reduces the densification rate. Usually, the solid precursor exhibit a linear shrinkage of 15-20 % during sintering process (Heunisch, Dellert, & Roosen, 2010), thus strengthens the ceramic membrane through densification.

The main goal for sintering step is consolidation of the microstructure by neck-formation among the ceramic particles. It consists of two stages; the first stage is combustion of organics, which is crucial in determining the achievement of a crack-free membrane. The second stage is sintering of the ceramic particles by densification to form grain growth or neck-forming. The chosen sintering temperature was below but approaching the melting point of the ceramic particles used, e.g. 1100-1500 ºC for α-alumina (Galusek, Ghillányová, Sedláček, Kozánková, & Šajgalík, 2012). Meanwhile, sintering at relatively low temperature (300-400ºC) and for a short time (few hours) do not produce thermally stable ceramic membranes. It also has an effect on pore size and the final phase composition of ceramic membrane. For example, the phase transition from γ-alumina to α-alumina takes place temperatures above 1000 ºC (Yalamaç, Trapani, & Akkurt, 2014). However, addition of other inorganic substances such as for example lanthanum oxide or titanium oxide can change the sintering temperature.

Hence, sintering process had a strong effect on the final properties of the ceramic membrane. The pore size can be increased at the cost of decreasing porosity by controlled sintering temperature in a range of 400-1000 ºC for most common membrane materials (Levanen & Mantyla, 2002). Furthermore, the sintering step consolidates the structure and give a require strength and hardness to the membrane but too high a sintering temperature may result in the loss of desire properties such as narrow pore size distribution. Consequently, these properties of prepared membrane were significantly affecting the membrane performance toward water permeation and selectivity.

2.5 Surface modification of alumina membranes

UF alumina membranes has been proven to be an effective process for the removal of natural organic matter and organic macromolecules such as proteins, sugars and humic substances (Alventosa-deLara, Barredo-Damas, Alcaina-Miranda, & Iborra-Clar, 2014; Gaucher et al., 2003; S. Khemakhem & Amara, 2012; X. Shi, Tal, Hankins, & Gitis, 2014). The only problem is the fouling effect during the operation. As contaminants are removed from waste water, they would stay at the surface of the membrane, resulting in cake formation and pore blockage (X. Shi et al., 2014). This phenomenon will cause a fouling effect in the alumina membrane process as well as reduce the separation performance of the membrane process. Thus, the surface character of the alumina membrane needs to be further modified to enhance its anti-fouling properties.

Generally, alumina membranes have a naturally moderate hydrophilic character which has a contact angle within the range of 40-50° (DeFriend, Wiesner, & Barron, 2003). The hydrophilic character is known as a water-loving property on a ceramic surface. Hydrophilic membrane features highly polar properties which have the ability to absorb water molecules by forming a hydrogen bond (Mendret et al., 2013). Indeed,

the hydrophilic character retains high surface tension on an alumina surface to repel foulants by reducing adhesion. Meanwhile, strong adhesion between foulants and the membrane surface will cause a fouling effect. Thus, hydrophilic membrane has anti-fouling properties (Mustafa, Wyns, Vandezande, Buekenhoudt, & Meynen, 2014). Anti-fouling properties are important in protein separation and purification. However, alumina membrane is intrinsically hydrophilic due to an oxide material contained in the hydroxyl group. In order to enhance protein separation and purification, a superhydrophilic character of the alumina membrane surface is more preferable.

Researchers focus on two great potentials in surface modification which are superhydrophilicity (contact angle < 5°) and superhydrophobicity (contact angle > 150°) (Kang et al., 2012). This attraction is due to the enhancement of its anti-fouling and self-cleaning applications. For instance, Maguire-Boyle and Borron (2011) implemented a superhydrophilic surface by coating cysteic acid onto an alumina membrane (Maguire-Boyle & Barron, 2011). Cysteic acid with contains of Zwitterionic was functionalised alumina coated ceramic to achieve comprehensive wettability when in interaction with water. Numerous hydrogen bonds form between both moieties and solvent during the coating technique. Thus, the superhydrophilic character was performed with increasing permeability and flux of membrane process. Meanwhile, superhydrophilic membranes also can be produced using glass particles as a modified material on a membrane surface (Özgür & Şan, 2011). A contact angle of 8° was achieved from a mixture of quartz and glassy additives consisting of zeolite and glass frit. Moreover, the prepared glassy pore wall membrane could stand high thermal and chemical processes.

However, the application of polymer as a modifier material could have drawbacks such as a reduced resistance to high thermal and chemical exposure through industrial

applications (Özgür & Şan, 2011). To overcome these problems, inorganic materials were selected as the modifier materials due to their properties of high thermal and chemical stability and mechanical strength (Q. Chang, Zhou, Wang, Wang, & Meng, 2010). Therefore, the application of inorganic materials with nano-size particles as modifier materials was studied in order to enhance their hydrophilic character (Garcia-Ivars, Alcaina-Miranda, Iborra-Clar, Mendoza-Roca, & Pastor-Alcañiz, 2014). For example, nano-TiO_2 particles were used as a hydrophilic modifier on commercial alumina MF membranes (Q. Chang et al., 2014). These nanoparticles did not form a separate layer but increased the hydrophilic character of the membrane surface. It should be mentioned however, that one of the limiting factors against the application of nanoparticles as modifier materials on a membrane surface is pore clogging (Q. Chang et al., 2010). Furthermore, the preparation of a nanoparticle solution also required the sol-gel technique, a high-cost process. Therefore, the selection of modifier materials still needs to be explored for future study in ceramic surface modification.

2.5.1 Surface modification techniques

Surface modification aims to further decrease the effective pore size and change the chemical nature of the surface (Tang & Li, 2013) resulting in the decline of the fouling effect during the protein separation process (S. Zhou et al., 2014). Currently, the study of modification on the alumina membrane is significant, particularly with its focus on the modifier material selection and the development of modification methods. There are two classification methods of surface modification; the chemical method and the physical method (Chu, Wang, & Chen, 2005). Generally, physical modification comprises of machine-aided approaches such as ion beams, plasma, flame and radiation. In bioseparation practice, the physical method is extensively applied to improve the surface of bone tissue and is widely used in tissue engineering applications (Treccani et al., 2013). Chemical modification is the direct reaction of certain chemical solutions on

the membrane surface. Usually, this method is used to enhance membrane permeability in order to reduce membrane fouling and enhance membrane selectivity (Peng Lee & Mattia, 2013). Meanwhile, selected modifier materials could also contribute to the surface modification process via the coating or grafting techniques, thus improving the surface property and fouling resistance of modified membranes.

The preparation techniques and modifier materials used for the surface modification of alumina membranes and the resultant membranes' features and applications are presented in Table 2.2 in reference to previous research. As can be seen, various modifier materials and techniques were used to modify the membrane surface. Mostly, focus was given to the modification of alumina membrane by coating with nanoparticle materials (Q. Chang et al., 2010; Qi et al., 2010; Rahman & Padavettan, 2012) where ceramic membranes were coated with nanoparticles such as sol titania or beohmite in resulting composite membranes. Furthermore, it improved permeability and enhanced the flux (J. Kim & Van der Bruggen, 2010) as well as the chemical resistance of alumina ceramic in highly acidic and alkaline solutions (Dong et al., 2011). On the other hand, composite membranes could also be produced via grafting techniques.

In the case of coating, the coated layer may be easily washed-out during filtration. Meanwhile, the layer produced via the grafting technique is more reliable and durable when applied to modifying the membrane surface, but the method is complicated and time-consuming. Prior to the wide use of coating and grafting techniques, the membrane surface was usually activated by the in-situ hydrolysis technique to introduce an active intermediate interface on the membrane surface (Cao, Zhang, Nguyen, Zhang, & Ping, 2008). Thus, the application of coating and grafting techniques into the surface modification of alumina ceramics will be discussed in more detail in the next sub-section.

Table 2.2: Preparation techniques of surface modified alumina membranes

Technique	Speed&Time	Calcined	Substrate	Modifier	Feature	Application	Ref.
Dip Coating	0.02 ms^{-1}	1150 °C, 1 h	Dics, 0.41 % (P)	Martoxide alumina	0.08-0.14µm (D)	Gas permeation	(Falamaki, Naimi, & Aghaie, 2006)
	20 min at 23±1 ◦C	-	Dics, 13 mm (D), 60µm (T), 0.2µm (S), 25–50% (P)	Alkanoic acid (octanoic acid and octadecanoic acid)	Hydrophobic	Protein adsorption	(C.-S. Chang & Suen, 2006)
	10cm/min for 99s	400 °C, 3 h	Dics, 0.2 µm (S)	TiO_2 sol	0.2 µm (T)	Photocatalytic reactor	(Mendret et al., 2013)
	-	350 °C, 4 h	Flat sheet	Ferroxane nanoparticles	~5 µm (T), 150.3 nm (S), & 5 µm x 5 µm (R)	Fouling study	(De Angelis & de Cortalezzi, 2013)
	1 mm/s for 10 s	700 °C, 3 h & 600 °C, 3 h	Tube, 4mm (T), 12 mm (D), 70 mm (L)	Boehmite sol & Silica sol	Permselectivities increase with temperature	Permselectivity of H_2/CO_2 and H_2/N_2	(Jabbari et al., 2014)
	10 cm/min	400 °C, 3 h	Disc, 0.2 µm (S), 50 mm (D) &1 mm (T)	TiO_2 nanoparticles	0.2 µm (S)	Photocatalytic degradation	(Mendret et al., 2013)
	0.01 ms^{-1} for 10 s	650 °C, 2 h	Tubular, 5 nm&100 nm (S)	Boehmite sol	0.16 µm (T)	Gas separation	(Ananthakumar et al., 2000)
	Immersion & hydrolysis for 6h	850 °C, 2 h	Tubular, 40%(P) & 0.2 µm (S)	Aluminium isopropoxide	12.5 % (P), 26 ° (CA)	Oily wastewater	(Q. Chang et al., 2010)
	Immersion for 24h & hydrolysis for 6h	600 °C, 2 h	Tubular, 40% (P) & 0.2 µm (S)	Zirconium tetrachloride	100 nm (T) & 20° (CA)	Oil emulsion	(J.-e. Zhou, Chang, Wang, Wang, & Meng, 2010)

Table 2.2 (continued): Preparation techniques of surface modified alumina membranes

Technique	Speed&Time	Calcined	Substrate	Modifier	Feature	Application	Ref.
Dip Coating	Immerse into the channels	-	Tubular & hollow, 1.2 ± 0.1 µm (S) 35 ± 2 vol% (P)	Cellulose acetate	~35 µm (T) & 10-20 nm (S)	Industrials effluents (high organic contents)	(Nataraj et al., 2011)
	20 cm/min for 3 min 30 s	800 °C, 3 h	Tubular, 1.4 µm (S)	Boehmite sol & titania sol	100 nm (S)	Water purification	(Manjumol et al., 2011)
	Immersion & heat at 85 °C for 3h	950 °C, 2 h	Tubular, 40% (P) & 0.2 µm (S)	$Ti(SO_4)_2$ & urea	30 nm (S) & 8° (CA)	Oil emulsion	(Q. Chang et al., 2014)
	Immersion for 24h	65 °C, 10 min	Tubular, 20 nm (S)	Polydopamine & Polyethyleneimine	26 - 79 nm (T)	Pervaporation dehydration	(G. M. Shi & Chung, 2013)
	Immersion and heat	600 °C	Disc, 4.5 cm (D), 2 mm (T)	Boehmite sol &	4 µm (T), 5 nm (S), 16 nm (R)	Nano membrane	(Kheirollahi, Abdellahi, Emamalizadeh, & Sharifi, 2015)
	-	550 °C, 4 h	Dics, 0.3-0.8 mm (T) & 25-30 mm (D)	Boehmite sol	0.5 µm (T) & 10 nm (S)	Microbial separation	(N. Das & Maiti, 2009)
Spin Coating	2000 rpm for 1 min	-	Disc, 0.02 µm (S) & 25–50% (P)	Bovine dermal collagen	35 nm - 60 nm (T) & 34.5° (CA)	Biomolecular separations	(Malaisamy, Lepak, Spencer, & Jones, 2013)
	1000 r/min for 30 s	500 °C, 5 h	Disc, 0.7 µm (S), 30 mm (D) & 2 mm (T)	Aluminum hydroxide gels	136.3° (CA) & 360 L /h m^2 bar (WF)	Proteins separation	(Ke et al., 2013)
	2400 rpm for 18 s	400 °C, 2 h	Disc, 23 mm (D), 0.14 µm (P), 1.4 mm (T)	Titanium tetraisopropoxide (sol-gel)	Supporting CMS membrane with high adhesion	H_2/CO_2 and H_2/CH_4 separation	(Tseng et al., 2016)

Table 2.2 (continued): Preparation techniques of surface modified alumina membranes

Technique	Speed&Time	Calcined	Substrate	Modifier	Feature	Application	Ref.
Grafting	24 h under nitrogen	100 °C, 12 h	Tubular, 0.2, 0.5 & 0.8 μm (S)	Fluoroalkylsilanes	> 90 ° (CA)	Osmotic evaporation	(Vargas-Garcia, Torrestiana-Sanchez, Garcia-Borquez, & Aguilar-Uscanga, 2011)
	Coupling reaction 24h & ultrasonic 30 min	100 °C, 6 h	Hollow, 42.8% (P) & 0.7 μm (S)	Fluoroalkylsilanes	130 ° (CA), 42.9 $Lm^{-2}h^{-1}$ (WF) & 99.5% (SR)	Oil emulsions	(H. Fang, Gao, Wang, & Chen, 2012)
	Soaking for 12 h	120 °C, 2 h	Disc, 3 mm (T) & 30 mm (D)	Alkoxysilane	126.0° - 140.0° (CA)	Oil emulsion	(Gao, Ke, Fan, & Xu, 2013)
	Immersed for 30 min	120 °C, 3 h	Tubular, 0.1 μm (S)	zinc chloride, 2-methyl imidazole & sodium formate	Hydrophobic	Ethanol-water & acrylic acid-water	(Tang & Li, 2013)
	Pour gel into substrate & autoclave	400 °C, 4h	Tubular, 0.2 μm (S) 30 mm (L)	ZnAPSO-34 gel	High crystallinity	CO_2 separation	(Abbad Brahim, Azeddine Lounis, Sylvie Condom, & K. Taibi, 2013)

*Note: P=porosity, S=size, CA=contact angle, T=thickness, D=diameter, WF= water flux, SR=salt rejection, R=roughness and L=length

2.5.1.1 Coating technique

Membrane surfaces can be coated using various coating techniques such as dip coating (Mittal, Jana, & Mohanty, 2011), spin coating (Ke et al., 2013) and spray coating (Di Girolamo, Brentari, Blasi, & Serra, 2014). In view of its low cost and simplicity, the dip coating technique is the preferred technique in many applications. Membranes for UF and NF can be prepared using the coating process to acquire a small pore size of about 1-100 nm (N. Das & Maiti, 2009). Meanwhile, coating solution can be obtained using the sol-gel technique to fabricate fine powder (K.-H. Lee, Youn, & Sea, 2006). The sol-gel technique is a suspension preparation of small particle-sized materials such as bohemite sol (Ananthakumar et al., 2000), titania sol (Manjumol et al., 2011) and ferroxane nanoparticle (De Angelis & de Cortalezzi, 2013) as shown in Table 2.2. Table shows that most researchers studied titanium as the alkoxide precursor in the sol-gel technique for preparing the coating solution. This is because titanium alkoxide is an extremely reactive organic solvent that requires effective control during preparation (Manjumol et al., 2011).

The dip coating method is generally used in the development of composite membranes (Cao et al., 2008; Jana et al., 2011; Jannatduost, Babaluo, Abbasi, Ardestani, & Peyravi, 2010; Kasperski, Weibel, Estournès, Laurent, & Peigney, 2013). Composite membrane usually consists of two or more layers of different materials. For example, alumina-polymer composite contains alumina as support and polymer at the top layer that acts as a penetration and surface covering material (Poletto et al., 2013). Currently, alumina-polymer composite is widely applied due to its unique combination of properties. The alumina support has high mechanical strength, thermal and chemical stability, while polymer has high selectivity (Chu et al., 2005). However, there are two issues in the preparation of alumina-polymer composite (Samei, Mohammadi, & Asadi, 2013). Firstly, porous alumina requires highly mechanical strength as the support of

composite. Secondly, polymer solution needs to be prepared as a thin layer to enhance membrane permeability. This thin polymer layer reduces the pore size of ceramic, thus offering high selectivity and increased flux (Nataraj et al., 2011).

On the other hand, control over the thickness of the polymer layer on the alumina support is a crucial problem (Jana et al., 2011). The minimum thickness of the coated layer is offered as maximum in substrate surface roughness of the membrane (Falamaki et al., 2006). Moreover, the thickness of the composite membranes is influenced by dipping time via dip coating. Falamaki et al., (2006) applied the dip coating technique on an alumina MF membrane by focusing on coating time in order to prepare the desired membrane pore size in the range of 0.08 - 0.14 μm (Falamaki et al., 2006). Meanwhile, an increase in the coating time resulted in more defects on the membrane surface during sintering (Mendret et al., 2013). In addition, cost and time of preparation of the membrane increased due to the increase in coating time.

Recently, coating materials have become the focus of the study of surface modification on ceramic membranes in order to produce a nano pore sized coating layer (Yang & Yen, 2013). Nataraj et al. (2011) applied cellulose acetate as a polymer coating onto the tubular α-alumina ceramic membrane (Nataraj et al., 2011). The pore size of the resultant membrane was decreased by 10 - 20 nm from the original pore size of 1.2 μm. Furthermore, cellulose acetate was selected as the coating material due to its advantages such as excellent adhesion to ceramic surfaces, flexibility, commercial feasibility and low cost. Meanwhile, De Angelis and de Cortalezzi (2013) used ferroxane nanoparticles as the coating material on the alumina support (De Angelis & de Cortalezzi, 2013). As a result, the nanoparticles were distributed homogeneously on the alumina surface with an average pore size of 75 nm. Moreover, the alumina

composite demonstrated protein separation with a high selectivity and reduced pore size as well as a reduced fouling effect.

2.5.1.2 Grafting technique

The grafting technique involved immersion of the ceramic membranes in a grafting solution for chemical modification of the membrane surface. Chemical modification occurred by condensation reaction within the reactive group due to the grafting solution and hydroxyl groups on the oxide surface of the membranes (Kujawa et al., 2013). As a result, stable covalent bonds were created between the membrane surface and grafted materials. Mostly, silane groups (H. Fang et al., 2012; Gao et al., 2013; Vargas-Garcia et al., 2011) were selected as grafting materials on the surface modification of alumina ceramic as shown in Table 2.2. Silane groups were reacted with hydroxyl groups on the alumina surface in order to convert the surface character to hydrophobic from its naturally hydrophilic state (Kujawa et al., 2013). According to Hendren et al., (2009), the hydrophobic character enhances by increasing the molecular chain length of silane groups in a grafting solution (Hendren, Brant, & Wiesner, 2009). Hence, the highest length of molecular chain causes more penetration into the pore structure of the membrane surface. These changes of character are applicable for gas separation and oily wastewater treatment (H. Fang et al., 2012; M. Khemakhem, Khemakhem, & Amar, 2013) but not for bioseparation and purification processes.

As previously mentioned, the hydrophilic character of the alumina surface is appropriate for reducing the fouling effect during the bioseparation and purification processes. Therefore, the grafting technique could also be used to enhance the hydrophilic character of the membrane surface by using hydrophilic grated materials. This modification used direct monomer grafting onto a ceramic surface. For example, Cao et al., (2008) used acrylic acid as the grafting monomer by free-radical graft

polymerization on silica membrane (Cao et al., 2008). As a result, a ceramic-polymeric pervaporation membrane was prepared with a highly hydrophilic character. To date, researchers are still researching new grafted materials to be used to enhance the hydrophilicity character of alumina membrane.

2.5.2 Recent developments in graphene derivatives on alumina membranes

Nowadays, researchers are looking for new modifier materials which can be applied in surface modification on ceramic membranes such as carbon-based materials. Carbon-based materials such as graphene were explored due to their unique and environmentally friendly properties (H. Huang, Ying, & Peng, 2014). Graphene was discovered in 2004 (Jing Dong, Zhaahui Yao, Tianzhang Yang, Lili Jiang, & Shen, April 2013) and it consists of a mono-atomic thickness of carbon atoms with a two-dimensional structure. Equally important, it has a large surface area, excellent outstanding chemical resistance and high mechanical properties (Chen, Bi, Yin, & You, 2014; J. Liu, Yan, & Jiang, 2013). Furthermore, graphene-based materials could be formed into nano size membranes which exhibit low fictional flow of water (Joshi et al., 2014). Therefore, the application of graphene derivatives in alumina modification has great potential and needs to be explored in more detail. Two practical methods for preparation of graphene are the chemical and mechanical cleavage methods (M. Zhang et al., 2014). The chemical method (K. Wang, Wang, Fan, Yan, & Wei, 2011) has been widely applied in the oxidation process of graphite to exfoliate graphite oxide sheets. The reduction process will then form graphene films. As a result, graphene films were successfully achieved in large scale production.

The addition of graphene into alumina powders using the blending technique offered new opportunities in alumina based composite preparation (Athanasekou et al., 2014; B. Chen et al., 2014; Porwal et al., 2013). The preparation of a graphene-alumina

composite depends on the degree of exfoliation and amount of crystalline defect in the graphene network (Ramirez & Osendi, 2014). Crystalline defect principally differs according to which graphene derivative is used from the selection which includes reduced graphene oxide (rGO), graphene oxide (GO), graphite (Gt) and graphite oxide (GtO) (Hegab & Zou, 2015; Inagaki & Kang, 2014). Meanwhile, the dispersion of graphene derivatives in an alumina suspension strongly depend on their van der Waals interactions that essentially tend toward aggregation (K. Wang et al., 2011). Hence, the agglomeration in alumina based composite could cause densification during the sintering process (B. Lee, Koo, Jin, Kim, & Hong, 2014a). As a result, using the blending technique to produce alumina-graphene composite is less effective without a detailed mechanism process on alumina-graphene suspensions.

2.5.2.1 Challenges in the fabrication of graphene-alumina composites

The fabrication of graphene-alumina composites involves three key issues which are quality of graphene production, homogeneous dispersion of graphene in alumina suspension and retention of graphitic structure during the sintering process (Porwal et al., 2013). The problem of homogeneous dispersion occurs due to the strong tendency of graphene compounds to agglomerate as a consequence of their inherent hydrophobicity and their high specific surface areas (Rincón, Chinelatto, & Moreno, 2014). To overcome this problem, a wet milling process is used on the alumina powders and graphite in ethanol instead of using graphene directly. Exfoliation of the graphite into graphene and uniform mixing of both powders is thus achieved in just one step. However, some graphite agglomerates remained in the suspension and the graphene that is produced is of a low quality. This approach has subsequently been improved using a solution of graphene platelets in dimethylformamide for better dispersion (J. Liu, Yan, Reece, & Jiang, 2012). So far, two main issues have been solved, which are the

synthesis of graphene sheets and the preparation of a homogeneous mixture of graphene in an alumina powder (Rincon et al., 2014).

Addressing the issue of graphitic retention structure through the sintering process, researchers are still researching the use of the Spark Plasma Sintering (SPS) (J. Liu et al., 2013; Porwal et al., 2013; K. Wang et al., 2011). SPS is a new sintering technique which is less time consuming due to high heating rates exceeding 300°C/min compared to conventional sintering. On the other hand, current focus is also being given to other graphene derivatives like graphene oxide on alumina based composite fabrication (Centeno et al., 2013; Fan, Estili, Igarashi, Jiang, & Kawasaki, 2014; Rincon et al., 2014). The details of this application are presented in the next sub-section.

2.5.2.2 Graphene oxide as a noble graphene derivative

Graphene oxide (GO) is a graphene derivative which has a flake-like structure in the micron scale (Jing Dong et al., April 2013). GO can improve the membrane's wetting ability due to its high hydrophilic functional group properties. In order to achieve GO structure, graphene surface was modified by attaching water molecules to change its wettability properties from hydrophobic to hydrophilic. GO surface consists of oxygen groups and carboxyl groups which could be suitable for further modification. The oxygen groups can enhance the solubility and dispersion ability of the GO in the ceramic matrix (Yuan & Liew, 2014). Meanwhile, the Hummer Method created carboxyl groups on the GO structure due to the oxidation of graphene by strong acids.

The Hummer method (N. M. Huang, Lim, Chia, Yarmo, & Muhamad, 2011) was used to prepare the GO by oxidizing graphite. The method uses a combination of potassium permanganate and sulphuric acid to oxidize graphite. Moreover, GO nanosheets offer an ultrathin, high flux and energy efficient sieving membrane due to their unique two-dimensional, outstanding mechanical strength and good flexibility (Pei

& Cheng, 2012). Currently, the performance of the GO membrane was focused on the separation of small molecules. This is due to the special structure of the GO membrane which features a high hydrophilicity character and less toxicity. It has possible applications in the biological field (Yuan & Liew, 2014).

However, the structure of GO is still under debate and a popular structural model as shown in Figure 2.5 was proposed by Lerf and Klinowski (Smith & Freeman, 2014). GO is mostly composed of carbon and oxygen in atomically thin, plate-like structures. According to this model, several oxygen-containing groups decorate the basal planes (hydroxyl and epoxide groups) and edges (carbonyl and carboxyl groups) of GO (H. Huang et al., 2014).

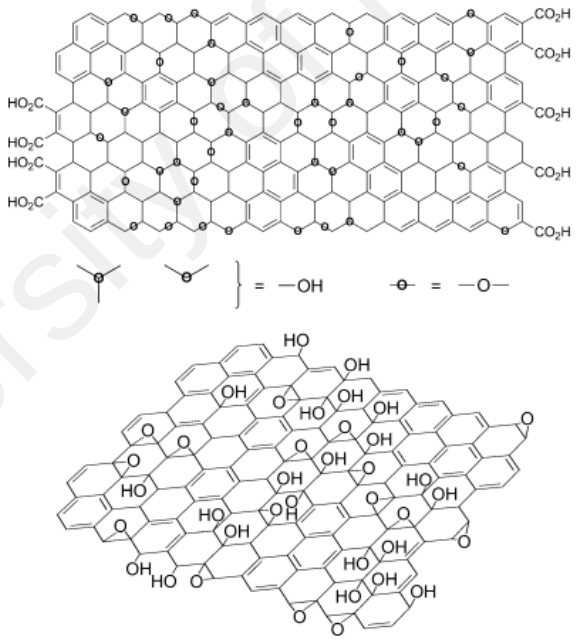

Figure 2.5: The structure of GO proposed by Lerf and Klinowski (Smith & Freeman, 2014)

The existence of these oxygen functional groups in GO can be readily dispersed in an aqueous medium and can form well-dispersed aqueous without any addition of surfactants or stabilising agents. In the dispersion of water, GO sheets are highly negatively charged and the result is the ionisation of the carboxyl groups. Moreover,

these functional oxygen-containing groups provide many reactive reactions for a variety of modification, which can be used to develop a series of functionalised GO-based membranes with significantly enhanced separation performances (Compton & Nguyen, 2010). The functionalized GO also known as GO framework (GOF), where other functional groups attached to GO structure such as boronic ester (Burress et al., 2010), silane group (Lou, Liu, Liu, Shen, & Jin, 2014) and tannic acid (M.-Y. Lim et al., 2017). The GOF has potential in the fabrication of alumina-graphene derivative membrane for water permeation application.

2.5.2.3 Fabrication of alumina-graphene derivative membranes

Currently, the application of GO as a graphene derivative on alumina based composite fabrication has earned great attention due to its high permeation and selectivity performance. However, fabrication techniques of GO-alumina membranes still require deep investigation in order to obtain outstanding high permeability with excellent selectivity and stability. The main advantages of GO among other graphene derivatives are highly negative suspension and a high polar character due to the ionisation of the carboxylic acid and phenol hydroxyl groups (H. Huang et al., 2014). The negative charge of the GO sheets provides strong electrostatic repulsion to prevent overlapping among the GO sheets. Meanwhile, the polar character of GO consists of electrosteric and electrostatic forces to allow good dispersion in polar solvents such as water (Rincon et al., 2014). From experimental measurement, the water contact angles for GO and graphene were 30-60° and 87-127° respectively (N. Wei, Peng, & Xu, 2014). GO had a highly hydrophilicity character due to its oxygen-rich groups. Therefore, these factors are in favour with enhancing the water permeability of alumina modified membranes.

Generally, the GO's reactions are classified into two methods which are reduction (removing oxygen groups) and chemical functionalization (adding other chemical functionalities) (Dreyer, Park, Bielawski, & Ruoff, 2010). A few applications of graphene derivatives into alumina for composite preparation were shown in Table 3. The dispersion of graphene derivatives in alumina suspension has two methods; either powder or colloidal processing routes. Mostly, researchers have used the powder processing method due to its simplicity and less time-consuming preparation. In most cases the suspension is dried and the resulting powder mixture is then compacted by axial pressing. However, the colloidal processing method offers a better quality of dispersion through the surface charges modification of the ceramic and graphene derivative powders (Porwal et al., 2013) resulting in a highly reliable and uniform microstructure.

It can be seen in Table 2.3 that most of the graphene-alumina composites were tested for a beneficial effect on the enhancement of conductivity (Inam, Vo, & Bhat, 2014) and reinforced mechanical properties (B. Lee et al., 2014a). The first report on a graphene-alumina composite was published in 2009 (T. He, Li, Wang, Zhu, & Jiang, 2009). The study was implemented 5 % graphite into alumina suspension via the milling process in ethanol at room temperature. The electrical conductivity was found to be 5709 S/m for the composite with a minimum thickness of 3-4 nm. Meanwhile, Lee et al. have reported a strategy to synthesise a GO-alumina mixture using the Powder Processing Method (B. Lee, Koo, Jin, Kim, & Hong, 2014b), resulting in an increment of up to 21% in the flexural strength considering the alumina as reference material. In conclusion, most researchers have tested the graphene-alumina composite for an improvement in mechanical properties such as hardness, fracture toughness and flexural strength.

These enhancements can be significantly improved by loading relatively low graphene derivatives into alumina suspensions. For instance, Centeno et al. reported an improvement of 50 % in the fractural strength of graphene reinforced alumina composite with the addition of only 0.22 vol% of GO (Centeno et al., 2013). However, more recently, GO was used as a grafting material on the alumina surface in order to produce the composite structure as shown in Figure 2.5 as reported by Lou et al. (2014). This method uses the silane group 3-Glycidoxypropyltrimethoxysilane (GLYMO) as a linker between the alumina surface and the GO in the Grafting Technique.

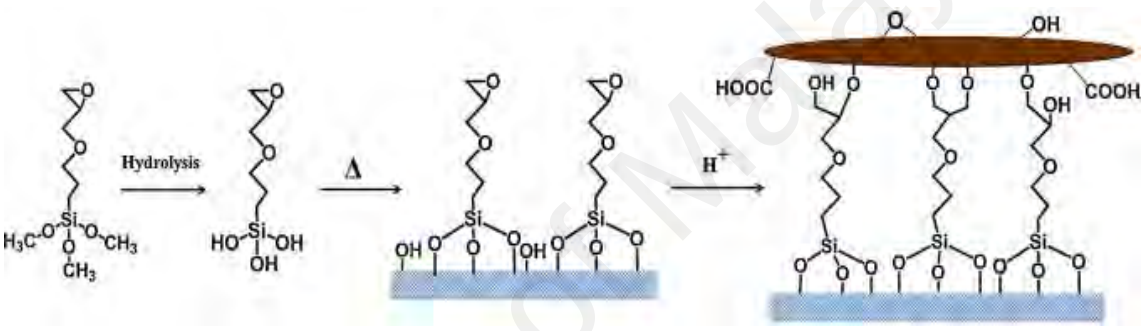

Figure 2.6: Schematic of formation of GO/ceramic composite membrane by Lou et al. (2014) (Lou et al., 2014)

However, an important issue is the interfacial adhesion between the separation and support layers (Lou et al., 2014). The enhancement of interfacial adhesion is necessary to prevent the membrane layer peeling off from the ceramic surface. Therefore, grafting the GO onto the alumina surface is presumably the best alumina based composite fabrication option in order to enhance its hydrophilicity character. Due to protein separation and purification, high hydrophilic properties could improve the flux permeation and selectivity as well as reducing the fouling effect. Thus, a future prospect here is the improvement of the alumina-based composites using GO as a modifier. In order to attach GO onto an alumina membrane, the linker must be good enough to hold the bonds. The major future challenge of introducing a linker is the mechanism happening during the composite membrane preparation.

Table 2.3: Application of graphene derivatives into alumina membranes

Graphene derivatives		Alumina	Preparation method	Sintering	Features	Ref.
Graphite	Exfoliation (50 mesh)	Powders (2μm)	Colloidal method: ball milling	159MPa & 160°C for 24h	Cold modulus of rupture, CMOR (21.31 ±0.28 MPa) & modulus of elasticity, E (3.10 ± 0.06 GPa)	(Q. Wang et al., 2014)
Graphene	Liquid phase exfoliation (2.5-5 mg/mL)	Powders (200nm)	Powder method: ultrasonic bath & ball milling	1350°C, 50MPa with 100°C/min	Facture toughness improvement of ~40%	(Porwal et al., 2013)
	Rapid thermal expansion/exfoliation (T=6-8 nm & L= 15-25 μm)	Powders (150nm)	Powder method: sonication & ball milling	1500-1550°C, 50MPa with 100°C/min	Flexural strength (523 ± 30 MPa) & fracture toughness (4.49 ± 0.33 MPa $m^{½}$)	(J. Liu et al., 2013)
	Nanoplatelets (T=1-5 nm)	Powders (500nm)	Powder method: ultrasonic & ball milling	1500°C & 25MPa	Fracture toughness (6.6 MPa $m^{1/2}$)	(Y.-F. Chen et al., 2014)
	Nanopowders	Powders (<50nm)	Powder method: ball milling	1250–1450 °C , 10–70 MPa with 25–50 °C/min	Fully dense nanocomposite had higher crystallinity, thermal stability and electrical conductivity	(Inam et al., 2014)
	Exfoliation (~1.3 mg/mL)	Powder (~0.1 μm)	Colloidal method: ball milling and dried by rotary evaporator	1250–1600 °C with 50 MPa for 5 min	Nanocomposite with high fracture toughness (3.8 MPa $m^{½}$) , electrical conductivity (~20.1 S/m)	(Çelik, Çelik, Flahaut, & Suvaci, 2016)

Table 2.3 (continued): Application of graphene derivatives into alumina membranes

Graphene derivatives		Alumina	Preparation method	Sintering	Features	Ref.
Graphene oxide (GO)	Hummers method (0.5 mg/mL)	Powders (70nm)	Powder method: ultrasonic & mechanical stirring	1300°C, 50MPa with 100°C/min	Toughness (5.21 MPa $m^{½}$) & conductivity (172 Sm^{-1})	(K. Wang et al., 2011)
	Hummers method (1-3 g/L)	Powders (150nm)	Colloidal method: mechanical stirring & centrifugation	1300-1500°C, 80MPa with 100°C/min	Low resistivity (15 Ωcm), mechanical strength (630 MPa) & fracture strength (~185 MPa)	(Centeno et al., 2013)
	Monolayers (SA=103m^2/g, L=1-4μm & T= 0.7-1.2nm)	Powders (0.35μm) with zirconia (100nm)	Colloidal method: tape casting	1400°C, 80MPa with 100°C/min	Viscosities (523 mPas at shear rate of 250 s^{-1}) & thicknesses (50 μm)	(Rincon et al., 2014)
	Hummers method (powders)	Powders	Powder method: sonication & ball mill	1400°C, 50MPa with 100°C/min	Flexural strength (425 MPa), hardness (2294 Hv) & fracture toughness (10.5 MPa $m^{1/2}$)	(B. Lee et al., 2014b)
	Modified Hummers method (Colloid)	Powders (0.2μm)	Colloidal method: sonication	1573-1673 K & < 6 Pa	Relative density (98.90 %) & average grain size (471 ± 144 nm)	(Fan et al., 2014)
	Modified Hummer method (1mg/mL)	Substrate (S=110nm & P=35%)	Dip-coating for 30 s	50 °C	Hydrophilicity (68.3°) & total flux (461.86 g/(m^2h))	(Lou et al., 2014)

2.6 Protein recovery

Protein recovery in biotechnology downstream process are required to be emphasis for an alternative to produce value-added product which is left-over proteins in wastewater stream. Proteins are considered sensitive macromolecules due to their three-dimensional structures and needed to be processed at mild operating conditions. They are generally produced at very low concentrations with many impurities having quite similar physicochemical and biological properties as target proteins and at the same time (A. Saxena et al., 2009). The proteins need to be processed for enhancing their purity and concentration in aseptic conditions to avoid any contamination. All these require a moderate purification technique with high purity and selectivity for the final product. Several techniques for the protein recovery process were implementing, as shown in Table 2.4 which regarding to their aim of application. In biotechnology industrial process, the available techniques could be combined more than two in the whole process which depends on the end-use of the protein product.

Conventionally, packed bed chromatography (PBC) also has been used for bio-separation technique (Orr, Zhong, Moo-Young, & Chou, 2013). The technique is limited either employ good separation with low purity or can handle in large volume of feed but with poor selectivity. This involves large number of steps in the downstream processing of protein-based biopharmaceuticals, resulting in reduces the overall yield. For purification of products such as monoclonal antibodies and plasma proteins, there is a significant amount of interest in alternatives to PBC technique (L. Wang, Mah, & Ghosh, 2009; Yu, McLean, Hall, & Ghosh, 2008). Therefore, the membrane technology technique in this application still on the top due to lower cost as well as promising in industry for high purity of proteins (Hassan et al., 2013).

Table 2.4: The available techniques for protein recovery

Process aim	Technique
High-productivity and low-resolution	Cell disruption
	Centrifugation
	Precipitation
	Liquid-liquid extraction
	Microfiltration
	Ultrafiltration
High-resolution, low-productivity	Ultracentrifugation
	Packed bed chromatography
	Affinity separation
	Electrophoresis
High-resolution, high-productivity	Membrane chromatography
	Monolith column chromatography

The membrane technology-based processes such as UF, MF and membrane chromatography (MC) are promising techniques for protein recovery that are being examined in industry and academia. The ceramic membranes have been used in the protein recovery such as food and beverage processing, drinking water treatment, biotechnology, and pharmaceuticals due to their promising properties. In food and beverage processing as well as in drinking water treatment, good chemical stability of the ceramics is appreciated since it makes it possible to use more rigorous cleaning agents (Salehi, 2014; Silva, Paskocimas, Oliveira, Nascimento, & Zille, 2015). Meanwhile, for the biotechnology process, the biocompatibility of ceramic membranes is important as well as their resistance to microbial attack and biological degradation (La Flamme et al., 2007). Moreover, it is beneficial to use ceramic membranes for viscous fluids of feed, since they are more stable at high pressures and it is also possible to use higher filtration temperatures in the process.

Although alumina membranes have been widely introduced in protein recovery (Treccani et al., 2013), there is still limited study on the fouling effect. Therefore, in order to further advance the use of alumina membranes, it is necessary to understand the chemical and physical phenomena involved. The efficiency of protein recovery highly depends on membrane fouling (Saxena, Tripathi, & Shahi, 2008). Membrane fouling may be caused by pore size constriction, pore blockage and a macromolecular aggregate of proteins (Mahesh Kumar & Roy, 2008). A number of mechanisms would cause protein accumulation on the membrane surfaces which are hydrogen bonding, van der Waals forces, electrostatic attraction and hydrophobic interactions (Yeu et al., 2009). All these phenomena will result in membrane fouling by reducing the flux permeation process. Thus, the enhancement of the surface properties of the alumina membrane surface is one of the solutions to minimize membrane fouling.

2.6.1 Protein as foulant

A protein is a biopolymer composed of basic building blocks called amino acids with naturally made up of to 20 different amino acids (R Ghosh, 2003). Generally, proteins are abundantly found in living cells and have various biological functions such as protective (antibodies), transport (haemoglobin), catalysts (enzymes), structural (collagen) and regulatory (hormones). Majority of these proteins are found in various microbial, plant and animal sources. In order to be further used in food industry, bioproduct and pharmaceutical, the proteins need to be processed or purified to achieve vary degree stage depends on that applications. During the application process via MF or UF particularly, the proteins could act as foulant that caused a fouling phenomenon. For instance, in dairy fluids contain a variety of solids including proteins, minerals, lactose and fat (Le et al., 2014). These components have been noted to foul membranes at varying degrees. It is generally accepted that proteins and minerals account for the majority of foulant in dairy membrane operations **(**Adams**,** 2012**).** Meanwhile, lactose is

not considered to be an important foulant, but could become trapped in the foulant matrix during NF process (Bipasha Das, Sarkar, Sarkar, Bhattacharjee, & Bhattacharjee, 2016).

Protein constitute a large proportion of the foulant layer in most dairy membrane processes because the charged and hydrophobic regions within their structures are able to interact with other feed components and the membrane itself (Curtis & Lue, 2006). More specifically, the negatively charged milk proteins may engage in either electrostatic attractions with positively charged membranes or cation-mediated electrostatic attractions to negatively charged membranes. Two parameters that contribute higher foulant of proteins during water filtration, which are proteins concentration and its chemistry properties (Y. P. Lim & Mohammad, 2010). According to mass transfer effects, flux decreases exponentially with increasing concentration of the feed fluid. This theory addresses concentration polarization specifically, it impacts fouling phenomenon. Generally, increasing the concentration of a feed stream of proteins increases the level of reversible foulant (that which can be removed by cleaning) (D'Souza & Mawson, 2005). This amounts to an increase in observed cake layer formation and a decline in flux.

Meanwhile, the chemistry of proteins will also impact its fouling potential by physical (Y. P. Lim & Mohammad, 2010). Previous research has determined that BSA, like other proteins, exhibits maximum membrane deposition to membranes at its isoelectric point. (Saxena, Kumar, Tripathi, & Shahi, 2010) Consequently, flux minimum during the filtration of protein solutions are also observed at the isoelectric point of the protein, as this is the pH at which a protein is least soluble. Thus, the nature of the electrostatic relationship between the protein and membrane is also important. As previously mentioned, proteins have an affinity for binding to membrane surfaces,

particularly hydrophobic ones (Salgın, Takaç, & Özdamar, 2005). The fouling phenomenon during dairy filtration is due to the protein foulant's hydrophobic interaction with the membrane, thus by making the membrane as hydrophilic as possible reduces the chance of protein adsorption (Y. P. Lim & Mohammad, 2010).

2.6.2 Reduction of fouling mechanism

Membrane fouling for protein recovery process is heavily influenced by protein adsorption on the membrane surface, pore blocking, cake layer formation, and depth fouling (Jamal, Chang, & Zhou, 2014). Therefore, it is crucial to understand the effects of proteins chemistry including ionic strength, divalent ion concentration and pH, membrane properties such surface charge and hydrophobicity/hydrophilicity character, and the interactions between proteins-membrane surface on the fouling behaviour (S. Lee, 2013). The fundamental of the physical properties of membranes is essential to provide the water treatment industry and the manufacturers with practical guidelines for the selection of membranes with optimal performance. Ceramic membranes are made of metal oxides which are generally more hydrophilic than most polymeric materials and may assume different surface potential that develops from different surface modification.

The membrane properties such as membrane hydrophilicity/hydrophobicity character, pore size, surface roughness, and membrane charge should be considered to predict the extent of fouling. The impact of membrane hydrophilicity on fouling has already been addressed. The pore size, or more accurately, the ratio of the pore size to the rejected proteins is also important. Despite the enhanced adsorption capacity of relatively large pores (C. Wang et al., 2010), flux will be reduced to a greater degree if a narrower pore becomes fouled to the same extent as a larger pore, simply because there is less open space to be lost. Minimizing surface roughness reduces the risk of fouling

simply by taking away points at which foulant can easily attach to the membrane (Ramon & Hoek, 2013). On the other hand, membrane surface charge is yet another consideration. In general, the biological proteins are negatively charged at neutral pH, thus the negatively charged membranes or even neutral membranes would less foul than the positively charged membrane during protein filtration (Breite, Went, Prager, & Schulze, 2015). This fundamental was given to the conclusion that the negative charge of membrane surface is more preferable in protein separation and purification in order to avoid the fouling mechanism.

2.7 Summary

Pressure-driven membrane filtration processes such as MF, UF and NF provide opportunities in the protein recovery by purifying and concentrating. However, widespread acceptance of these processes has not yet fully utilized due to membrane fouling. Membrane fouling is the accumulation of proteins, on the surface or within the pores of a membrane. Fouling prolongs processing times, increases energy and cleaning costs, decreases separation efficiency, and, in severe cases, may lead to irreversible clogging of the membrane. While membrane fouling cannot be eliminated completely, nevertheless could limit its development by choosing membrane materials which adsorb less foulant, optimizing processing conditions such as cross-flow velocity, temperature, pre-treatment process to reduce their tendencies to foul, or event pursue with modified the membrane surface to avoid fouling. Recently, focused was given to surface modification of ceramic membrane in order to improve the surface properties due to its anti-fouling. In this review, many research works have explained the surface modification of alumina ceramics in order to enhance the separation process by reducing fouling. Furthermore, this review also revealed the available modification techniques to create alumina membranes with high hydrophilicity thus high performance in protein separation. There are two main approaches to enhance the

performance of alumina ceramic membranes to reduce the fouling effect and increase membrane selectivity. Thus, surface modification on alumina ceramic membranes is an attractive technique in order to reduce membrane fouling in protein separation. As a result of this review study, graphene derivatives are viewed as having high potential to serve as modified materials. Future studies are needed to address the issue of hydrophilic character on chemically modified GO sheets. GO films as grafted materials and the preparation of an alumina-GO composite are still lacking, especially on the performance study of protein recovery processes.

CHAPTER 3: MATERIALS AND METHODS

3.1 Materials

A commercially available alumina powder with three different powder diameters of 1 μm (alpha, surface area 10 m^2/g), 40 – 50 nm (gamma/alpha, surface area 32-40 m^2/g) and 10 nm (gamma/alpha, surface area 100 m^2/g) [purchased from Alfa AESAR] were used as ceramic materials. Polyethersulfone (PESf) [Veradel 3000P, Solvay], Arlacel P135 [Corola, Malaysia] and *N*-methyl-2-pyrrolidone (NMP) [Synthesis Grade, Merck] were used as binder, dispersant and solvent, respectively to prepare the ceramic suspension. Meanwhile, sodium hydroxide (NaOH) was used as an alkali medium and acid nitric (HNO_3) was used as an acidic medium. Both chemicals were purchased from Sigma, Malaysia.

Meanwhile, Graphite flakes (code no 3061) were purchased from Asbury Graphite Mills, Inc (Asbury, NJ), sulphuric acid (H_2SO_4, 98%), phosphoric acid (H_3PO_4, 85%), potassium permanganate ($KMnO_4$, 99.9%), and hydrogen peroxide (H_2O_2, 30%), were purchased from Merck (Darmstadt, Germany). Hydrogen chloride (HCl, 37%) was purchased from Sigma Aldrich (St Louis, MO). All these chemicals were needed in the synthesis of GO using simplified Hummer's method. Diamine groups for this study are ethylenediamine (EDA), butylenediamide (BDA) and phenylenediamine (PDA) are used as cross-linker agent to prepare GOFs. Bovine serum albumin (BSA, Mw of 66KDa), egg albumin (EA, Mw of 45KDa), trypsin (TR, Mw of 20KDa) and lysozyme (LSZ, Mw of 14.3KDa) are selected as model proteins for proteins recovery study. The following chemicals were obtained from Sigma Aldrich, Malaysia.

3.2 Preparation of alumina dope

Four main components in ceramic dope are alumina powder, NMP, PES and Arlacel P135 for inorganic powders, solvent, binder and dispersant, respectively. Start with Arlacel P135 was dissolved in NMP solvent prior to the addition of alumina powders with three different particle sizes of 1, 0.04–0.05 and 0.01 μm at ratio of 7:2:1. The dope was mixed well using an approximate alumina/balls ratio of 2 for 24 hours in a planetary ball milling machine (NQM-2 Planetary Ball Mill) and rate was fixed at speed of 182 rpm. Mixing was performed for further 24 hours after addition of PES. The homogeneous dopes were degassed under vacuum while stirring until no bubbles could be seen at the surface (~ 1 hr). Then the dope was ready to use for rheological characterization and proceed with phase inversion step for the next step of alumina membrane fabrication.

In this study, the alumina loading was investigated in order to determining desirable solid precursor as well as alumina membrane. Thus, the alumina loading was adjusted with different weight percent (wt.%) from total weight (300 g) of ceramic dope as present in Table 3.1. Meanwhile, the amount of Arlacel P135 was 1.5 wt.% from total weight of ceramic dope and the amount PES is 10 wt.% from total weight of alumina powders (with three different particles sizes). All these ceramic dopes were used to study the rheological characterization by viscosity measurement using Rheometer (TA instruments) with cone and plate geometry at shear rate 0 – 100s^{-1} at room temperature.

Table 3.1: Composition of alumina dope with different alumina loading (wt.%)

Alumina loading (wt.%)	Alumina powders (g)			NMP (g)	PES (g)	Arlacel P135 (g)
	1 μm	0.05 μm	0. 01 μm			
56	117.6	33.6	16.8	110.7	16.8	4.5
57	119.7	34.2	17.1	107.4	17.1	4.5
58	121.8	34.8	17.4	104.1	17.4	4.5
59	123.9	35.4	17.7	100.8	17.7	4.5
60	126.0	36.0	18.0	97.5	18.0	4.5

3.3 Preparation of GO and GOF suspensions

The synthesis of GO was used a simplified Hummer's method as reported by N. M. Huang et al., (2011) (N. M. Huang et al., 2011). Start with oxidation of graphite using acidic mixing of sulphuric acid: phosphoric acid, H_2SO_4:H_3PO_4 (360:40 mL) and $KMnO_4$ (18 g) using a magnetic stirrer. After complete the reaction, the colour of mixture changed from dark purplish green to dark brown. Second step is to stop the reaction using hydrogen peroxide, and the colour of mixture changed to bright yellow, indicating a high oxidation level of graphite. The last step is washing method used three times of 1 M HCl aqueous solution and repeatedly with deionized water until a pH of 4-5 was achieved. The washing process was carried out via a centrifugation technique with a centrifugation force of 10,000 rpm. During the washing process with deionized water, the graphite oxide experienced exfoliation, which resulted in the thickening of the graphene solution, forming a GO gel.

The prepared GO gel was modified using diamine-functionalize in order to form facile GO frameworks (GOFs) which to enhance the stability and compatibility of GO sheets. 100 mL of GO suspension (at different concentration) was sonicated for 15 min and 5mL of diamine (EDA, BDA or PDA) was added by let them mix well using ultrasonic. Preparation of GOFs using ultrasonic at 60 °C for 1 hr in order to complete the reaction and form homogeneous suspension. The GOFs will use as grafting material on alumina surface to prepared GOFs/Alumina composite membrane. The concentration of GO suspension is very important factor to influence the final product as selective of composite membrane. Thus, a vary concentration of GO suspension was used are 5, 10 and 15 ppm.

For the GO properties study, the GO gel was dried at 60 °C overnight onto disc glass and peel off and also known as GO sheet to measure field emission scanning electron

microscopy (FESEM), contact angle, thermogravimetric analysis (TGA), differential scanning calorimetry (DSC), Fourier transform infrared (FTIR) spectroscopy, X-ray powder diffraction (XRD) and X-ray photoelectron spectroscopy (XPS). The XRD patterns of GO was recorded with a scanning rate of 1 per minute in a 2θ range from 10 to 80 with Cu Ka radiation (k = 1.5418 Å) to characterize the inter layer spacing of GO sheet and to determine its purity. The thermodynamic state and kinetic process of low-temperature deoxygenation reaction of GO have been investigated for better understanding on the reduction mechanism by TGA and DSC.

Meanwhile, both GO and GOF suspensions were characterize for some analysis that significant effect on their changes of suspension properties using zeta potential (ZP) and particles size distribution (PSD). The ZP and PSD were analysed by using Malvern instruments at vary GO concentration of 5 – 50 ppm and vary pH of GO suspensions using dilution of NaOH and HNO_3 in order to analysed the stability of the suspensions.

3.4 Fabrication of flat-sheet alumina (FSA) membrane

In this preparation, the aim is to determine the optimum condition to fabricate FSA membrane using statistic tool of central composite design (CCD) method from response surface methodology (RSM). The statistical approaches was found to be the best methodologies for optimisation as they consumed minimum time and resources (Ahmad, Low, Shukor, & Ismail, 2009). This method was conducted with the aid of Design Expert software (version 6.0.6). The design of experiment (DoE) for this method involved two factors (blade gap and sintering temperature) with four responses (mechanical strength, pure water flux, shrinkage, and porosity). The DoE was applied with these two factors were set at three levels namely low (−1), centre (0), and high (+1). These low and high values were chosen after performing preliminary tests and presented in Table 3.2. The DoE approach produced a total of nine experimental runs.

The results from the experiments were analysed using ANOVA for quadratic model performed at 95% level of confidence to establish its significance (Wee, Tye, & Bhatia, 2010). The data collection was analysed mathematically and statistically using CCD for modelling the influenced factors with several responses.

Table 3.2: Experimental independent factors.

Factors	Factor code	Unit	Level and range		
			-1	0	1
Blade gap	A	mm	1.0	1.5	2.0
Sintering temperature	B	°C	1300	1400	1500

The FSA membranes were fabricated using the phase inversion with tape casting and sintering method. The alumina dope was casted on a glass sheet using a doctor blade with different gaps of 1.0, 1.5, and 2.0 mm. The casted film was immersed in a water bath for 24 h for phase inversion technique (W. He, Huang, Gao, Winnubst, & Chen, 2014). Milli-Q ultrapure water was used as the coagulant in the water bath. The film was dried at room temperature for 24 h and later cut into a disc shape in diameter of ~70 mm. Then, the disc-shaped film was sintered using two-step heating in a muffle furnace (Magna Value, Malaysia) as shown in Figure 3.1.

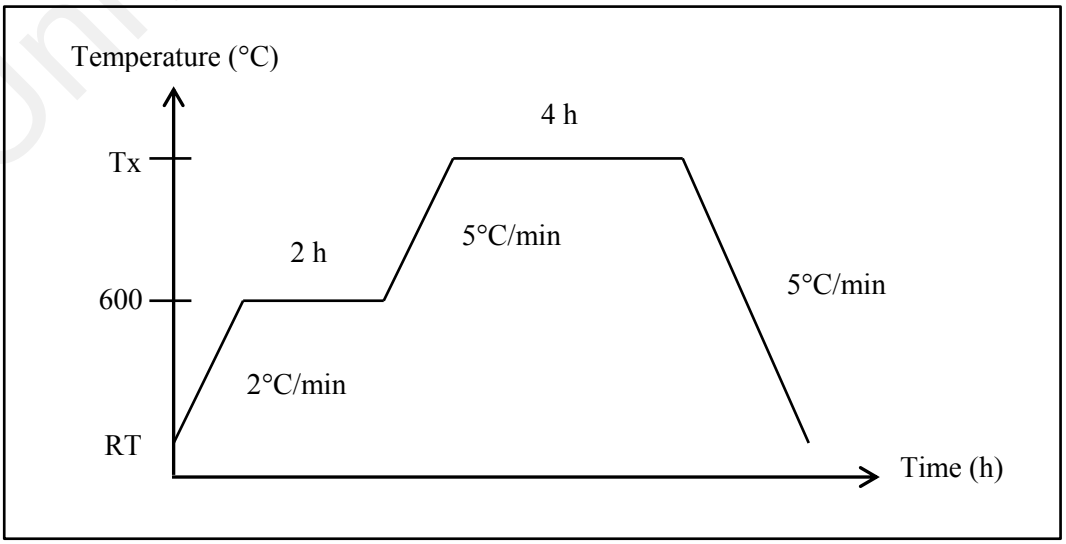

Figure 3.1: Sintering profile using two stages of heating

The first stage is removing the binder at 600 °C and the latter is formation or rearrangement of inorganic particles at elevated temperature which is target temperature (Tx). The Tx most probably around 60 – 80% of melting temperature for inorganic powder (Darcovich, Toll, Hontanx, Roux, & Shinagawa, 2003). In this study, inorganic material was used alumina powder with melting point of 2051 °C, thus the target temperature was in the range of 1200 to 1600 °C. From the figure, the furnace temperature was first increased at a rate of 2 °C/min to 600 °C was carried out for 2 h. The temperature was then further increased to 1300, 1400, and 1500 °C as selected Tx at 5 °C/min and was held for 4 h for the final sintering. Finally, cooling was carried out to room temperature at a rate of 5 °C/min.

3.5 Fabrication of hollow fibre alumina (HFA) membrane

The preparation of alumina membrane in hollow fibre configuration was carried out using extrusion technique-based phase inversion, whereby the parameter employed is presented in Table 3.2. The as obtained alumina dope was degassed for 1 hour, and then was transferred to 200 ml Harvard stainless steel syringes with a tube-in orifice (OD = 3mm, ID = 2.8mm). The suspension was then extruded into a coagulation bath that contained tap water with the extrusion rates of 10 mL/min, bore fluid rate of 10 mL/min and air gap of 15 cm to an external coagulant bath.

Table 3.3: Spinning parameters for fabrication of HFA membrane

Spinning parameters	
Extrusion rate (mL/min)	10
Bore fluid rate (mL/min)	10
Air gape (cm)	15
Internal & External coagulant	Tap water
Temperature of coagulant	Room temperature (25 °C)

The extrude HFA precursors were immersed in the external coagulant bath overnight for the solvent/non-solvent process and this overall process was demonstrated in Figure 3.2. Further with cut the HFA precursors (OD = 1.38mm, ID = 1.02mm) into 35 cm of length and complete dried in room temperature for another 24 h. The last step was sintered the HFA precursors using two-step profile via a tubular furnace (XL-1700) using aforementioned sintering profile.

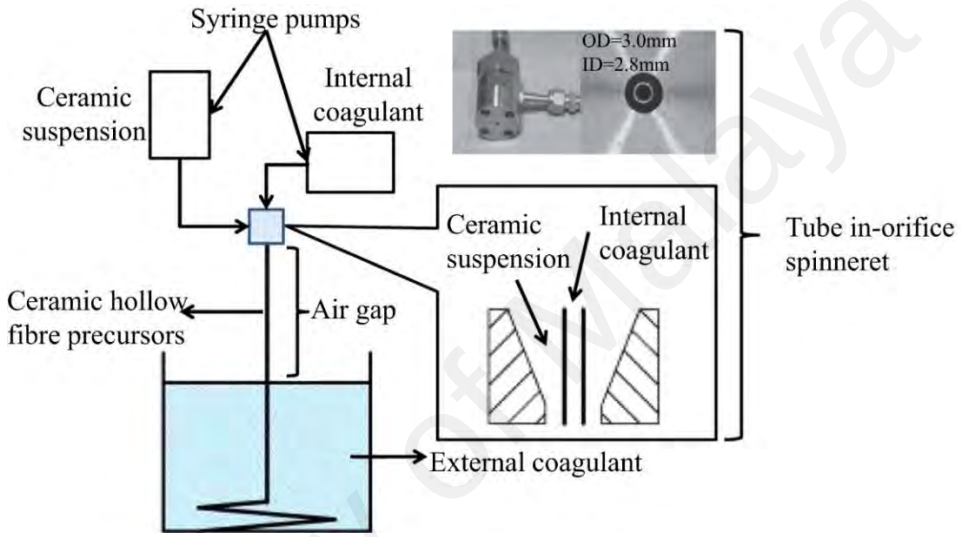

Figure 3.2: A schematic diagram for spinning-based phase inversion technique as reported by Abdullah, et. al (2016) (Abdullah et al., 2016)

3.6 Fabrication of composite alumina membrane

Composite membrane fabrication on both FSA and HFA membrane by incorporated with prepared GOFs. Two methods were used for deposition of GOFs which are pressure driven deposition (PDD) and vacuum deposition (VD) for FSA and HFA membrane, respectively. The PDD method was used a dead-end filtration module with nitrogen gas supply as presented in Figure 6.1. A 100 ml of GOFs suspension was immediately transfer into dead-end module after complete ultrasonic for 1 hr at 60 °C. Then, the suspension was pressurized onto the surface of FSA membrane at 0.5 bar. This step was repeated for other GOFs suspension at vary GO concentration and diamine monomers. Meanwhile, the VD method was used in order to deposit GOFs on

HFA membrane as shown in Figure 3.4. The HFA membranes as support were first potted into ¼ inch national pipe thread (NPT) male connectors and sealed with epoxy resin at both the connector and at the hollow fibre end was connected on the vacuum pump. Then, the VD was run by turn on the vacuum pump for 1 hour to attach the GOFs sheets at the outer layer of HFA membrane.

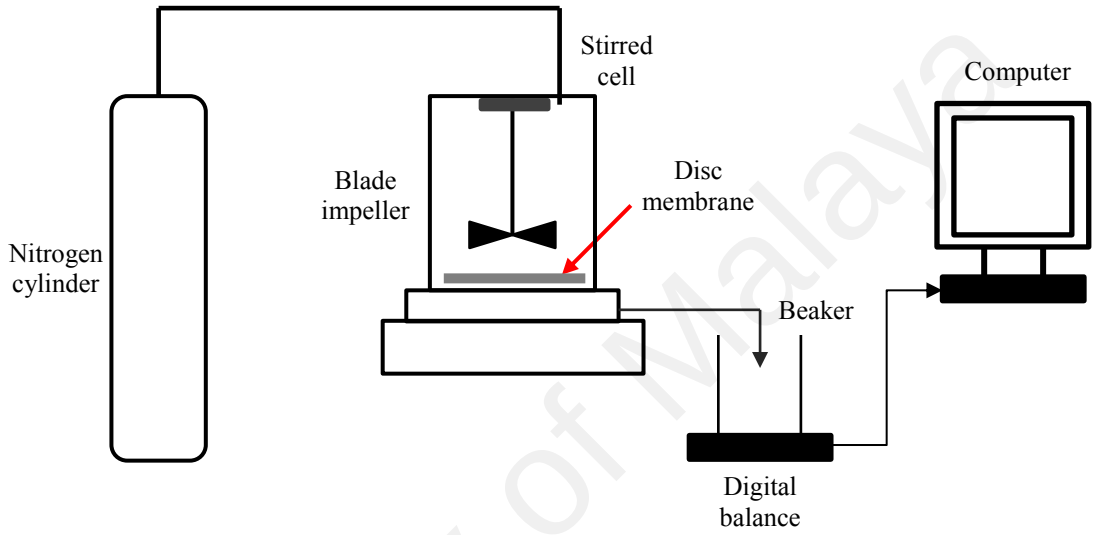

Figure 3.3: Schematic diagram for pressure driven deposition (PDD) using a dead-end filtration system

During the deposition step, the positively charged diamine groups (EDA, BDA and PDA) at the GOFs suspension bind to the negatively charged groups at the surface of alumina membranes via electrostatic attraction (Shao et al., 2016). The GO suspension without diamines-functionalization also prepared to form GO/A and presented as control. After finished GO and GOF deposition step, the modified membrane was dried at 80 °C for 24 h using drying oven in order to cross linking the GO and GOFs layer onto the membrane's surface. For the FSA, five modified membranes were prepared at vary GO concentration and designated as 5GOF(EDA)/FSA, 10GOF(EDA)/FSA and 15GOF(EDA)/FSA composite membranes. Meanwhile, the HFA membrane, three modified membranes were prepared at different diamine monomers which are

GOF(EDA)/HFA, GOF(BDA)/HFA and GOF(PDA)/HFA composite membranes. After complete modification method, these composite membranes were ready to proceed with characterizations and performance test.

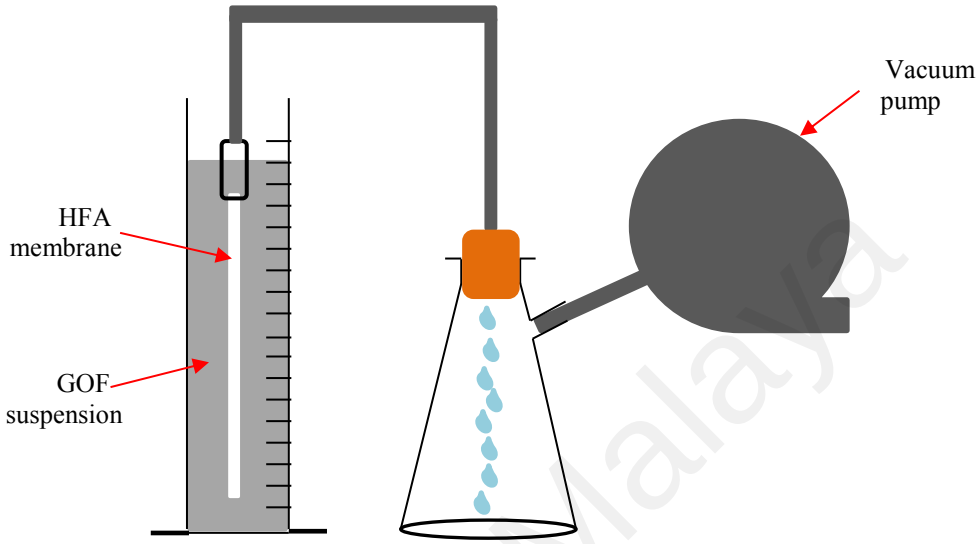

Figure 3.4: Fabrication of HFA composite membrane using vacuum deposition (VD) method

3.7 Membrane characterizations

Morphology study consisted of the surface and cross-section structure was measured using scanning electron microscopy (SEM, Philip) for the prepared alumina membranes. SEM images were recorded at the accelerated voltage of 10 to 20 kV to examine surface morphology. In addition, the modified membranes were further observed their morphology structure using field emission scanning electron microscope (FESEM, Carl Zeiss Microscopy, North America) for a better resolution image. Both alumina support and modified membranes were gold coated by sputter coater to produce electrical conductivity images of the sample before measured their morphology structure. For surface area measurement, a standard procedure was employed for the analysis of the B.E.T. (Brunauer Emmet Teller) gas adsorption measurement. The pore size distributions of the membranes were identified using Porometer (Beneflux Scientific, Belgium). In this method, the prepared membranes with a diameter of 2 cm were

immersed in porefil (surface tension of 16 dynes/cm). After that, the membranes were analysed using nitrogen gas with increasing pressure.

The measurement of porosity of the FSA membranes was calculated by Archimedes' principle using ultrapure water as an immersing medium. To determine the porosity of prepared alumina membranes, the sample was dried at 120 °C for 3 h and weighed (W_{dry}). The sample was then placed in Milli-Q water overnight and weighed again (W_{wet}). Their porosities were calculated using Eq. (3.1) with known total volume (V_{sample}) and density of Milli-Q water (ρ_{water}) (Bakhtiari, Samei, Taghikarimi, & Mohammadi, 2011). Shrinkage rate was measured using percentage of mass loss of alumina membranes after sinter. The shrinkage (Sh) in diameter is defined by Eq. (3.2). Where d_i and d_f are the initial (before sintering) and final (after sintering) diameters of the membrane, respectively.

$$\text{Porosity } (\varepsilon) = \frac{W_{wet} - W_{dry}}{\rho_{water} \text{ X } V_{sample}} \text{ x } 100 \qquad \text{Eq. (3.1)}$$

$$\text{Shrinkage (Sh)} = \frac{(d_i - d_f)}{d_i} \text{ x } 100 \qquad \text{Eq. (3.2)}$$

Meanwhile, the alumina support and modified membrane's surface wettability was investigated using a water contact angle measurements system with the sessile drop method. The drop soaking rate was determined based on the change in water contact angle within the first 15 second. Values of at least five different samples were averaged. An X-ray photoelectron spectrometer (XPS) was utilized to measure the surface chemical compositions of the modified FSA membranes. XPS full-scan spectra were recorded within the range from 200 to 1200 eV resolution. The XPS result was used to obtain the obtained atomic concentration of elements and degree of cross-linking between FSA membrane and GOFs layers. From the element's calculation, O/N ratio

was obtained as shown in Eq. (3.3) to further calculate the degree of cross-linking using Eq. (3.4) as reported by Lai et al., (2017) (Lai et al., 2017).

$$\frac{O}{N} = \frac{3m+4n}{3m+2n} \quad \text{Eq. (3.3)}$$

$$\text{Degree of cross} - \text{linking} = \frac{m}{m+n} \text{ X } 100 \quad \text{Eq. (3.4)}$$

The flexure strength of the prepared alumina membranes was measured by three-point bending test using universal testing machine (Instron Model 4469, USA) provided with a load cell for 10 kN. For the FSA membrane were performed on a 70 × 20 mm rectangular bar with a span length of 50 mm and a crosshead speed of 5 mm/min. Meanwhile, for the HFA membrane, the sample was in length of 70 mm. The flexure strength was calculated using Eq. (3.5) and Eq. (3.6) for HFA and HFA membrane, respectively. Where the σ is flexure strength (MPa), F is load applied (N), L is length of support span (mm), b and t are width and thickness, respectively of FSA membrane (mm), and D and d are outer and inner diameter, respectively of HFA membrane (mm).

$$\text{Flexure strength } (\sigma) \text{for FSA membrane} = \frac{3FL}{2bt^2} \quad \text{Eq. (3.5)}$$

$$\text{Flexure strength } (\sigma) \text{for HFA membrane} = \frac{8FLD}{\pi(D^4 - d^4)} \quad \text{Eq. (3.6)}$$

Last but not least, the surface roughness of the modified HFA membranes was characterized using an atomic force microscopy (AFM) (PARK XE-100, SCHAEFER Technology GmbH), obtained by tip scanning with a scanning size of 1.5 µm × 1.5 µm.

3.8 Membrane performances

For the performance test of pure water flux (PWF) was evaluated under nitrogen gas as pressure in dead-end system as shown in Figure 3.3 previously. A dead-end system was used to test the PWF of the support and modified FSA membranes. The membrane

system consists of a holder with diameter of 6 cm in cylinder shape, a pressure vessel and a digital balance that measures the permeate flow rate and sends data to a PC for recording in Riskey software (version 1.34, A&D Company). The pure water flux was measured under a transmembrane pressure of 0.5 bar. A volume of 2 L of deionized water was passed through the membrane sample with active surface diameter of 60 mm at 0.5 bar and the time of flow-through was recorded with time interval of 30s. PWF of the membranes were calculated using Eq. (3.7), where J is the PWF ($L/m^2h.bar$), Q is the volume of water permeated (L), A is the effective membrane area (m^2), and t is the sampling time (h).

$$\text{PWF (J)} = \frac{\text{Q}}{\text{A X t}} \qquad \text{Eq. (3.7)}$$

Meanwhile, for the HFA membrane, the PWF and proteins recovery were determined using cross-flow filtration system at 2 and 5 bar for support and modified membrane, respectively. Proteins recovery was used for different proteins with specific molecular weight and radius size as shown in Table 3.3. For the measurement of protein recovery rate was calculate using Eq. (3.8), where the C_1 and C_2 are proteins concentration at feed and permeate, respectively.

$$\text{Protein Rejection (\%)} = \frac{C_1 - C_2}{C_1} \text{ X } 100 \qquad \text{Eq. (3.8)}$$

Table 3.4: Proteins with their molecular weight and average solute radius

Protein	Molecular weight (kDa)	Average solute radius (nm)
Bovine serum albumin	69	4.5
Egg albumin	45	3.3
Trypsin	20	2.15
Lysozyme	14.3	1.9

The antifouling study was performed with long-term filtration using LSZ protein which is the smallest protein model in this study. The performance test was collected on a digital balance, and the cumulative mass of permeate was recorded in a computer every 3600s via a RS-232 connection in order to calculate the flux for 24 h duration for each permeation, starting firstly with water flux, J_1 (L/m^{2}h) and followed by protein flux, J_P (L/m^{2}h) and secondly with water flux, J_2 (L/m^{2}h) which is carried out after washing with deionized water. In order to evaluate the antifouling property of membranes, the flux recovery ratio (FRR) and the total fouling ratio (Rt) were calculated as follow:

$$\text{FRR}\ (\%) = \frac{J_2}{J_1}\ \text{X}\ 100 \qquad \text{Eq. (3.9)}$$

$$\text{Rt}\ (\%) = 1 - \frac{J_P}{J_1}\ \text{X}\ 100 \qquad \text{Eq. (3.10)}$$

Where the Rt is the sum of reversible fouling ratio (Rr) and irreversible fouling ratio (Rir). The Rr defines the fouling produced by concentration polarization, meanwhile the Rir designates the fouling caused by adsorption or deposition of protein molecules on the membrane surface. Rr and Rir can be calculated using the following equations, respectively:

$$\text{Rr} = \left(\frac{J_2 - J_P}{J_1}\right)\ \text{x}\ 100\% \qquad \text{Eq. (3.11)}$$

$$\text{Rir} = \left(\frac{J_1 - J_2}{J_1}\right)\ \text{x}\ 100\% \qquad \text{Eq. (3.12)}$$

CHAPTER 4: RESULTS AND DISCUSSIONS

4.1 Effect of alumina loading on the alumina dope

Three different particle sizes of alumina powder were used, and those are 1 μm, 50 nm and 10 nm. The application of smaller size alumina particle (10 nm) into alumina dope may be beneficial under certain circumstances as a reduction in membrane pore size and an increase in mechanical strength of final product, which is alumina membrane. However, the addition of smaller particles leads to aggregation due to high van der Waals interaction. Therefore, there is a maximum alumina loading that can be achieved to avoid aggregation during alumina dope preparation. Furthermore, it is difficult to form asymmetric membrane structures when the dope viscosity is above a certain level. A good alumina dope must have an acceptable rheology behavior.

Five alumina dope was prepared with different alumina loading which are 56, 57, 58, 59 and 60 wt.% of alumina loading. The evolution of the viscosity curve with shear rate at 10 to 100s^{-1} for the alumina dope with different alumina loading was displayed in Figure 4.1. The viscosity study is an important parameter for dope handling during casting process on glass sheet using doctor blade. From the viscosity curve, the rheological behavior of the prepared dopes can be described as having a pseudoplastic behavior; in which the viscosity decreases as the shear rate increases. Furthermore, dopes with different alumina loading indicate various viscosity values via all range of shear rates. In addition, at certain shear rates, the viscosity of the dope increases as the alumina loading increases.

From the figure, at an alumina loading of 56wt.% and 57wt.% resulted in a lesser viscosity value of ~12 and ~17 Pa.s, at a shear rate of 30 s^{-1}, respectively. These values are good enough for dope mobility on glass plate by doctor blade at a speed of 3 cm/s. However, at an alumina loading of 58 wt.% and 59 wt.%, the dope is slightly difficult to move on the glass plate during casting. At 60 wt% of alumina loading had a viscosity of ~50 Pa.s, which is highly viscous and makes it very hard to flow and stick on ceramic jar. From the overall viscosity result, the alumina dope with 56 and 57 wt.% alumina loading have a good rheology behavior due to better flowability during casting step using doctor blade with speed of 3 mm/s. Kingsbury et al. (2009) studied the morphology structure on the prepared alumina dope having 58.7wt.% alumina content with viscosity value of 12 Pa.s at shear rate of 30 s^{-1}. At this viscosity value, an adequate morphology with finger and sponge structures via phase inversion and sintering technique could be produced (B. F. K. Kingsbury & K. Li, 2009). Therefore, the alumina dope with 56 and 57 wt.% of alumina loading have a good casting behavior and could produce a desired alumina membrane.

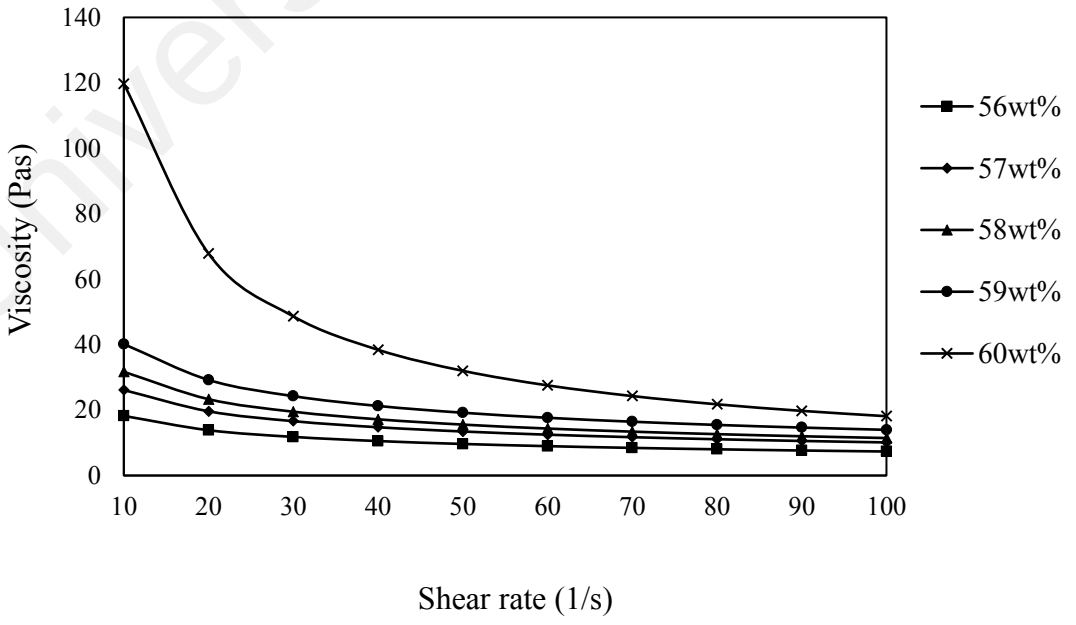

Figure 4.1: Viscosity curve of alumina dope with different alumina loading in wt.%

4.1.1 Alumina membranes at different alumina loading

All the prepared alumina dopes were used in the next step in the alumina membrane fabrication, which is the phase inversion step with casting technique. The dopes were casted at a blade gap of 0.5 mm on glass plate using doctor blade and are directly immersed in a coagulation bath (miliQ pure water) for overnight. Then, the solidified alumina precursor (with a thickness of ~0.5 mm and 7 x 2 cm of rectangular shape) was dried and made to go through the sintering step at a sinter temperature of 1300 °C to produce alumina membranes. Figure 4.2 shows the topographic images of the prepared alumina membranes at different alumina loading after being sintered at 1300 °C. When using the 56 wt.% of alumina loading, the prepared alumina membrane cracked. Meanwhile, the rest of these membranes have bent slightly at the corner. This is due to the shrinkage phenomena that happens during sintering process which could effect the mechanical strength of the prepared alumina membranes. Furthermore, this shrinkage is an expected phenomena during sintering especially when the solid precursor is too thin (< 0.3 mm for all the prepared alumina membranes) and resulted in the bending effect at the edge part.

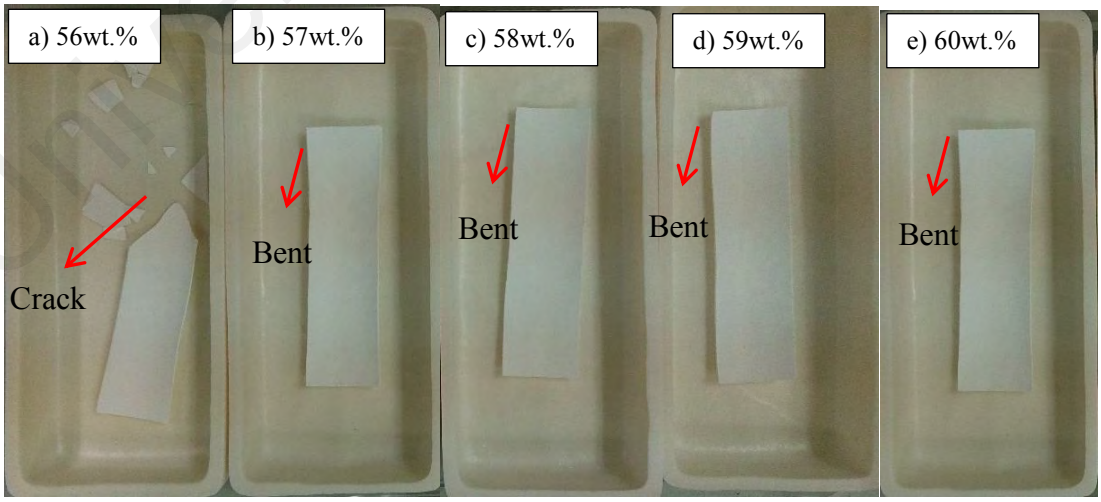

Figure 4.2: Photographic images for alumina membranes after sintering at 1300 °C

Meanwhile, Figure 4.3 presents the SEM image for all the prepared alumina membranes which indicate the surface morphology structure. The dark spots were referred as pores or macrovoid formation of the membrane surface. From the figure, the highest alumina loading of 60 wt.% in alumina dope resulted in less porosity with probably less pore size due to less dark spots. Meanwhile, more dark spots were obtained at the lowest alumina loading (56 wt.%) was most probably due to high porosity (42.68 %) of alumina membrane as shown in Table 4.1. The high porosity could defect the membrane due to the crack effect, which is observed when using 56 wt.% of alumina loading, as shown in Figure 4.2.

On the other hand, the increase in alumina loading in alumina dope was found to increase the viscosity. Thus, high viscosity most probably increase the density of the prepared alumina membrane. So, it is obvious that the higher the density, the lower the porosity or vice versa. The results shown in Figure 4.3, satisfies the trend reported in Table 4.1. Porosity of the alumina membrane is decreased with higher alumina loading in alumina dope. However, all these prepared alumina membranes do not have too much difference in shrinkage value. That is, the shrinkage of prepared alumina membrane does not increase or decease monotically with the increase of alumina loading. The high value for shrinkage is mainly due to the sintering temperature and the grain growth which result in the gaps among the alumina particles becoming narrower (Qin et al., 2014). Thus, the shrinkage do not really depend on alumina loading but is most significantly related to the sintering temperature.

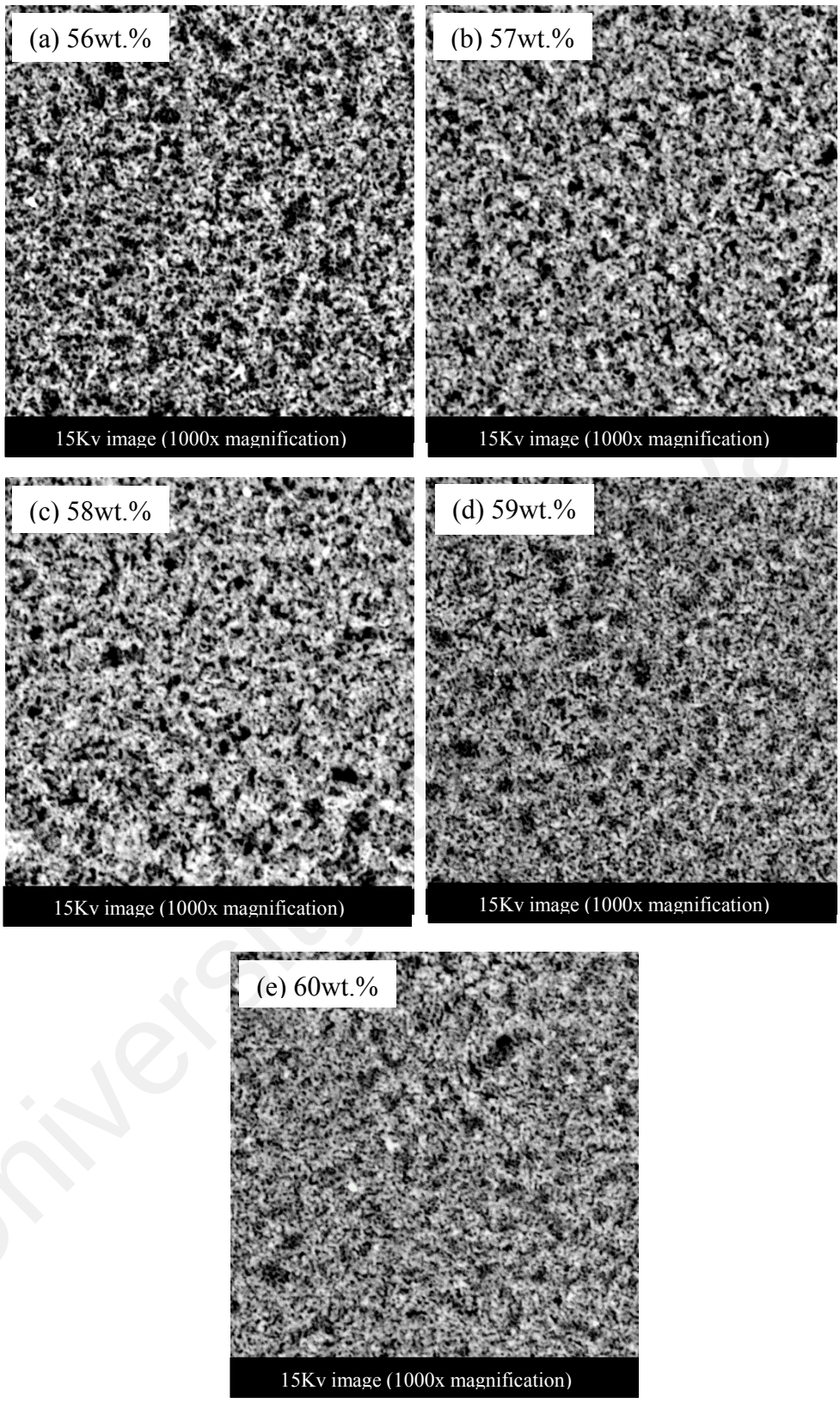

Figure 4.3: SEM images of prepared alumina membranes at different alumina loading in wt.%

From the SEM structure, the alumina particles were close to each other and the sintering neck among the alumina grains was formed, which provides the flexure strength of the alumina membrane. The flexural strength of porous ceramic membranes depend on the sintering neck among the alumina grains (Zhu et al., 2015). This indicates that the alumina loading in the alumina dope does influence the flexure property of the prepared alumina membrane. Thus, the membrane obtained at 60 wt.% of alumina loading has the highest flexure strength of 21.81 MPa. The highest flexure strength is due to the highest compact of alumina particles inside the prepared alumina membrane. Meanwhile, the less compact alumina particles lead to high pore size of the prepared alumina membrane which provides more porosity and results in less strength needed to fracture that membrane. At a composition of 56 wt.% of alumina loading, the membrane has the lowest value of flexure strength (16.63 MPa) due to high amount of porosity.

Table 4.1: Characteristics of prepared alumina membranes at different alumina loading

Alumina loading (wt.%)	Flexure strength (MPa)	Porosity (%)	Shrinkage (%)	BET surface area (m^2/g)
56	16.63	42.68	12.54	16.81
57	17.01	40.11	12.42	17.27
58	18.58	36.52	12.72	12.12
59	19.32	35.41	12.68	12.52
60	21.81	35.11	11.89	12.20

In addition, the BET surface area of the prepared alumina membranes was also analyzed, as presented in Table 4.1. At a composition of 57wt.%, the membrane has the highest BET surface area of 17.27 m^2/g, while at the composition of 58wt.%, the membrane has the lowest BET surface area of 12.12 m^2/g. From the eye observation, the high viscous dope produced more bubbles in the dope, which is very hard to remove. Thus, the trap bubbles in the dope were affected by high defects on the

structure of alumina membrane. This is due to the BET surface area is mainly dependent on the whole structure of alumina membrane, which is included at the middle layers. Furthermore, the higher BET surface area reduces the pore size of the prepared alumina membrane as well as increases its performance (Kujawa et al., 2013).

In overall, the suitable alumina loading in alumina dope for the fabrication of alumina membrane was obtained at 57 wt.%. In order to observe a more detailed morphology structure of the alumina membrane at 57 wt.% alumina loading, the field emission scanning electron microscopy (FESEM) was used to evaluate its surface structure at a high evolution image, as shown in Figure 4.4. At a resolution of 2 kV, the arrangement of alumina particles is not uniform and not compact enough at a sintering temperature of 1300 °C. Thus, further studies need to increase the sintering temperature in order to achieve a promising alumina membrane. From the figure, the estimated pore size was obtained at ~108 nm.

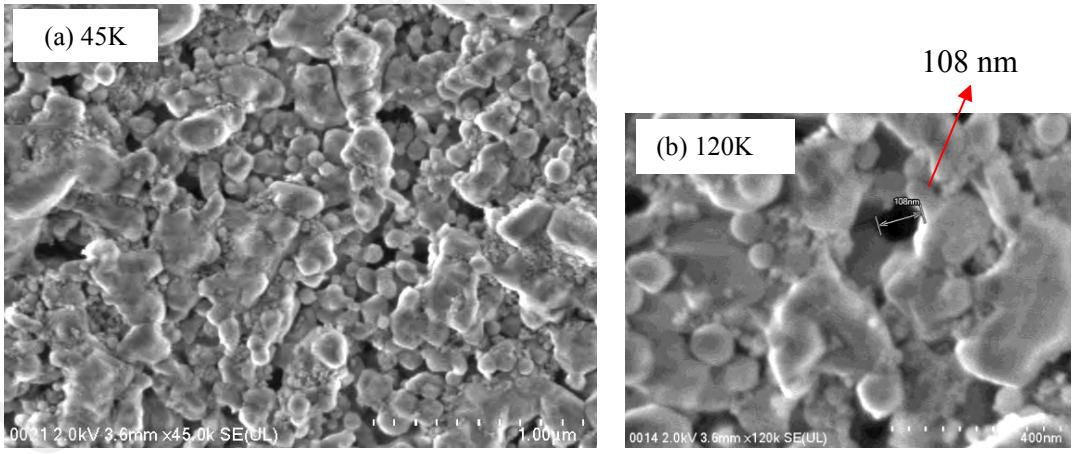

Figure 4.4: FESEM structure for 57 wt.% alumina loading of prepared alumina membrane at different magnification; (a)45 K and (b)120 K

It is well known that the highest alumina loading in alumina dope has to have the highest solid precursor density and the lowest shrinkage rate (Rincón et al., 2014). Hence, the dope suspension with alumina loading of 57 wt.% was taken as the optimum for this alumina dope preparation, since it presents high alumina loading while

maintaining the viscosity at a level that is low enough to allow casting process using doctor blade with speed rate of 3 cm/s to take place. Moreover, the alumina precursor provides an easy handling when shaping it into a disc shape. The obtained alumina precursor could be easily peeled off on glass plate and had a great uniformity structure without macroscopic defects as shown in SEM morphology. Thus, for the next section of alumina fabrication for flat-sheet and hollow fibre configurations, the 57 wt.% of alumina loading was used in alumina dope preparation.

4.2 Properties of GO and GOF suspension

4.2.1 The prepared GO gel

Several characterization techniques were measured to understand the unique physicochemical properties of GO, as these properties could greatly affect the subsequent GOFs synthesis and eventually the membrane fabrication. The GO suspension normally had a yellowish or light brown colour, indicating that the carbon lattice structure was distorted by the added oxygenated functional groups, since pure graphene or graphite is black in colour (Hu & Mi, 2013). A general characterization of synthesized GO gel was classified by concentration, pH, zeta potential, electrical mobility, conductivity and particle size. All these properties were shown in Table 4.2 to indicates the GO gel properties that are prepared by the simplified Hummer's method.

Table 4.2: Physicochemical properties of prepared GO gel

Properties	**Value**
Concentration (mg/mL)	10
pH	4-5
Zeta potential (mV)	-75.9
Electrical mobility (m^2/Vs x 10e-8)	-5.952
Conductivity (x10^{-5} S/m)	0.964
Particle size (nm)	1.6

Meanwhile, TGA and DCS were performed as presented at Figure 4.5. TGA was measured to monitor the level of reduction of GO during the heat treatment. Figure 4.5(a) present the TGA curve at a temperature range of 0 to 900 °C against the weight loss in percent. At a temperature less than 100 °C, the weight is slightly lost (~ 5%), and this loss is attributed to the elimination of physiosorbed and interlamellar water (P. V. Kumar et al., 2014). Starting at a temperature of 400°C to 800°C, the weight loss occurs rapidly around 90%. From this result, it could be concluded that GO would not reduce during the diamine-functionalization of GO at 60 °C to form GOFs.

A typical DSC curve with a heating rate 20°C/min is shown in Figure 4.5(b). Wide exothermic peaks were found at around 5°C and 100°C. During exothermic reaction, it has been found that a dramatic mass loss occurs due to the degassing of CO, H_2O and CO_2. GO is a key intermediate between graphite and graphene, which contains many kinds of oxygen functional groups, including epoxide (C-O-C), single-bonded on-top oxygen (C-O), hydroxyl groups (C-OH), and carbonyl (C=O). For a dry GO, a considerable mass loss will occur near 100 °C, accompanied by the release of CO_2, CO, and H_2O due to the deoxygenation of oxygen functional group. The enthalpy change of -1506 J/g is negative as the deoxygenation reaction is exothermic.

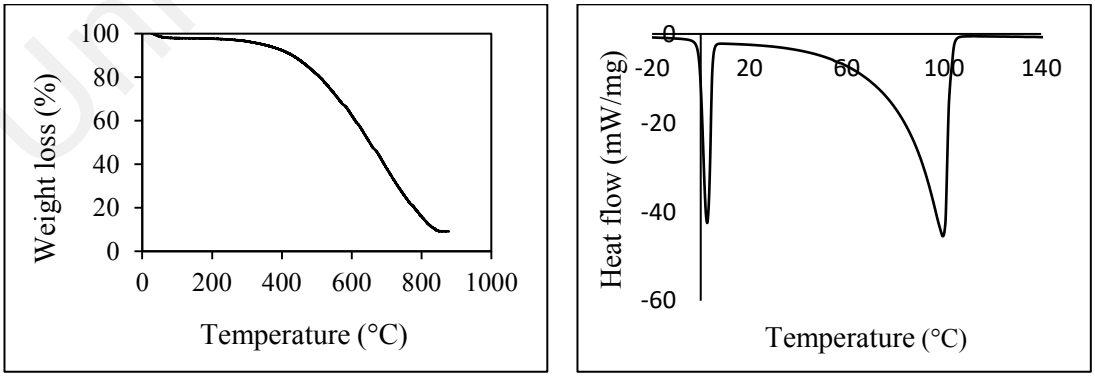

Figure 4.5: GO sheets properties (a)TGA curve and (b) DSC graph

The chemical structure of GO sheets was characterized in terms of FTIR, XRD and XPS. FTIR spectroscopy is recognized as an important tool to study different types of functional groups. Figure 4.6. as depicted, for the FTIR spectrum of GO sheet, the broad and intensive peak at ~3321 cm^{-1} denotes the hydroxyl (–OH) functional groups at the end of GO plane with symmetrical stretching vibrations (Allahbakhsh, Sharif, Mazinani, & Kalaee, 2014) and the peak at ~1637 cm^{-1} corresponds to the C=OO stretch of carboxylic group. The existence of carboxylic acid results in GO having electronegativity, and water nanochannels between each GO nanosheet are formed through electrostatic repulsion (W. Choi, J. Choi, J. Bang, & J.-H. Lee, 2013).

Meanwhile, the peak of ~1109 cm^{-1} indicates the existence of C–O stretching vibration, the peak at ~1282 cm-1 belongs to the C–OH stretching vibration and the peak at 1161 cm^{-1} arises from epoxide groups (C–O–C). Thus, all these peaks confirm the abundance of hydroxyl groups and carboxylic groups which can be utilized as active sites to graft functional molecules onto GO. The others various functional groups on the GO also could provide active sites for the bonding between GO layer and linker monomers to form multilayer of GO and GOF sheets.

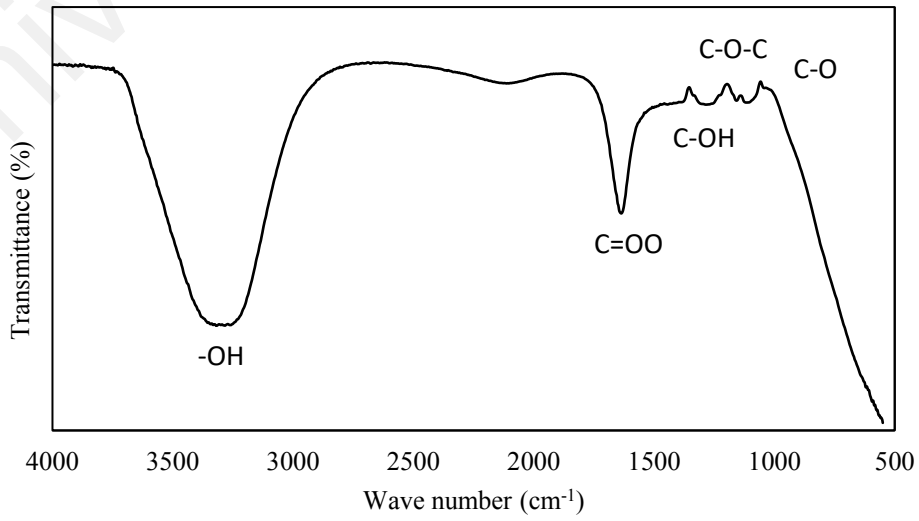

Figure 4.6: FTIR spectrum for GO sheet

The XRD analysis measured the degree of oxidation of graphite and the interlayer spacing can be obtained to form GO sheets. An XRD pattern of GO sheets was shown in Figure 4.7. The GO sheets exhibit a sharp peak at 10° which referred to GO characteristic (Lou et al., 2014). In contrast, the peak at ~26° refers to graphite characteristic that is not present in GO sheets. The peak of graphite has been shifted to the peak of GO due to the oxidation process in which functional groups are added on the GO, the interlayer spacing shifts from 0.34 to 9.63 nm.

In general, the GO interlayer spacing *d* in graphite oxide is around 0.6 – 1.0 nm depending on the degree of oxidation of graphite and the amount of water molecules intercalated into the interlayer spacing (J. Li, Zeng, Ren, & van der Heide, 2014). The increase of interlayer spacing reduces the interaction between GO sheets and thus facilitates the exfoliation of GO into dispersed GO nanosheets. Moreover, the enlarged interlayer spacing would be beneficial to quicken the transport of small molecules. However, this increment also causes the GO sheets to be easily wetted and swelled by water molecules (Y. Huang et al., 2015). Thus, the interlayer spacing of GO sheets could be altered for the optimum thickness in order to get high water permeability without swell.

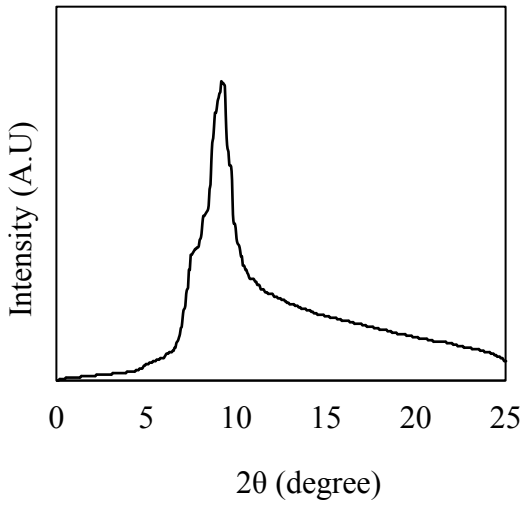

Figure 4.7: XRD spectra for GO sheets

In addition, elemental survey by XPS analysis also revealed that GO was free from any metal residues used during the chemical oxidation process, as shown in Figure 4.8(a). This is because the wide spectra which contain two major elements are oxygen (O 1s) and carbon (C 1s). It is generally accepted that oxygen present on GO is mainly in the form of epoxy (i.e., the bridge site oxygen) and hydroxyl groups. From the wide spectra, the ratio of carbon to oxygen (C/O) is 2.3. The typical value of C/O ratio in GO, which indicates the degree of oxidation, reported in the literature is in the range of 2−4 (An, Yang, Wang, & Liu, 2016). However, the GO structure is complicated by a rich variety of interactions: (1) between (adjacent) sp2 and sp3 carbon atoms, (2) between epoxides, (3) between hydroxides, and (4) between epoxide and hydroxide (L. Wang et al., 2010). Therefore, XPS analysis also can used to identify the types of carbon-oxygen bonds of GO.

The detail elemental analysis of C 1s was performed in Figure 4.8(b), which indicated the existence of hydrophilic oxygen-containing groups, such as the hydroxyl/epoxy and carbonyl/carboxyl groups. For C 1s spectra, 284.5 eV corresponds to the C-C, C=C and C-H bonds. Meanwhile, 286.7 eV and 288.3 eV are assigned to C-O and C=O/C=OO, respectively. Thus, the ratio of C-C/C=C/C-H:C-O:C=O/C=OO was 6.7:5.2:1, which is determined by using a percentage value of atomic concentration at C1s peaks. Typically, the GO contain a ratio of epoxy:hydroxyl:carbonyl/carboxyl in the range of 3−8:0.4−5:1−4 (An et al., 2016). The different ratio value due to the partial carbon−carbon bonds of oxygen-containing functional groups linked on the GO sheets break. The data from Figure 4.8(b) show that about 52.08 % of carbon was not oxidized, 40.15 % had C-O bond (representing hydroxyl and epoxide groups), and 7.77 % had COOH bond.

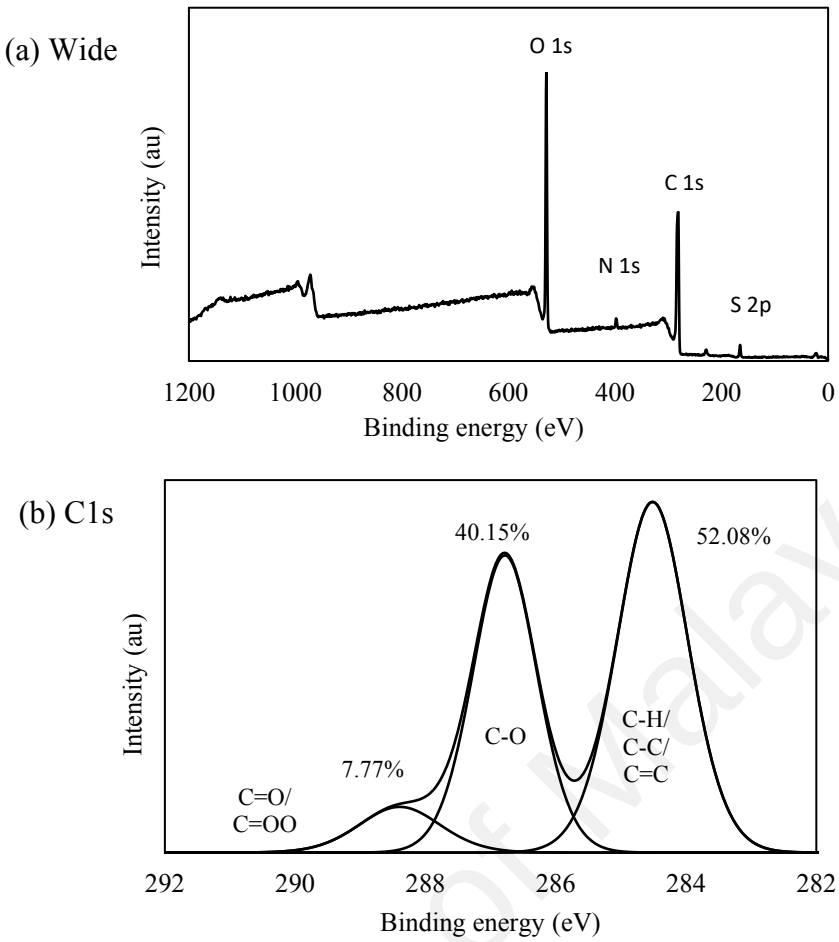

Figure 4.8: XPS analysis for GO sheet (a) wide spectra and (b) C 1s spectra

Overall, the synthesized GO using the simplified Hummer's method in this work reveals that it is a simple and convenient method. This work confirms the existence of oxygen functional groups by XPS and the presence of C-O and C=C bonds by FTIR analysis. Also, the exfoliation of graphene sheets is confirmed by FESEM image. Thus, the synthesized GO shows many interesting and unique properties that can be applied in a variety of applications. Their unique properties that contain highly oxygenated groups at the plane and edges could be functionalized with other groups in order to improve their performance. GO can be best described as a single layer planar hexagonal array of carbon atoms to which functional groups, including carboxylic acid, hydroxyl, epoxy, and carbonyl groups, are attached to. This property opens up many opportunities for

chemical reactions and schemes, including self-assembly and thin films processing, to exploit the beneficial properties of GOF.

4.2.2 GO and GOF suspensions

Homogeneous and stability of GO and GOF suspension are important factor for the selective layer formation. In this part, only one GOF has been used to determine its stability in suspension form, which is GO-EDA functionalization. Generally, highly dispersed suspension is of great benefit to the formation of integrated selective layer. The concentration of GO suspension is a crucial factor to influence the separation performance. A series of GO suspension is investigated from 5 to 50 ppm. A highly dilute concentration of GO was not effective to prepare a selective layer on ceramic support with good integrity, since a lot of defects appeared on the surface of the composite membrane. On the contrary, a selective layer that is too thick will easily peel off after swelling (Lou et al., 2014). To control the process of dispersion of GO and GOF, a fundamental understanding of their suspension behaviour is also necessary. Meanwhile, pH is another important parameter to be considered, and it is closely related to the physiological activity suspension. As the GO and GOF particle was titrated with NaOH or HCl, the resulting change in the pH of the particles leads to the agglomeration of the graphene-based colloidal particles due to the changes of functional groups in these suspensions. Recent analyses indicated that the carboxyl groups (-COOH) play a key role in determining the solution behaviour of GO (W.-N. Wang, Jiang, & Biswas, 2012). Thus, the behaviour of GO and GOF nanosheets were determined at a varying GO concentration in the range of 5 to 50 ppm and varying pH in the range of 2 to 12 at a concentration of 10 ppm.

The GOF was prepared by adding 5 mL of EDA into 10 ppm of GO suspension which was later subjected to sonication for 1h at 60 °C. As observation from naked eyes, the colour turned from light brown into blackish brown, where the GO nanosheets were modified with diamine functionalization to form GOF nanosheets. Both suspensions had their properties of mean particle size and zeta potential evaluated at varying concentration and pH. These parameters influence the stability of GO and GOF suspension to work as selective layer on surface modification later.

4.2.2.1 Zeta potential

The stability of GO and GOF particles in the suspension has been attributed to the electrostatic repulsions between ionized carboxyl groups, which can be interpreted by measuring their zeta potential. Generally, particles with zeta potential in the range of -30 mV to + 30 mV are considered stable due to electrostatic repulsion (Kashyap, Mishra, & Behera, 2014). When GO gels are dispersed in water, the carboxyl and hydroxyl groups on the GO sheet are ionized and these groups makes the GO suspension highly negative charged. Figure 4.9 illustrated the changes of zeta potential for GO and GOF suspension at varying concentration. From the figure, it can be observed that the GO suspension was negatively charged at all concentration in the range of 5 to 50 ppm, except that the GOF suspension had positive charges at a lower concentration (5 and 10 ppm). This is due to the higher amount of NH group in the diamine monomers at these concentrations. All the GO suspension at a varying concentration had a higher negative value of zeta potential than the GOF suspension, and the highest is at 30 ppm of GO which is -29.4 mV.

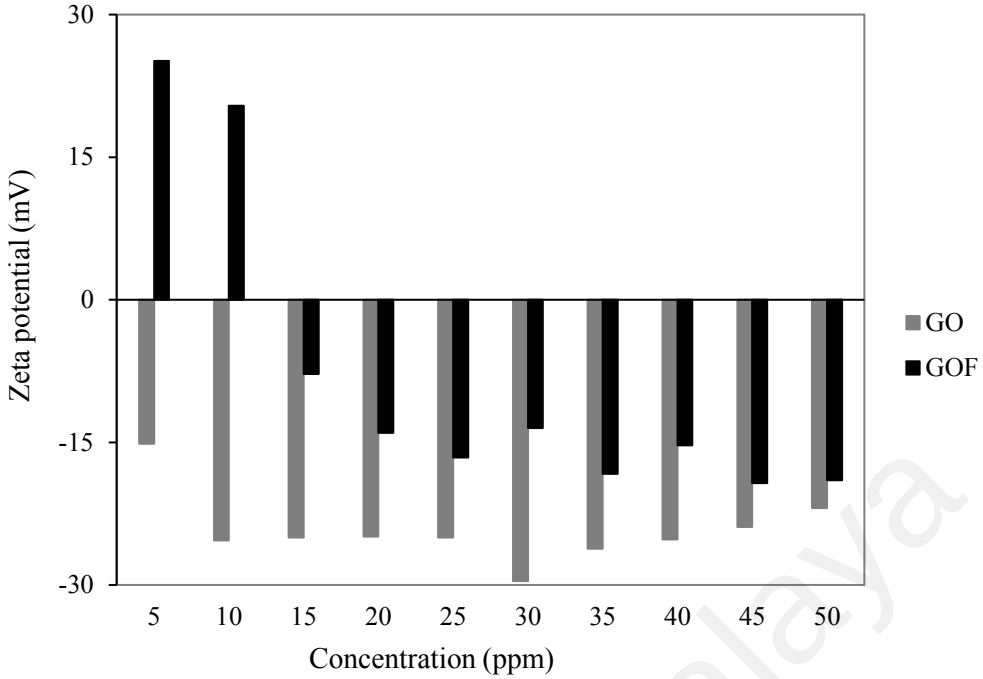

Figure 4.9: Zeta potential of GO and GOF suspension at different concentration of in the range of 5 to 50ppm

Oxygen containing functional groups present on the GO sheets renders GO highly hydrophilic. As a result, the electrostatic repulsion allows GO sheets to be easily dispersed in water at concentrations up to 3000 ppm, as reported by Song et. al (2016). The electrostatic repulsion affects the mobility of ions with different electric charges. Moreover, the selectivity of GO membrane is achieved by the size exclusion from the interlayer space of the GO membrane, electrostatic interaction between different ions and negatively charged GO sheets, and ion adsorption including cation-π interaction and metal coordination to GO sheets (Song et al., 2016). Thus, the zeta potential value of GO and GOF particles were important in order to prepare a good surface character of the modified membranes. Overall, all the GO and GOF suspension at a concentration in the range of 5 to 50 ppm had a stable condition with good dispersion property.

Meanwhile, Figure 4.10 shows the zeta potential for 10ppm of GO and GOF at varying pH. From the figure, GO and GOF suspensions are pH sensitive, and an

effective dispersion of particles occur within the pH range of 2 – 4 and 8 – 12 for GO and GOF suspension, respectively. However, the GO suspension was shown to have positive charge at pH2, which reflects the fact that the edge carboxyl groups are highly protonated at pH 2, resulting in weak electrostatic repulsive forces. These observations reinstate our findings from the zeta potential measurements that GO suspension is more stable in the acidic range, while the GOF suspension is stable in the alkaline range. As a result, it can be observed from Figure 4.10 that the highest zeta potential is obtained at pH 10 (-52.7 mV) for GO suspension. Meanwhile, for GOF suspension, the value of zeta potential for all respective pH was positively charged due to the diamine linker containing the positively charged NH group. This positive charge occurred due to the protonation of NH group into the GO nanosheets, thus decreasing the electrostatic repulsion between them, and eventually resulting in the expected increased thickness of GOF film as compared to GO film used as a selective layer on the ceramic membrane.

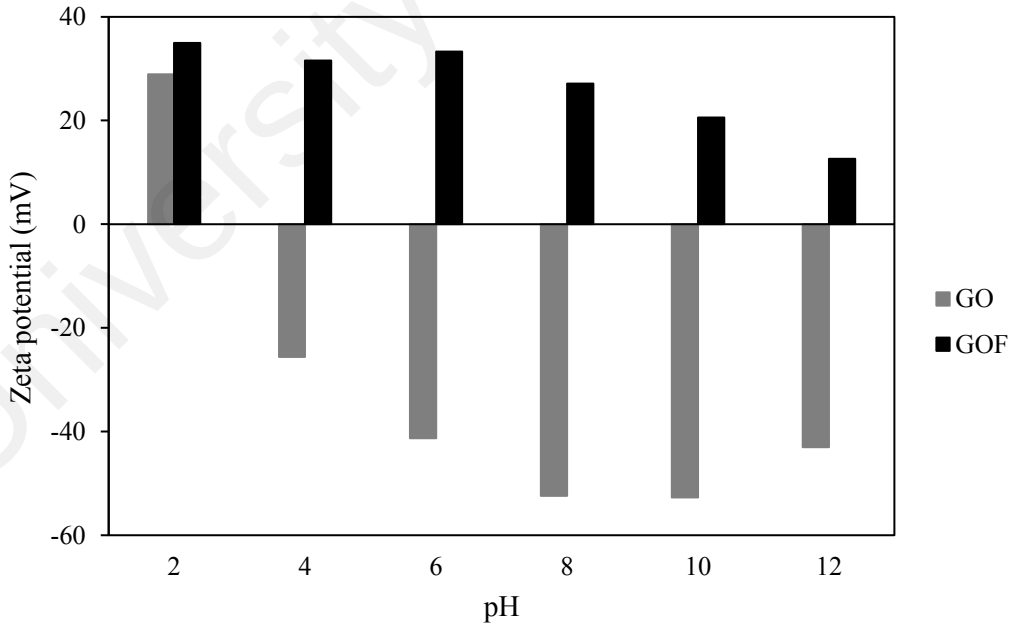

Figure 4.10: Zeta potential for 10 ppm of GO and GOF suspensions at vary pH of in the range of 2 to 12

4.2.2.2 Mean particle size

The particle size distribution of GO and GOF particles in suspension was measured using dynamic light scattering (DLS) method as shown in Figure 4.11 and 4.12 at varying concentration and pH, respectively. From the graph, the mentioned value is the mean value of particle size distribution of GO and GOF suspensions. Generally, the DLS was used to determine particle size of spherical shape but for other shapes such as flakes, GO and GOF may exhibit slightly incorrect size. However, the DLS is used to evaluate the size changes of GO and GOF at both the varying concentration and pH. Overall, both GO and GOF suspension had no specific trend, but we observed that almost all GOF suspension had a higher mean particle size than GO suspension, except at the concentration of 40 and 45 ppm as shown in Figure 4.11. This phenomenon is due to the mean particle size which was difficult to measure because it is very much influenced by the dispersion and stability of particles in the suspension.

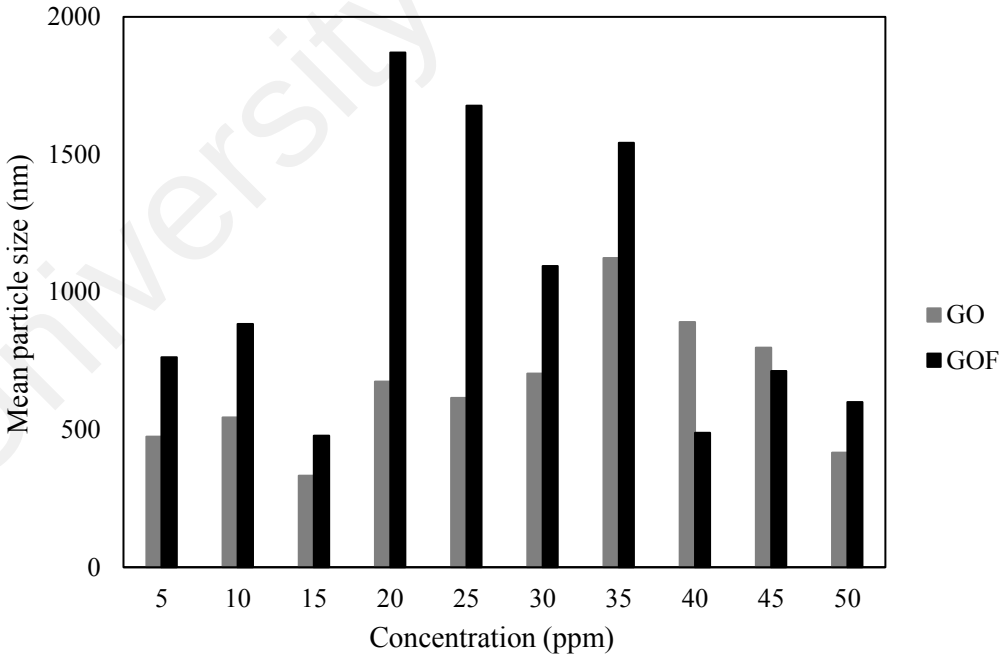

Figure 4.11: Mean particle size of GO and GOF suspensions at different concentration in the range of 5 to 50ppm

Some particles were agglomerates and as they are highly charged, the particle keeps moving due to electrostatic repulsion that occurred. From the Figure 4.11, GO and GOF suspension exhibited a mean particle size in the range of 333 to 1124 nm and 478 to 1870 nm, respectively. GOF suspension had higher mean particle size compared to GO suspension for all concentration except at concentration of 40 and 45ppm. Generally, GOF structure had more length of the interlayer spacing due to the addition of diamine functional groups on GO structure. Thus, higher interlayer spacing of GOF structure generates a high value of mean particle size. As shown in the figure, the mean particle size was inconsistent regardless of the increment concentration of GO and GOF. The phenomenon was due to the agglomeration tendency of particles in the different concentrations of GO and GOF suspension which affect the mean particle size. For example, the agglomeration was occurred at the highest mean particle size of 1870nm and 1124nm for GOF at 20ppm and GO at 35ppm, respectively.

From Figure 4.11, the mean particle size of GO suspension varied in the range of 538 to 1762 nm, and at a pH 12 exhibits higher size, which is over 1700 nm (~1.7 μm). The corresponding hydrodynamic diameters of GO nanosheets measured by DLS is also related to zeta potential. These findings suggest that the electrostatic repulsions between ionized carboxyl groups at the GO nanosheet edges provide the major barrier preventing the GO sheets from aggregating. Thus, the bigger mean particle size of GO suspension could provide an agglomeration of particle due to a higher value of the zeta potential. Meanwhile, for the GOF suspension, the mean particle size varied in the range of 604 to 1834 nm.

However, we observed that for GOF suspension, in the pH range of 6–10, the mean particle size remains almost the same size in alkaline condition as shown in Figure 4.12. The NaOH titration, to change the pH value of particles could introduce a

hydrogenating agent to remove the oxygen functionalities from the suspensions to form an activated graphene sheet. These activated sheets begin to stabilize themselves in the suspension by reducing their effective size. On the contrary, when titrated with HCl, the suspension was increase in H+ ions, which gradually increases the sheet size of particles. At an extreme pH at 2, GOF suspension had a higher mean particle size due to the agglomeration of particles, over 1800 nm (1.8 μm).

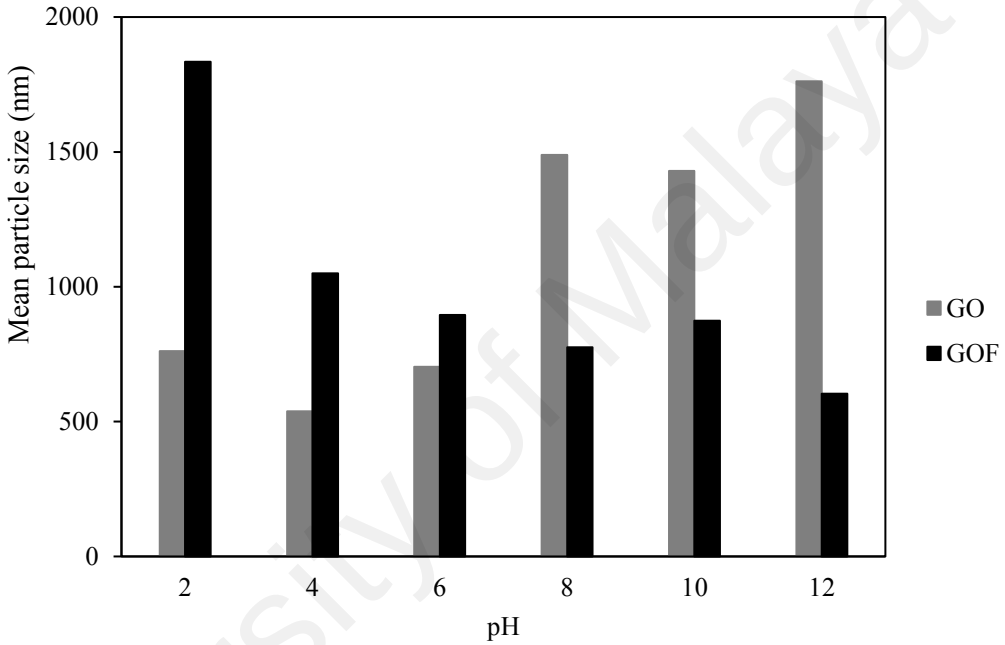

Figure 4.12: Mean particle size of GO and GOF suspensions at different pH of in the range of 2 to 12

Overall, the GO suspension was stable at an acidic condition due lesser mean particle size which is within the range of stable zeta potential value. The stability of GOF suspension was attributed to a strengthened electrostatic stabilization under the alkaline conditions, as the repulsion between the negatively charged sheets should increase at higher pH values. Thus, the repulsion lies within their threshold limits, the GO and GOF were stable, and above a threshold limit, the sheets begin to agglomerate and destabilize themselves.

4.2.3 Overview of GOF structure

GO was synthesized using the simplified Hummer's method in this work, which is a simple and convenient method of synthesis. This work confirms the presence of C-O and C=C bonds by FTIR analysis and the existence of carbon functional groups by XPS. Also, the exfoliation of graphene sheets is confirmed by FESEM image. Thus, the synthesized GO shows many interesting and unique properties that can be applied in the formation of GOF via diamine functionalization process. On the other hand, the zeta potential measurements of GO and GOF revealed that both suspensions had a surface charge of −25.7 ± 0.7 mV at pH 4.0 and +20.6 ± 1.1 mV at pH 10.0, respectively. This indicated that the GO nanosheets are negatively charged at pH 4.0, mainly due to the presence of carboxylic acid groups, while the GOF nanosheets are positively charged at pH 10.0, because of amine functional groups.

In this part, the EDA was used as reactive amine groups on the long alkyl chain reacting with oxygen functional groups on the GO surface, creating new C−N bonds, and leading to broad chemical cross-linking, as shown in Figure 4.13. The GOF, with perfect arrangement, were fabricated by introducing the diamine monomers as the cross-linking agent between the GO sheets. The diamine molecules fix the orientation of the GO layers to stabilize the GO and covalent bond during the drying process (Y. S. Kim et al., 2014). This approach provides a facile method for fabricating a GOF sheets with excellent selectivity properties to be used as precursors in the preparation of selective layer materials on alumina support. Generally, for the native graphene structures, the natural interlayer distance is 0.34 nm (Burress et al., 2010). For GO structure, the natural interlayer distance is around 0.7 nm due to the presence of O and OH groups. Thus, it is important that we expand the interlayer distance without filling the space between GO layers in order to introduce water molecule pathways.

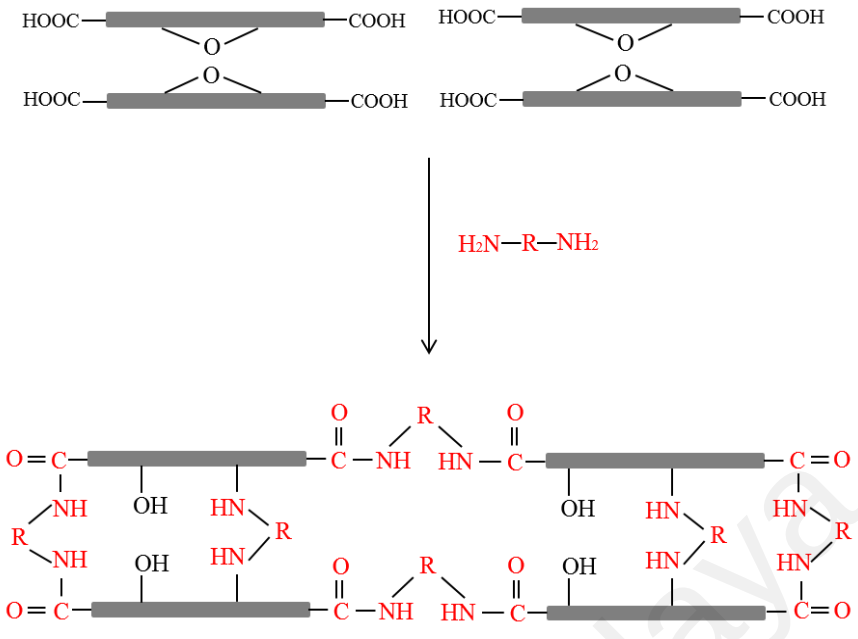

Figure 4.13: Idealized graphene oxide framework (GOF) using diamine monomers linker (Jia, Wang, Shi, & Wang, 2016)

GO and GOF suspension were found to be stable in the concentration range of 5 to 50 ppm, with good dispersibility as evidenced by zeta potential and mean particle size. Meanwhile, at a varying pH in the range 2 to 12, the GO suspension was more stable in the acidic condition while GOF suspension was more stable in the alkaline condition due to their properties on zeta potential and mean particle size, as explained previously. As shown in Figure 4.14, an idealized GOF structure was proposed by adding diamine (NH) groups in the GO structure, which also presented in the study of Jia et al. (2016). The structure was occurred as a condensation reaction between amine and hydroxyl, resulting in carboxyl/amidation mechanism (Jia et al., 2016). These finding was useful in the fabrication of GO and GOF as a selective layer on surface modification process later. From the results, both GO and GOF suspension was highly significant on the changes of concentration but has a low significant on the changes of pH. Thus, in order to further use GO and GOF suspension as a selective layer on ceramic membrane via surface modification, these suspensions could adjust their concentration in order to form the best performance from the modified membranes.

4.3 Properties of flat-sheet alumina (FSA) membranes

4.3.1 Analysis of variance (ANOVA)

Table 4.3 shows the design layout and responses for each experiment obtained through CCD. All experiments were done in triplicates and average values were taken. From the analysed model, blade gap and sintering temperature as known as A and B factor respectively were observed to influence the flexure strength (FS), pure water flux (PWF), shrinkage, and porosity. The optimal operating condition of the membrane fabrication process was determined by those experimental response models. Meanwhile, Tables 4.4 and 4.5 demonstrate the ANOVA and its summary for the respective responses.

Table 4.3: Design layout and properties of prepared FSA membranes

Membrane	A: Blade gap (mm)	B: Sintering temperature (°C)	Flexure strength, FS (MPa)	Pure water flux, PWF ($L/m^2.h$)	Shrinkage, (%)	Porosity, (%)
M1	1	1300	444	1387	4.55	63.71
M2	1	1400	496	1566	8.15	57.43
M3	1	1500	697	1716	13.86	45.18
M4	1.5	1300	227	1382	5.61	60.63
M5	1.5	1400	268	1565	8.89	54.27
M6	1.5	1500	434	1649	14.47	36.68
M7	2	1300	114	790	6.01	60.11
M8	2	1400	124	970	9.3	53.08
M9	2	1500	142	1332	15.96	36.38

Table 4.4: The ANOVA for respective responses

Response	Model terms	Sum of squares (SS)	Degree of freedom (DF)	Mean square (MS)	F-value	P-value
Flexure strength (FS)	Two-factor interaction	316114	3	105371	57.45	0.0003
	A	263509	1	263509	143.68	< 0.0001
	B	39870	1	39870	21.74	0.0055
	AB	12735	1	12735	6.94	0.0462
Pure water flux (PWF)	Quadratic	744100	3	248000	44.13	0.0105
	A	414500	1	414500	73.75	0.0004
	B	215800	1	215800	38.40	0.0016
	A^2	113800	1	113800	20.24	0.0064
Shrinkage	Quadratic	139	3	46	509.15	< 0.0001
	A	4	1	4	40.67	0.0014
	B	132	1	132	1449.77	< 0.0001
	B^2	3	1	3	36.99	0.0017
Porosity	Quadratic	818	3	273	65.36	0.0002
	A	47	1	47	11.22	0.0204
	B	731	1	731	175.24	< 0.0001
	B^2	40	1	40	9.62	0.0268

Table 4.5: Summary of the ANOVA for respective responses

Model	Significant model terms	Standard deviation (SD)	Coefficient of variance (CV)	R^2	Adjusted R^2	Predicted R^2	Adequate precision
1) Flexure strength (FS) Two-factor interaction	A, B, AB	42.83	13.08	0.972	0.955	0.873	20.39
2) Pure water flux (PWF) Quadratic	A, B, A^2	74.97	5.46	0.964	0.942	0.866	18.11
3) Shrinkage Quadratic	A, B, B^2	0.3	3.13	0.997	0.995	0.989	54.44
4) Porosity Quadratic	A, B, B^2	2.04	3.93	0.975	0.96	0.919	20.32

4.3.1.1 Flexure strength (FS)

For FS, the *F*-value of 57.45 implies that the model was significant. There is only a 0.03% chance that the model with this large *F*-value was possibly created by noise. From the analysed model, blade gap (A) and sintering temperature (B) were found to influence the FS when the *P* value is less than 0.05. However, the blade gap (A) had the highest effect on the FS response due to its highest *F* value of 143.68. The equation to evaluate FS response in terms of coded factor presented in Eq. (4.1) is also known as the two-factor interaction model. Meanwhile, the R^2 for the suggested model is 0.972 which confirms the accuracy of the model as shown in Table 4.5.

$$FS = 327.33 - 209.50A + 81.33B - 56.25AB \quad \text{Eq. (4.1)}$$

The impact of both factors on the FS response is significant, as illustrated by the three-dimensional (3D) response surface plot in Figure 4.14. At a certain blade gap, when the sintering temperature was elevated from 1300 to 1500 °C, the MS response value increased. Maximum FS value of 697 MPa was attained when the blade gap was the lowest (1.0 mm) and the sintering temperature was the highest (1500 °C). This is probably attributed to the growth of grains and shrinkage of pores. Therefore, the FS response of alumina membrane can be intensified by increasing the sintering temperature (Qin et al., 2014). Meanwhile, at a constant sintering temperature, the FS response decreased with the increasing blade gap. The lowest FS value of 114 MPa was obtained from the highest blade gap (2.0 mm) and lowest sintering temperature (1300 °C). The possible reason behind the low FS value is attributed to the high porosity of the prepared membrane. As a result, the high membrane thickness could affect the membrane performance with low FS value. This impact is in line with the ANOVA result that evidenced the blade gap gave the utmost influence on FS response.

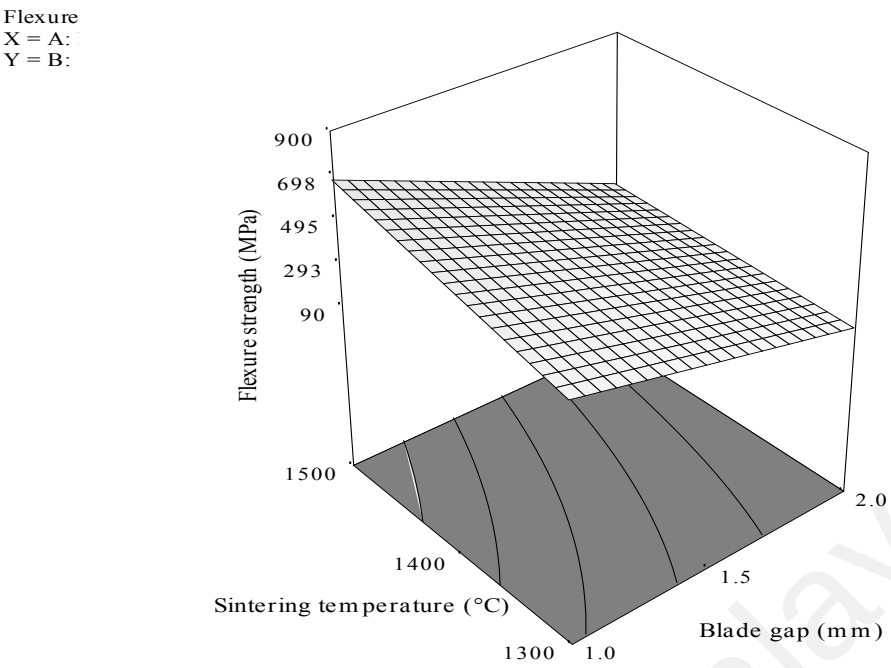

Figure 4.14: 3D graph for flexure strength of prepared FSA membranes

4.3.1.2 Pure water flux (PWF)

The *F*-value of 14.8 indicates the significance of the model and there is only a small percentage of 0.05% noise occurrence in this model. The lowest *P* value of 0.0004 for blade gap has the highest prominence on PWF. From ANOVA, it is evident that B^2 and AB terms are not as significant as the *P* values are higher than 0.05. Thus, the insignificant terms were removed in ANOVA, which could lead to the improvement of the regression model. The suggested mathematical equation for PWF response is the quadratic model as described in Eq. (4.2). This model fits well with the experimental results, as the value of R^2 (0.964), adjusted R^2 (0.942), and predicted R^2 (0.866) prove the reliability of the regression model for PWF response as shown in Table 4.5.

$$\text{PWF} = 1532 - 262.83A + 189.67B - 238.5A^2 \quad \text{Eq. (4.2)}$$

The 3D response surface for PWF is presented in Figure 4.15. It was observed that the highest PWF value of 1716 L/m^2·h was obtained by the membrane produced at the highest sintering temperature of 1500 °C and lowest blade gap of 1.0 mm. Overall, the

PWF response increased with the increasing sintering temperature and decreasing blade gap. This might be due to the high blade gap that produces thick prepared membranes. The thick prepared membrane could slow the permeation process through high mass diffusion. As a result, the blade gap had a higher significant influence on PWF compared to sintering temperature based on ANOVA.

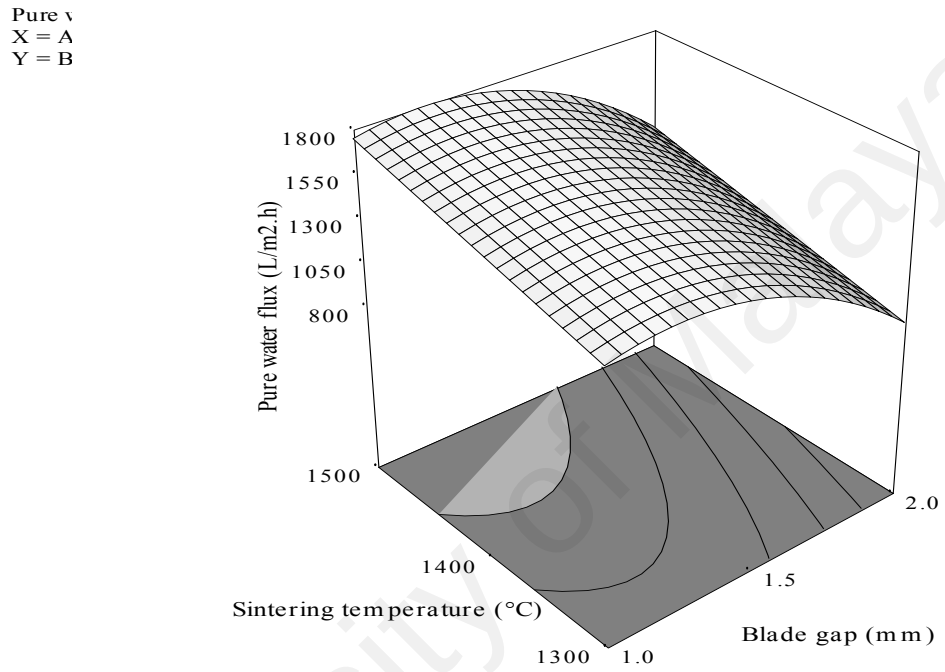

Figure 4.15: 3D graph for PWF of prepared FSA membranes

4.3.1.3 Shrinkage

The recommended model has a *P* value of less than 0.0001, which is very significant. It is obvious that the sintering temperature had the greatest impact on shrinkage response as its *P* value is smaller compared to the *P* value of blade gap. However, there is no major effect on the AB and A^2 on shrinkage response. Therefore, the coded model of shrinkage response was generated after removing the insignificant terms as presented in Eq. (4.3). This quadratic model also has a high R^2 value (0.997) and low coefficient of variation (CV) of 3.13, which explains the reliability of the regression model for membrane shrinkage as shown in Table 4.

$$\text{Shrinkage} = 8.78 + 0.79A + 4.69B + 1.30B^2 \quad \text{Eq. (4.3)}$$

The interaction between both factors on shrinkage response is shown in 3D response surface in Figure 4.16. The shrinkage greatly depends on the sintering temperature. At the sintering temperature of 1500 °C and 1.0–2.0 mm of blade gap, the shrinkage value considerably increased from 13% to 16%. Also, at the same sintering temperature of 1500 °C and the highest blade gap of 2.0 mm, more neighbouring particles of the membrane moved closer towards each other and eventually favoured quick sintering process compared to other membranes fabricated at low blade gap. Therefore, at a constant sintering temperature, the grain growth increased as the blade gap was increased. As a result, the porosity of membrane decreased sharply. Generally, a great in mechanical strength is noted at low porosity (Barma & Mandal, 2014). Thus, the highest blade gap of 2.0 mm and sintering temperature of 1500 °C resulted in the highest shrinkage (63.71%) and lowest porosity (4.55%). As a conclusion, the sintering temperature factor had the most significant effect on shrinkage response.

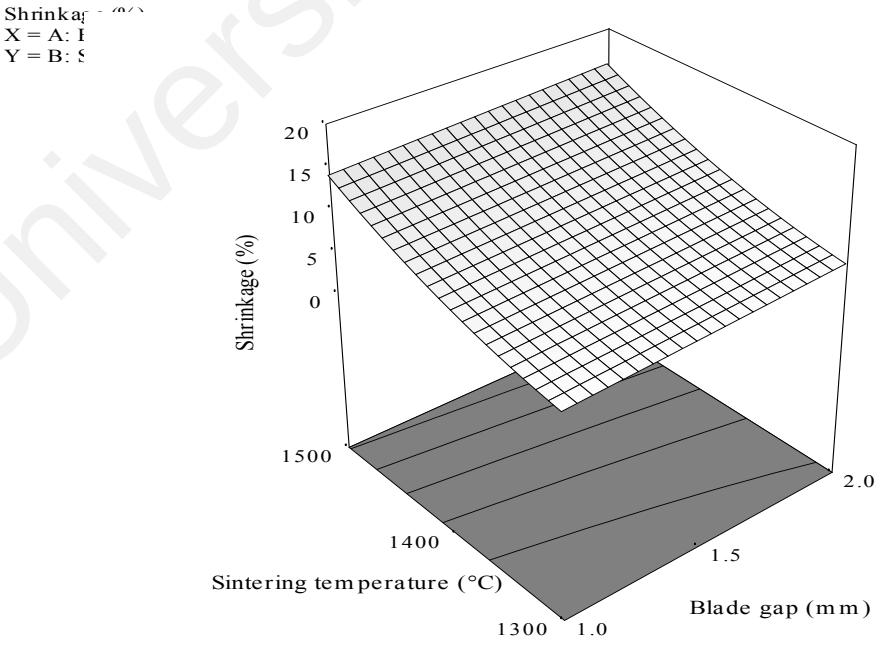

Figure 4.16: 3D graph for shrinkage of prepared FSA membranes

4.3.1.4 Porosity

The *F*-value of 65.4 with only 0.02% of noise reveals the high significance of the model. From the analysis, the *P*-value was lesser than 0.05 conforms all terms except for the A^2 and AB. These insignificant terms were removed from ANOVA to generate a quadratic model for P response as presented in Eq. (4.4). Meanwhile, the main significant effect was the sintering temperature due to its lowest *P*-value of <0.0001. This recommended model was in agreement with the high R^2 value of 0.975 and the low standard deviation of 2.04 as given in Table 4.5.

$$\text{Porosity} = 54.93 - 2.79A - 11.04B - 4.48B^2 \qquad \text{Eq. (4.4)}$$

Figure 4.17 shows the 3D response surface for porosity response. Generally, with the increasing sintering temperature, the shrinkage increased while porosity decreased. The rapid decrement of porosity was mainly due to the significant effect on shrinkage and grain growth, which caused the gaps between the alumina particles to become narrower (Qin et al., 2014). As a result, the porosity response had the highest impact on sintering temperature compared to the blade gap factor. Meanwhile, the porosity is significantly affect the mechanical strength of the prepared membranes (Meille, Lombardi, Chevalier, & Montanaro, 2012). At the high porosity of prepared membrane could be a result of low mechanical strength. The range of the desired porosity of porous membranes is 40–70 % (Barma & Mandal, 2014). In this study, all the prepared membranes have the porosity values in the range of 36% to 64%. As discussed before, a compact porous membrane can be obtained at higher blade gap due to high shrinkage. At the highest blade gap of 2.0 mm and sintering temperature of 1500 °C, the shrinkage was the highest. Thus, the porosity value of the prepared membrane was the lowest.

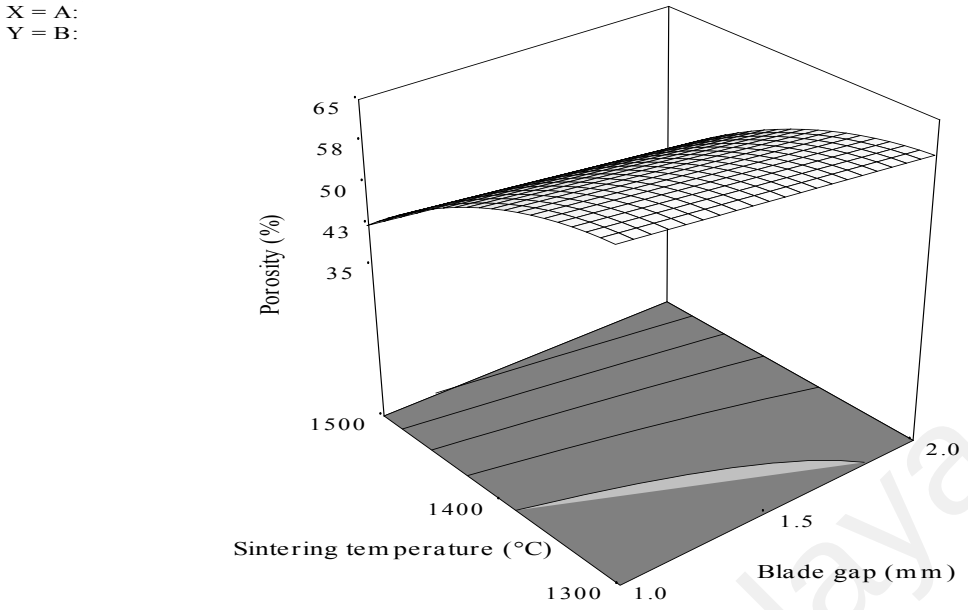

Figure 4.17: 3D graph for porosity of prepared FSA membranes

4.3.2 Morphology structure of FSA membranes

Morphology study was evaluated for all prepared FSA membranes (M1 - M9). Generally, the morphological structure was divided into three parts: membrane cross section, membrane surface and pore growth (Sun, Chen, Chen, & Li, 2007). Figure 4.18 shows the cross-sectional structure of the prepared membranes (M1 - M9) using SEM at 10 and 15 kV of accelerating voltage and at different magnification of 200 – 300x. The final thickness of the prepared FSA membranes was also obtained through SEM measurement. The thickness of the membrane decreased when the sintering temperature increased. The thinnest prepared membrane of 0.468 mm was labelled as M3, which uses lowest blade gap of 1.0 mm and highest sintering temperature of 1500 °C. This could be due to the fast removal of macrovoid structure at high sintering temperature and low blade gap during the sintering process. The removal of macrovoid could also improve the flexure strength of the prepared membrane.

All prepared FSA membranes have an asymmetric structure with slightly different internal structures. It can be observed that the top layer displays a finger like structure, whereas the bottom structure has sponge like structure. These arrangements occurred due to delayed demixing for the development of sponge like structure, and fast coagulation for the formation of finger like structure (Khayet, Cojocaru, & García-Payo, 2010). The thickness of the sponge like structure increased with increasing blade gap at certain sintering temperatures. The increment of sponge like structure could slow the water permeation. It also can be observed that the membrane at lowest sintering temperature had large macrovoid (yellow circled) as illustrated for MI and M4. Meanwhile, at the high sintering temperature for the high blade gap also contained large macrovoid as referred to M6 and M9. The phenomena might be happened due to movement difficulty of alumina particles to arrange as high thickness.

Generally, these large macrovoids could defect the flexure strength of the membrane (Khayet et al., 2010). On the other hand, at certain sizes and structure of macrovoids can be functional in separation process especially at the top layer of membranes. Therefore, the morphological structures of prepared FSA membranes need to carefully investigate on their surface structures to find the desired membrane. Since only the top layer has the separating ability, the membrane must have an excellent surface morphology to retain sufficient permeability. The surface structure was also evaluated using SEM for the prepared FSA membranes (M1 – M9) at different blade gaps and sintering temperatures are shown in Figure 4.19. It can be observed that alumina particles underwent neck growth with increases sintering temperature. The images of M3 and M9 clearly show the neck growth as high sintering temperature.

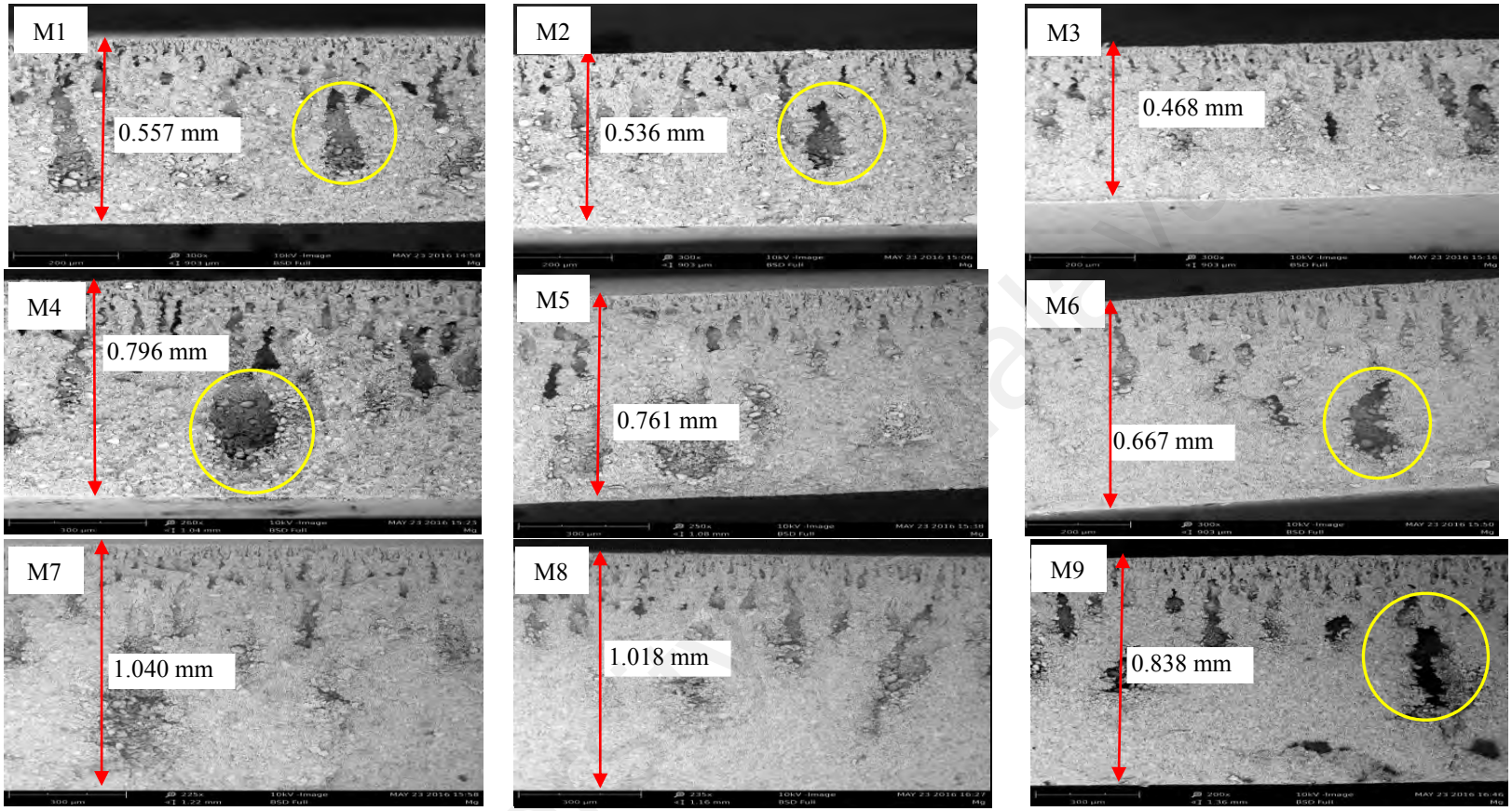

Figure 4.18: Cross-section structure of prepared FSA membranes using SEM

Meanwhile, the grain boundary decreases as increasing sintering temperature was observed. This might be due to the rearrangement of alumina particles (Barma & Mandal, 2014). When sintering temperature increases, agglomeration of fine particles will occur rapidly, leading to blocking the membranes' large pores. As a result, a significant grain growth occurs in the structure (Eskandari, Aminzare, Razavi hesabi, Aboutalebi, & Sadrnezhaad, 2012). However, the grain growth during the sintering process had significant effect on flexure strength of membranes. Along with increasing sintering temperature, the grain growth produced enhances the flexure strength (Zhu et al., 2015). There is also an influence of microstructure uniformity of flexure properties.

From the figure 4.19, grain boundary pores can be observed for all prepared FSA membranes. These boundary pores were known as macrovoid structure that could be seen in cross section structures. The boundary pores depend on sintering temperature during arrangement of alumina particles (J. Wang et al., 2015). At blade gap of 2.0 mm, there is a large pore existing along the grain boundaries, which is very difficult to be removed. It can be noticed that even when the sintering temperature is increased to 1500 °C, large pores still remain, as seen in M9. Thus, these large pores could affect the prepared FSA membrane when flexure strength decreases. On top of that, the surface structures do not merely justify the desirability of membrane permeation. The water permeation also depends on the pore size distribution of the prepared membranes. The pore size distribution is related to selectivity and performance of membrane during water treatment.

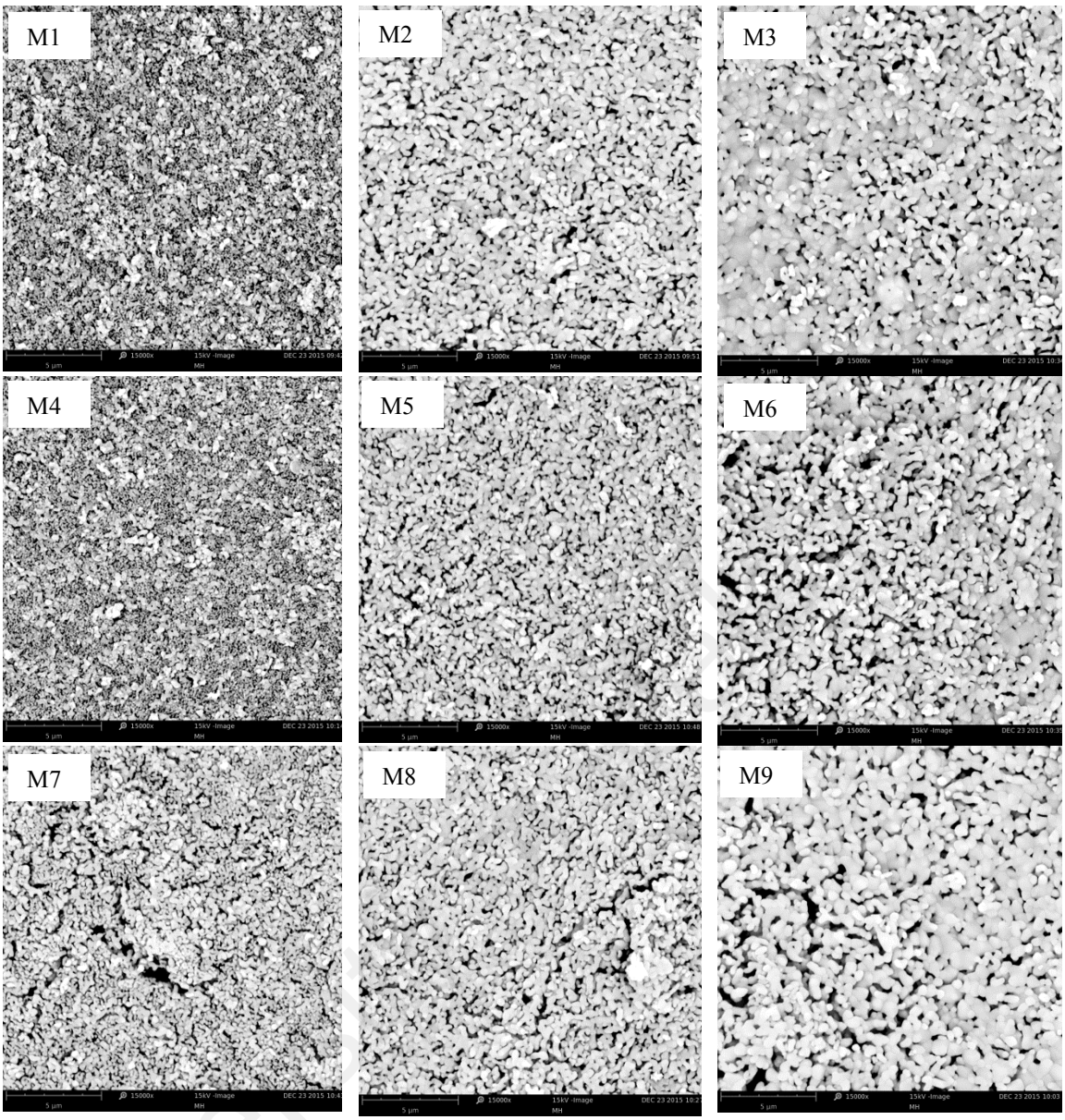

Figure 4.19: Surface structure of prepared FSA membranes using SEM

In addition, pore size distribution analysis of the prepared FSA membranes (M1-M9) was shown in Figure 4.20. As the sintering temperature increased, the average pore diameter decreased and the pore size distribution narrows down as well. This happened due to the pore shrinkage induced by high sintering temperature (Qin et al., 2014). Grain size decreases with increasing blade gaps at a certain sintering temperature, especially at 1500 °C. Whereas, at the lowest sintering temperature (1300 °C), the grain growth is accompanied by a broadening of pore size distribution. Furthermore, as shown

in M1 and M4, the pore size gives a bimodal distribution for a low sintering temperature of 1300 °C with the pore size within the range of 0.2 to 0.15μm. This phenomenon is due to the particle size distribution of alumina powders that was relatively inhomogeneous with three different sizes. The membrane pore structure is indeed mostly depended on the particle size distribution of alumina powders (Zhu et al., 2015).

The lowest pore size of 0.097 μm was obtained in the highest sintering temperature of 1500 °C and highest blade gap of 2.0 mm, in the M9 sample. However, the maximum number of pores and the narrowest pore size distribution was obtained at blade gap of 1.0 mm and sintering temperature of 1500 °C for the M3 sample. This prepared FSA membrane has the best pore size distribution with the narrowest distribution at the peak diameter size of 0.14 μm. As a conclusion of the morphology study, the lowest blade gap of 1.0 mm and highest sintering temperature of 1500 °C produced the desired morphology structure. As a result, this excellent morphology structure could perform better for water permeability with high selectivity.

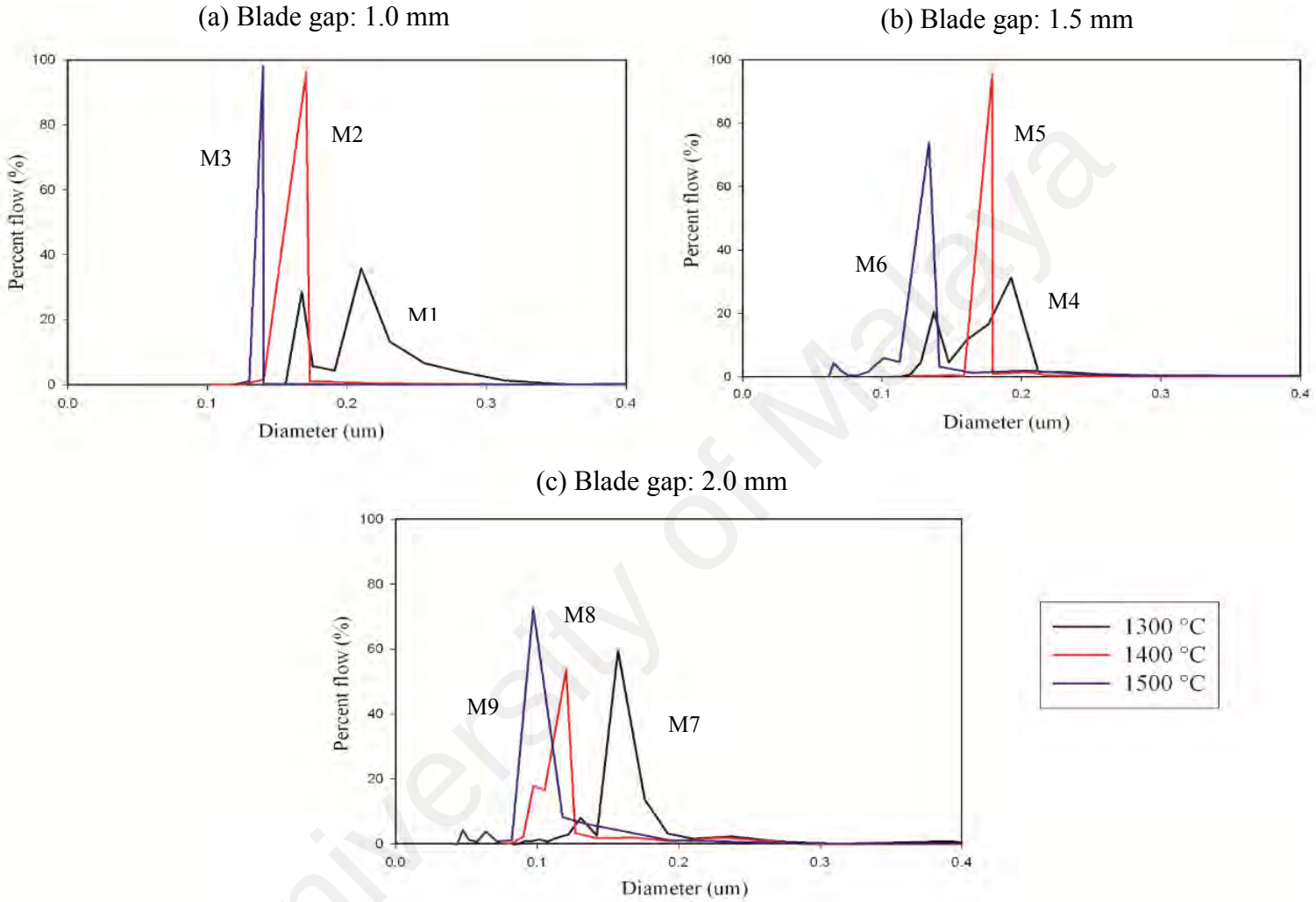

Figure 4.20: Pore size distribution of prepared membranes at (a)1.0mm, (b)1.5mm and (c)2.0mm of blade gap

4.3.3 Optimization of the prepared FSA membranes

The optimization step dealt with the analysis and improvement of responses using a CCD approach. Table 4.6 describes the constraints and limits considered for the optimisation goal. The ultimate goals for this flat sheet alumina membrane fabrication were high flexure strength, high pure water flux, and acceptable range of shrinkage and porosity. This optimisation method was calculated using a desirability function (D) for multiple responses as described in Eq. (4.5) (Ahmad et al., 2009). N, r_i, and d_i are the number of responses, significance of particular response, and partial desirability function for specific responses, respectively. The desirability value is used to satisfy all responses within the required limit to obtain a desired flat sheet alumina membrane.

$$D = \left[\prod_{i=1}^{N} d_i^{ri}\right]^{1/\sum ri} \quad \text{Eq. (4.5)}$$

Table 4.6: Set of goal for optimum condition

Name	Goal	Lower limit	Upper limit
Blade gap (mm)	is in range	1	2
Sintering temperature (°C)	is in range	1300	1500
Flexure strength (MPa)	maximize	114	697
Pure water flux (L/m^2.hr)	maximize	790	1716
Shrinkage (%)	is in range	4.55	15.96
Porosity (%)	is in range	36.38	63.71

Table 4.7 shows the optimum process parameter with the highest desirability value. This optimum membrane fabrication condition with 0.980 of desirability value was expected to be able to produce a desired flat sheet alumina membrane with high flexure strength and pure water flux. Only one solution was suggested to obtain the optimum value for responses at the highest value of desirability. The optimum fabrication parameters were recommended at the lowest blade gap of 1.0 mm and highest sintering

temperature of 1500 °C. The CCD optimisation result of the M3 sample is in agreement with the morphological structure analysis that found excellent cross section and surface morphology with the narrowest pore size distribution at the highest peak diameter of 0.14 μm.

Table 4.7: Optimized value for responses and highest value of desirability

Process parameter	**Response**					**Desirability**
A (mm)	B (°C)	FS (MPa)	PWF ($L/m^2.hr$)	Shrinkage (%)	Porosity (%)	
1.0	1500	674	1746	14	42	0.980

4.3.4 Performance of FSA membranes

4.3.4.1 Flux stability

Flux stability is perhaps the most critical factor in determining process and economic viability of separation applications with alumina membranes. In MF and UF applications, flux decay can be a serious problem that reduces the membrane performance. The selected membrane which is M3 was further experimented for validity performance of water permeation stability for 5 hours at 0.5 bar with 10 cycles (0.5hr/cycle). To be a good membrane for water treatment, it should not only have sufficient high pure water flux, but also good stability for long term operation under certain applied pressure. The PWF plotted against operating time were shown in Figure 4.21. It can be observed that the PWF of the membrane M3 are steady, varying from 1529 ± 24 to 1722 ± 16 $L/m^2.h$ at 0.5 barg. This implies that the M3 shows high stability, at least under this operating condition.

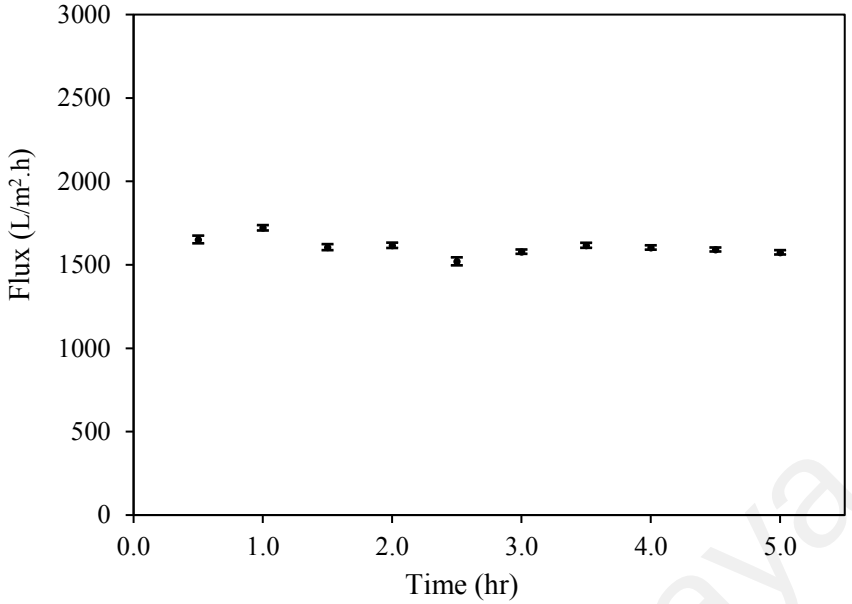

Figure 4.21: Flux stability of M3 for 5 hours duration with 10 cycles of pure water permeation at 0.5 barg

Meanwhile, Figure 4.22 shows the PWF at varying applied pressure up to 2.5 bar, which are suitable range for microfiltration (MF) of pressure driven application system. The PWF of M3 increased when the pressure applied increased from 0.5 to 2.5 barg. At the lowest applied pressure of 0.5 barg, the pure water flux is 1613 ± 13 L/m^2.h. Whereas, at the highest applied pressure of 2.5 barg, the flux value is 4361 ± 27 L/m^2.h. The flux increases linearly with the increase in applied pressure, consistent with the results obtained by Suresh et al. (Suresh, Srinu, Ghoshal, & Pugazhenthi, 2016). This is an important step to show that the selected membrane was stable in producing flux and is suitable in water treatment applications.

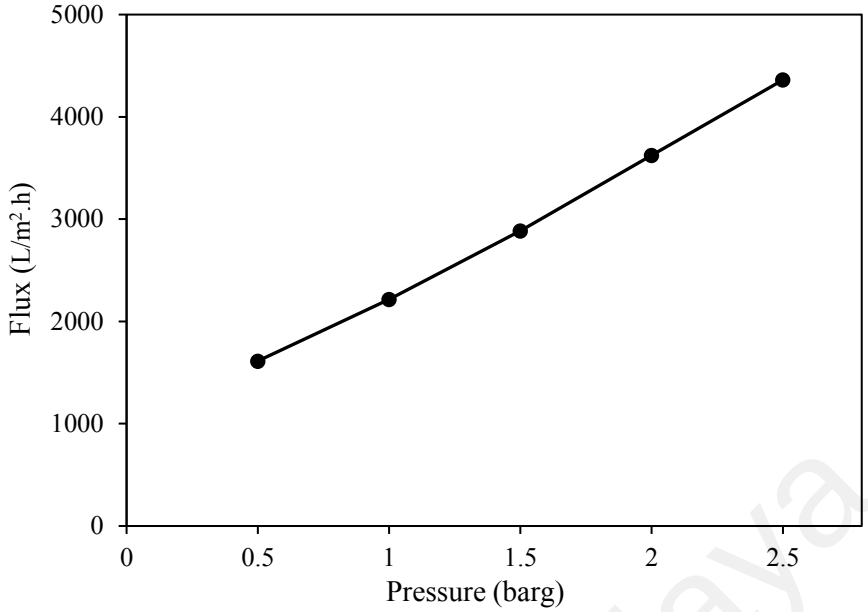

Figure 4.22: The PWF of M3 at varies applied pressure of 0.5 to 2.5 barg

4.3.4.2 Chemical stability

Alumina membranes are widely used in water treatments which not only demand high flux stability but also chemical stability. Generally, the extreme conditions on acidic and basic environment were very prone to cause membrane corrosion. Therefore, the selected membrane, M3 must have a good stability to chemical corrosion. In order to determine its chemical stability, the M3 was soaked at room temperature using acid medium (HNO_3 at pH = 1) and basic medium (NaOH at pH =14) for 10 days. FESEM-EDX analysis of the M3 before and after chemical stability test on highly acid and basic conditions was shown in Figure 4.23. It can be inferred from the figure that the aluminium (Al) composition of the M3 is almost the same in both acidic and basic media. The weight loss of Al compositions on acidic and basic media are 1.33 and 3.5 wt.% respectively. From the figure also shown that sodium (Na) element is presence (1.88 wt.%) after treated with basic media which is NaOH due to crystallization of NaOH on the M3 surface after 10 days immersion. The less weight percent of Na

crystalline on the M3 surface could slightly affect the water treatment application due to foulant increment.

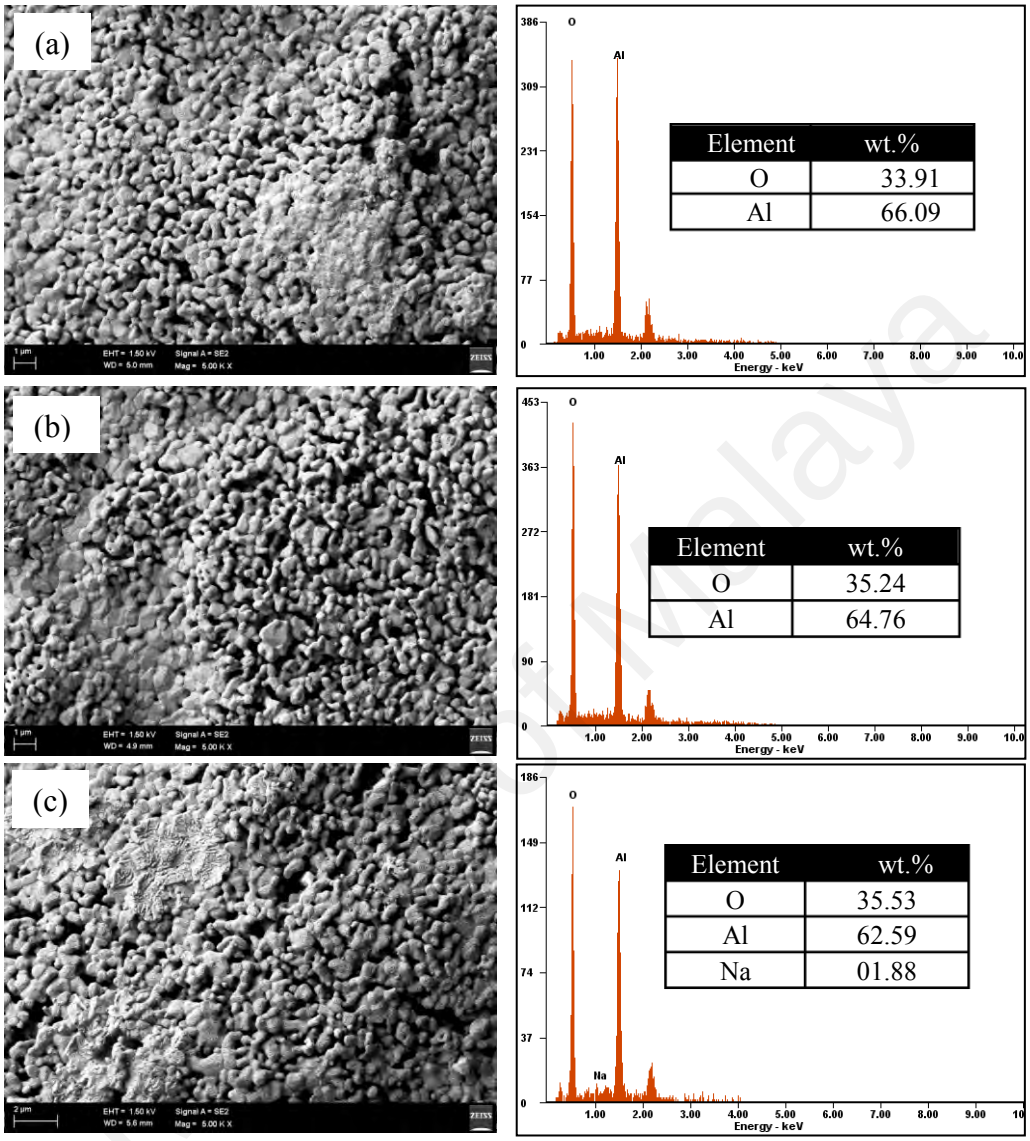

Figure 4.23: FESEM-EDX results for M3 (a) before and after treated with (b) acidic and (c) basic media

However, during ten days at atmospheric conditions the elemental loss done not exceed 4 wt.% which can be assumed not causing more damage in membrane surface. Thus, results reported that the M3 present a good chemical resistance in acidic medium than in basic one. These results are comparable with membrane prepared by Das et al. especially in basic medium (Bipul Das, Chakrabarty, & Barkakati, 2016). For overall, the FSA membrane structure and permeability can be significantly controlled by

manipulating the blade gap of casting and sintering temperature. The obtained optimum condition for desired FSA membrane requires the lowest blade gap (1.0 mm) and highest sintering temperature (1500 °C) which referred to M3. The M3 also exhibited high flux stability during the entire investigation period of 5 hours for 10 permeation cycles without decay and also had linear increment of flux values with the increasing applied pressure up to 2.5 barg. The validity of M3 proved to have high chemical stability with low elemental loss in highly acidic and basic media.

4.4 Properties of hollow fibre alumina (HFA) membrane

HFA membrane was prepared using a 57 wt.% of alumina loading via phase-inversion and sintering method, as applied for FSA membrane previously. Figure 4.24 illustrated the morphological structure of HFA membrane. As shown in Figure 4.24(a), the HFA membrane has the outer and inner diameter of ~1.3 and ~0.9 mm, respectively, and a wall thickness of ~0.2 mm. The membrane also has an asymmetric structure as shown in Figure 4.24(b), including a sponge-like structure at the center of the HFA membrane wall, which is nearly sandwiched by the finger-like structure from both the lumen and the shell side. Meanwhile, the surface of the HFA membrane exhibited pores on the surface due to the arrangement of alumina particles during sintering process, as shown in Figure 4.24(c).

In addition, Figure 4.25(a) and 4.25(b) showed the pore size distribution and surface roughness of HFA membrane via MIP and AFM analysis, respectively. The membrane had one peak diameter of 182 nm as shown in Figure 4.25(a), which is in the range of MF process. This peak diameter referred to the pore size of the prepared HFA membrane. Meanwhile, Figure 4.25(b) showed the surface texture of the HFA membrane with the average surface roughness (Ra) of 59.69 nm. The texture was depicted by the presence of dark regions (valley) and bright regions (peak) formed in

nonuniformly spaced manner. The displayed surface roughness was slightly lower than the Ra of the HFA membrane (62.85 nm), as reported by Abdullah et al. (2018) (Abdullah, Rahman, Dzarfan Othman, Jaafar, & Aziz, 2018). This characteristic may facilitate the selective layer with GO and GOF films onto the surface of the HFA membrane. Thus, these characterizations of HFA membrane were expected to have reduced the pore size and surface roughness after going through surface modification by incorporating new selective layer on this HFA membrane as a support membrane.

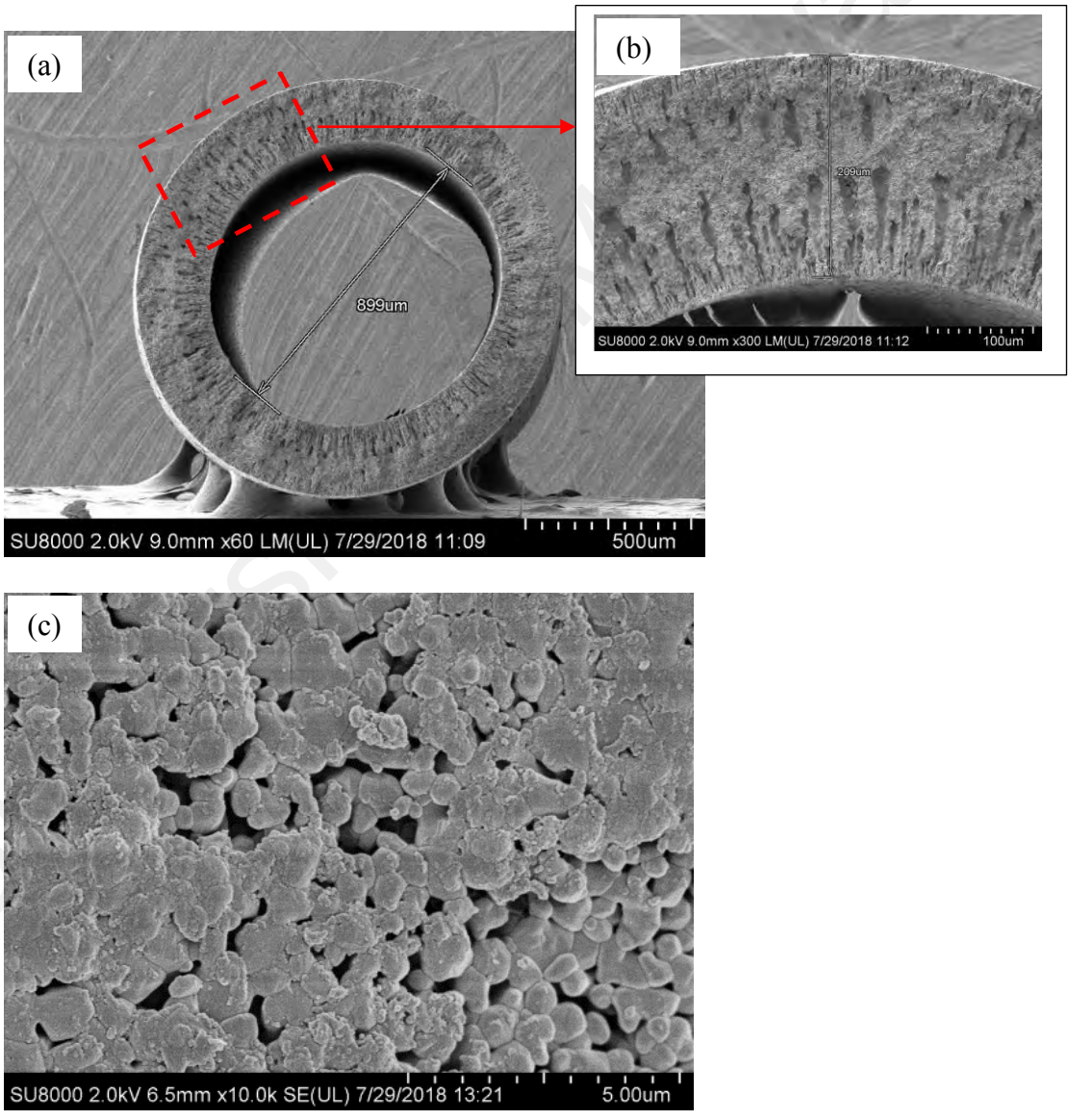

Figure 4.24: Morphology structure of HFA membrane for (a) cross-section at 60 and (b) 300 of magnification and (c) surface structure.

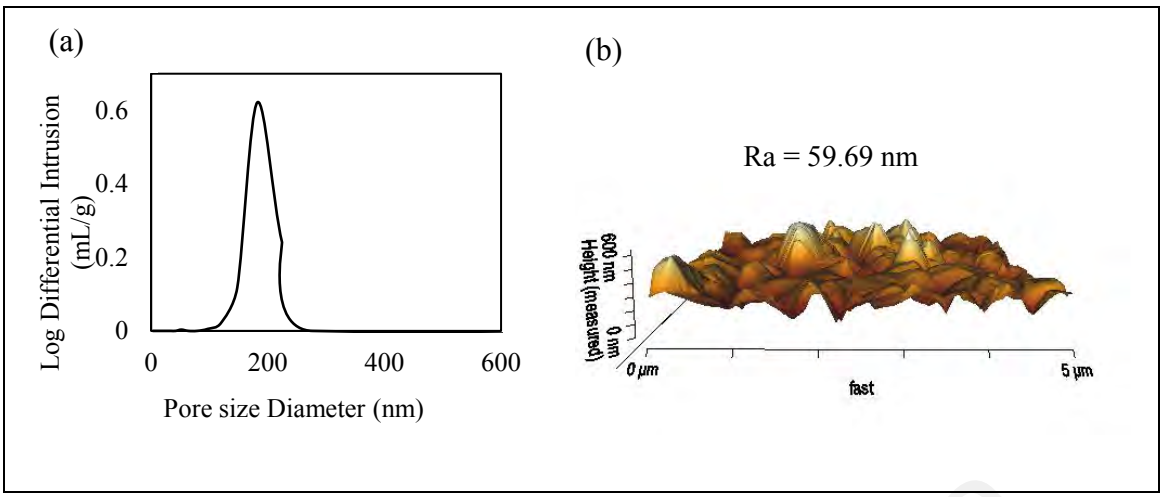

Figure 4.25: Properties of HFA membrane for (a) pore size distribution of MIP and (b) surface roughness of AFM

Overall, the fabrication of HFA membrane was successfully achieved by spinning and sintering method with fix parameter value as mentioned earlier. The properties of the prepared HFA membrane were slightly similar to that of the FSA membrane in terms of pore size distribution within the range of MF. Thus, in order to enhance their performance towards protein recovery, the prepared membranes for this study were incorporated with GOF in order to reduce the pore size and enhance the surface structure of the modified membrane. This surface modification was reported at the next subchapter discussing the formation of GOF/FSA and GOF/HFA composite membranes.

4.5 GOF(EDA)/FSA composite membrane

Generally, the GO concentration was A highly dilute GO concentration is not effective to prepare a GO film on ceramic support with good integrity, since a lot of defects appeared on the composite surface. In contrast, a GO film that is too thick will peel off easily after the drying process. Therefore, three GO concentrations (5, 10 and 15 ppm) were varied in order to prepare the GOF film as a selective layer on the GOF(EDA)/FSA composite membrane.

4.5.1 Morphology structure

Three GOF(EDA)/FSA composite membranes were prepared at different GO concentration of 5, 10 and 15 ppm to form 5GOF(EDA)/FSA, 10GOF(EDA)/FSA and 15GOF(EDA)/FSA composite membranes. The deposition efficiency can be noticed by the colour changes on the surface of composite membranes using naked eyes. The colour of composite membrane indeed gets darker with the deposition of higher GO concentration. Figure 4.26 presents the photographic image of composite membranes at different GO concentration on GOF(EDA) suspension. The photograph of these composite membranes was illustrated the deposition of GOF(EDA) film at different GO concentration, immediately after finish the modification process. In order to achieve the better selective layer, the film should fully cover the support surface. From the figure, all the GOF(EDA)/FSA composite membranes were obtained fully cover selective layer which are 5GOF(EDA), 10GOF(EDA) and 15GOF(EDA) films. However, for further observed their morphology structure, the FESEM-EDX was used to perform the present of the selective layer on FSA membrane.

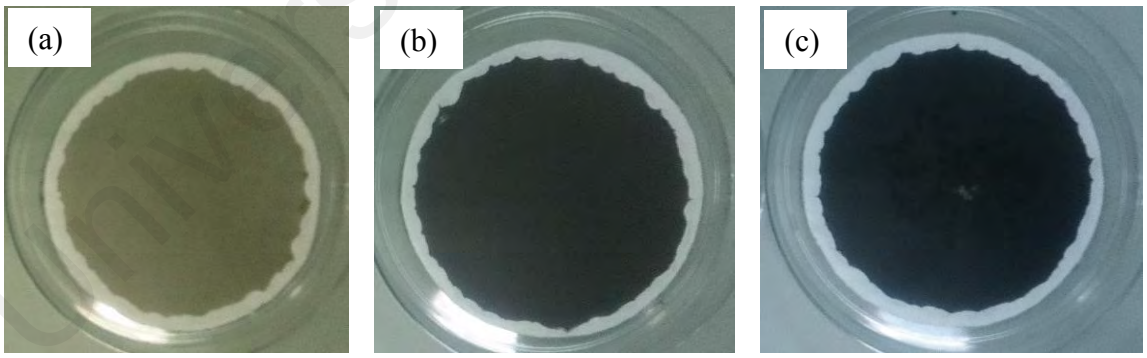

Figure 4.26: Photographic images of GOF(EDA)/FSA composite membranes at different concentration; (a)5ppm, (b)10ppm, and (c)15ppm

The surface structure presented by Figure 4.27 revealed that the GOF(EDA) films fully covered the surface of FSA membrane due to the monolithic structure (Y.-F. Chen et al., 2014). This monolithic structure was constructed from the intercalated GOF(EDA) sheets stacked together. However, the monolithic structures of all these

composite membranes have slightly different grains distribution due to different GO concentration. Among the composite membranes, the 5GOF(EDA)/FSA had a more uniform and smaller fracture surface. Meanwhile, the 15GOF(EDA)/FSA composite membrane had an uneven grain fracture due to high GO concentration that could result in the agglomeration of GOF(EDA) particles. From the EDX results, four elements exist on these GOF(EDA) composite membranes; which are carbon (C), nitrogen (N), oxygen (O) and alumina (Al). The Al element decreased as the GO increased in concentration, this is due to the fact that the 15GOF(EDA) film covered the FSA membrane with a certain thickness. Meanwhile, the C element is referred to the GO concentration which is the highest at 15GOF(EDA) film of 37.86 wt%.

On the other hand, the N element was obtained from EDA monomer and cross-links with GO structure to form a GOF(EDA) film. Among the GOF(EDA)/FSA composite membrane, the 10GOF(EDA) film contained the highest amount of N element (11.26 wt%) to create the cross-linking between GO structure and also form the adhesion between selective layer and support membrane. Meanwhile, the O element was attained from both the GO structure and FSA surface. Thus, the 5GOF(EDA)/FSA composite membrane had the highest O element amount (36.94 wt%) even its GO concentration is at the lowest (5ppm). Overall, these composite membranes discussed above were comparable with the FSA support membrane which only consists Al and O elements as mentioned previously at section 4.3.4.2.

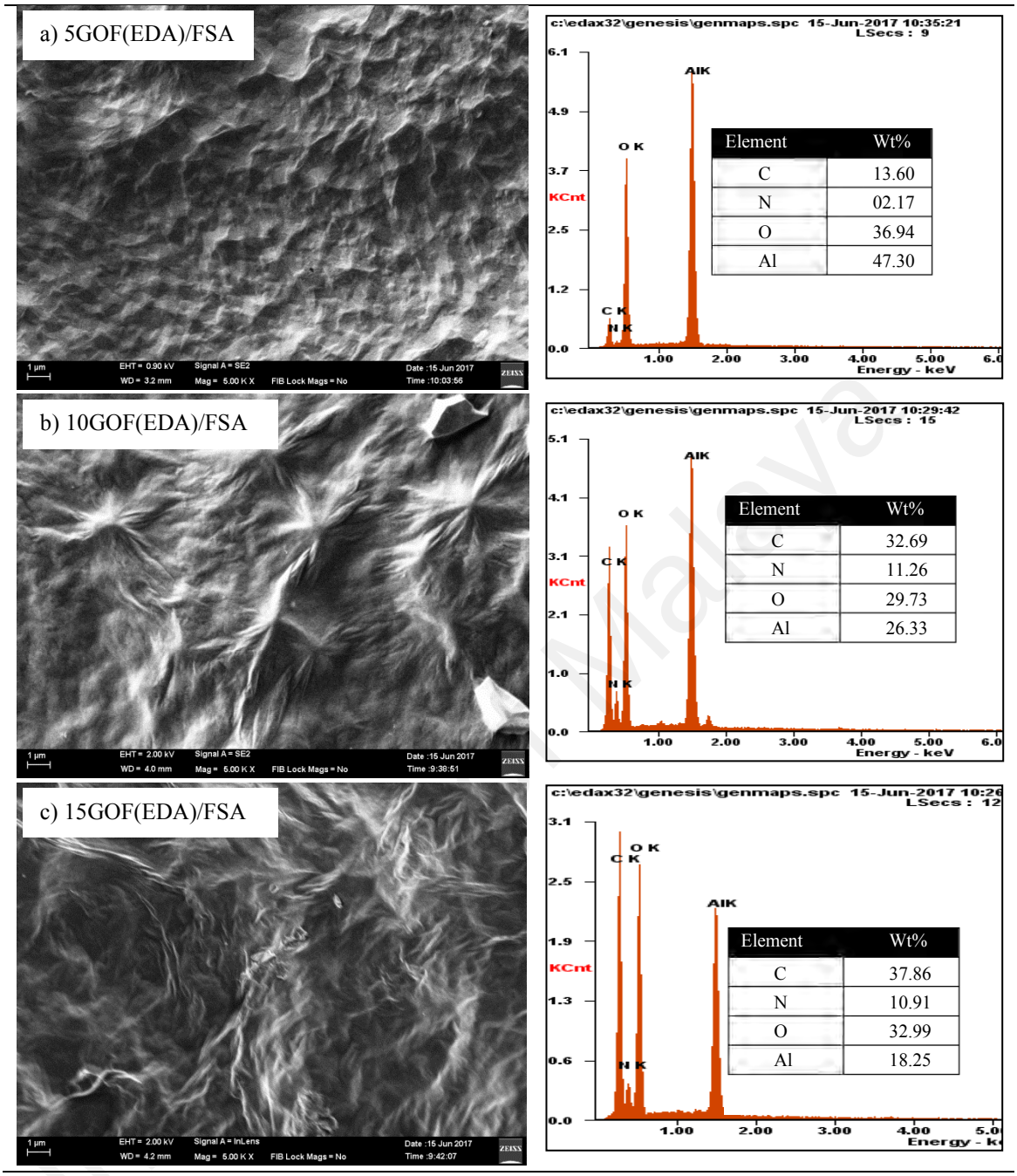

Figure 4.27: FESEM-EDX analysis of GOF(EDA)/FSA composite membranes at different GO concentration; a)5ppm, b)10ppm and c)15ppm

In addition, to confirm the thickness of the GOF(EDA) film as selective layer, cross-section morphology was observed for the composite membrane and compared with FSA support membrane. The cross-section structure observed in Figure 4.28, all the GOF(EDA)/FSA composite membranes had thin selective layer, which appeared due to GOF(EDA) films that successfully grafted on the support surface. However, the

5GOF(EDA)/FSA composite membrane at Figure 4.28(b) cannot measure its GOF(EDA) film due to very thin layer. Meanwhile, for the 10GOF(EDA)/FSA and 15GOF(EDA)/FSA, the selective layer form at thickness of ~61.41nm and ~124.39 nm, respectively. The result showed that the thickness of the GOF(EDA) film was increased at higher GO concentration. On the other hand, both 10GOF(EDA)/FSA and 15GOF(EDA)/FSA composite membrane appeared delamination GOF film which referred as defect selective layer formation.

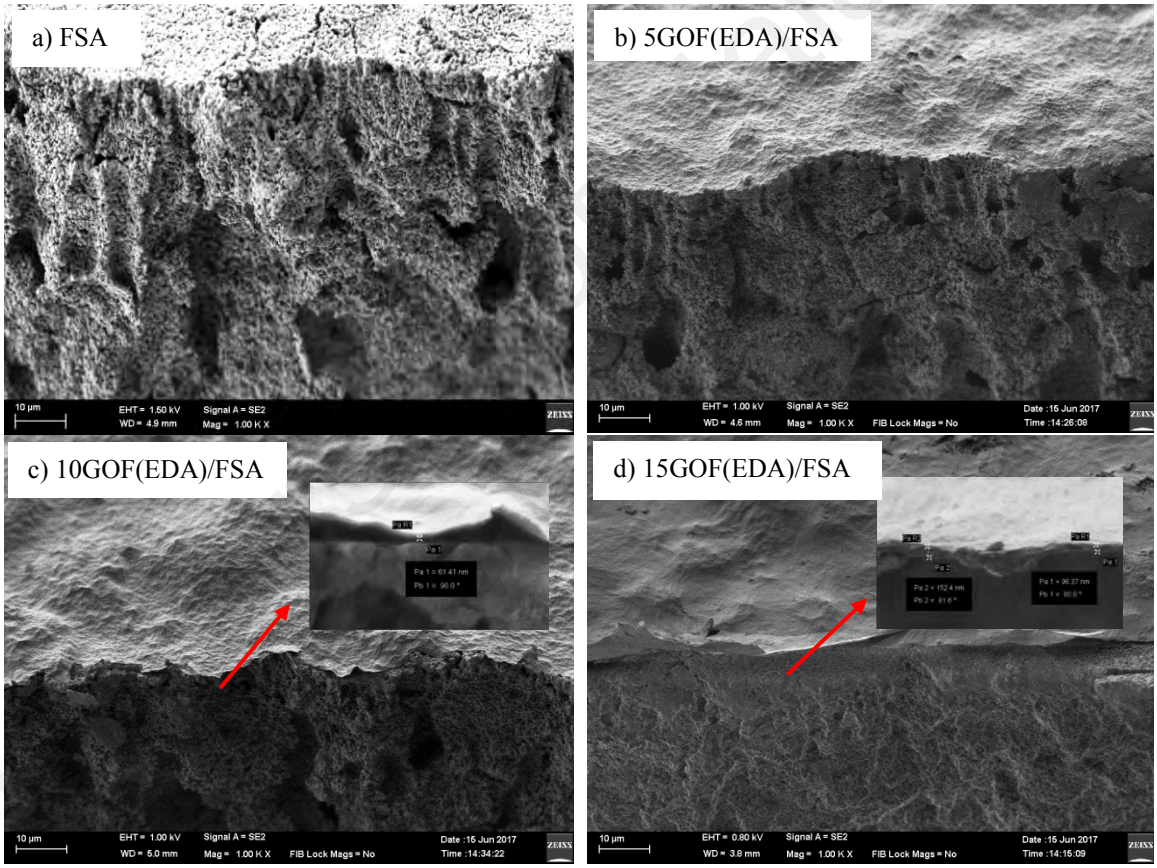

Figure 4.28: Cross-section structure of GOF(EDA)/FSA composite membranes at different GO concentration; a) FSA support, b) 5ppm, c)10ppm and d)15ppm

4.5.2 PWF performance

Generally, the thinnest selective layer would have a high PWF due to the lower permeation resistant. However, as the thickness of the selective layer increased, the water permeation becomes low due to high mass diffusion (Kattula et al., 2015). Figure 4.29 presents the PWF of the composite membranes at different GO concentration to evaluate the water permeation at the applied pressure of 3 barg for 60 min. All these composite membranes had a low PWF when compared to the FSA support membrane. Among the GOF(EDA)/FSA composite membranes, the highest PWF of 38.6 ± 1.1 $L/m^2.h$ is recorded at the lowest GO concentration of 5ppm, most probably due to the use of the thinnest GOF(EDA) film. Meanwhile, at a GO concentration of 10 and 15ppm, the PWF is almost the same, which are 24.3 ± 1.0 and 23.7 ± 0.6 $L/m^2.h$, respectively. The PWF performance was also related to the morphology surface and hydrophilicity character of composite membranes (Hegab, Wimalasiri, Ginic-Markovic, & Zou, 2015). Overall, due to the smoother surface and the use of the thinnest GOF(EDA) film of the 5GOF(EDA)/FSA composite membrane, the PWF value was the highest.

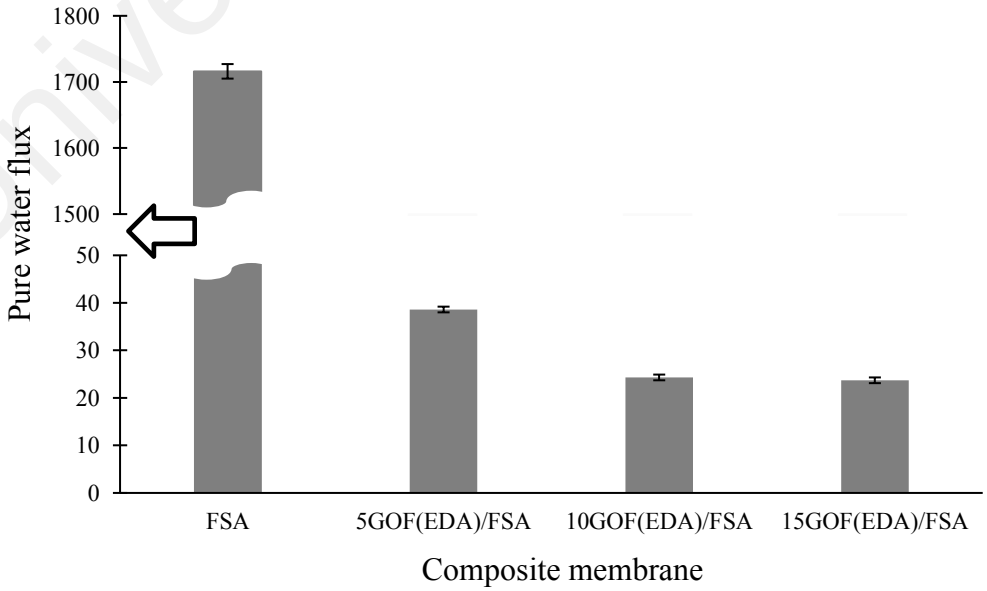

Figure 4.29: PWF of GOF(EDA)/FSA composite membranes at 3 barg for 60 min

The surface hydrophilicity was obtained by the contact angle measurement, which plays a significant role on the flux and antifouling performance of membranes. Generally, the smaller contact angle, the greater in hydrophilicity character (Zhao, Xu, Chen, & Yang, 2013). Hydrophilicity is water molecules being easily drawn to the inside of the membrane, hence increasing the flux of the membrane significantly. Figure 4.30 illustrates the hydrophilicity character using a contact angle of composite membrane when compared to the FSA support membrane. Generally, GO structure is highly hydrophilicity due to its high oxygen functional groups, which could enhance the PWF performance. However, by introducing the diamine monomers in GOF structure, the oxygen functional groups were reduced and led to a lower hydrophilicity character. This phenomenon was due to the cross-linking of EDA diamine monomers with GO structure after being heated at 60 °C for 1 hr during the diamine functionalization process (Hung et al., 2014).

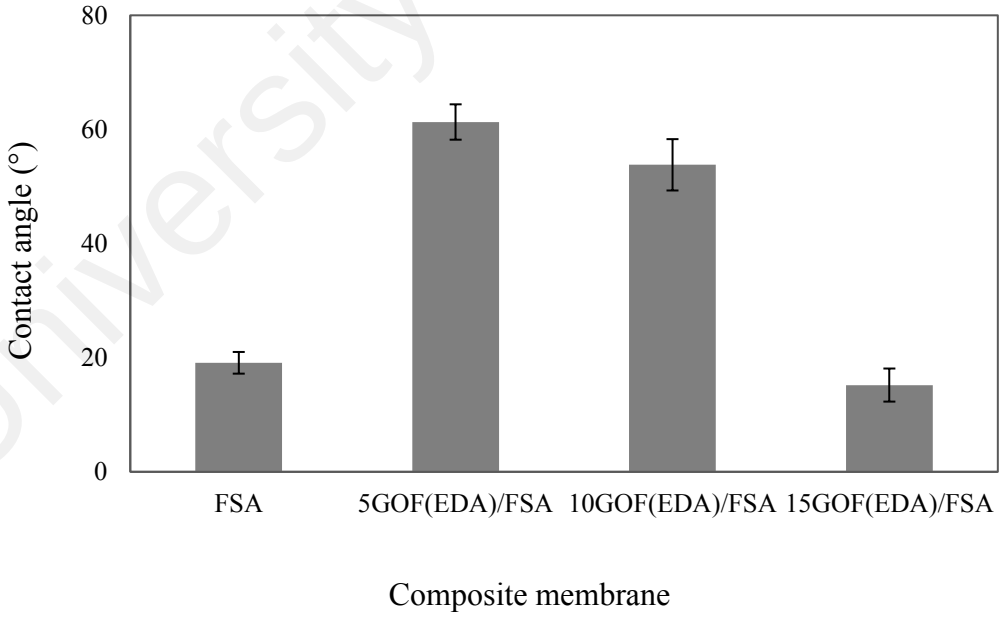

Figure 4.30: Contact angle of the top surface GOF(EDA) composite at different GO concentration

As shown in Figure 4.30, the contact angle decreased from 61.3 ± 3.1° to 15.2 ± 2.9° while the concentration of GO was increased from 5 to 15ppm, which indicated that the surface hydrophilicity was improved with the increase of GO content in GOF(EDA) film on the composite membrane. At 5ppm, the composite membrane had the highest contact angle of 61.3 ± 3.1° which refers to less hydrophilicity. However, this composite membrane also had the highest PWF value of 38.6 ± 1.1 L/m^2.h among the composite membrane. Meanwhile, at 10ppm of GO concentration was exhibited contact angle of 53.4 ± 4.5° with PWF value of 24.3 ± 1.0 L/m^2.h. At the highest GO concentration of 15ppm, the GOF(EDA) film had the lowest PWF of 23.7 ± 0.6 L/m^2.h with the highest hydrophilicity at the lowest contact angle of 15.2 ± 2.9°. However, the error percentage of contact angle value was in the range of 5 to 19%, which is acceptable in the range of hydrophilic value of 0 to 90°. Meanwhile, the contact angle value in the range of 90 to 180° was denoted as hydrophobic. Thus, it can be concluded that the hydrophilicity of the composite membrane consistently increased with a higher concentration of GO.

4.5.3 Degree of cross-linking

The degree of cross-linking between selective layer of GOF(EDA) film and support membrane of FSA was evaluated via XPS analysis. The XPS analysis was performed to calculate their elements on the composite membranes. Figure 4.31 presented the wide spectra of XPS analysis for GOF(EDA)/FSA composite membrane at different GO concentration and is compared with the support membrane, FSA membrane. As it can be clearly seen, only three elements; oxygen (O1s), carbon (C1s) and alumina (Al2s and Al2p) appeared on the FSA membrane, while composite membranes had four elements with an add on nitrogen (N1s) element. The nitrogen element was referred to EDA diamine monomer, which is successfully attached on these composite membranes. On the other hand, the carbon element was increased and the oxygen element decreased at a

higher GO concentration. From the wide spectra result, the amount of these elemental compositions, C/N ratio and degree of cross-linking were calculated and presented in Table 4.8.

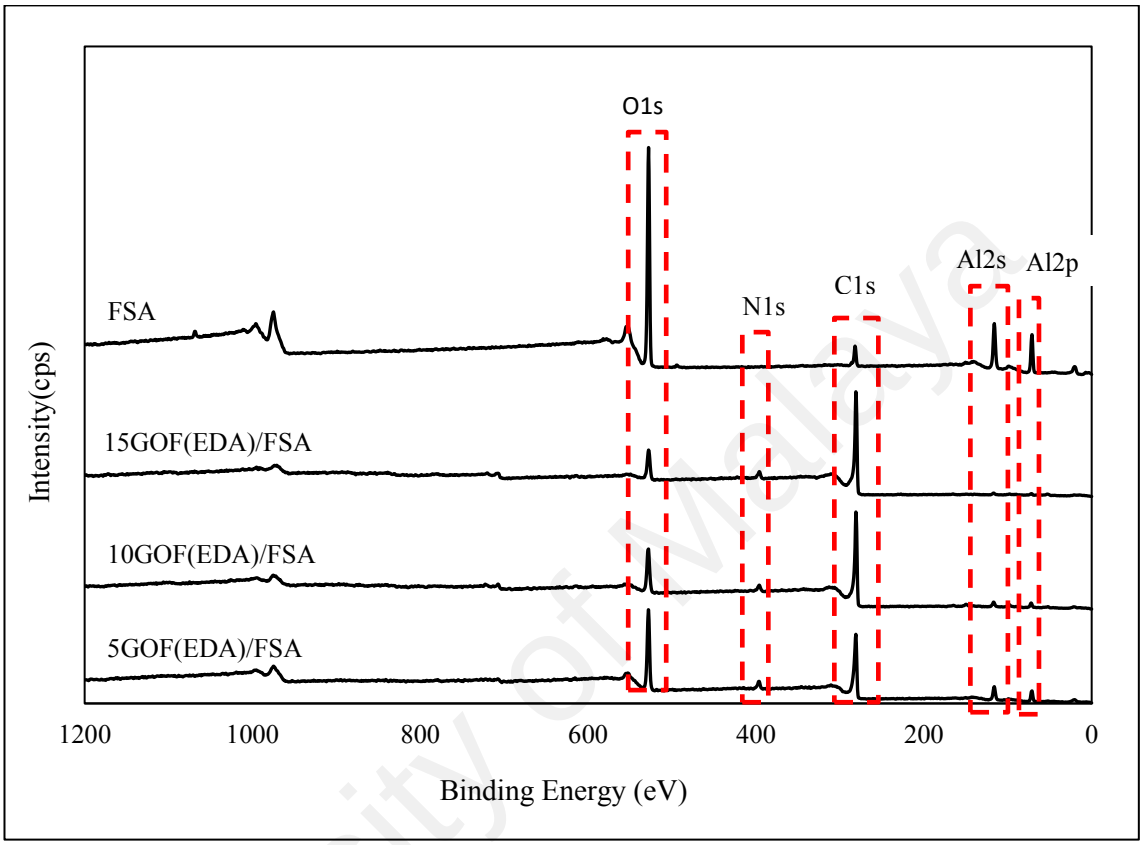

Figure 4.31: Wide spectra of XPS analysis for GOF(EDA)/FSA composite membrane at different GO concentration

In the formation of GOF(EDA) films, the oxygen element was covalently bonded with nitrogen elements to form cross-linking process. Thus, the O/N ratio was calculated to evaluate their cross-linking formation. The O/N ratio of 5GOF(EDA)/FSA composite membrane is higher when compared to other two composite membrane, indicating the formation of GOF(EDA) film having high amount of oxygen to attach to nitrogen. Thus, the 5GOF(EDA)/FSA had the highest degree of cross-linking (99.30%). Meanwhile, 10GOF(EDA)/FSA and 15GOF(EDA)/FSA composite membrane exhibited a degree of cross-linking of 82.27% and 32.10%, respectively. Due to degree of cross-

linking, we observed that the lowest GO concentration (5ppm) is a suitable concentration to form GOF(EDA) film as a selective layer on the FSA surface with a high PWF value. On the other hand, the other two composite membranes had a lower degree of cross-linking due to their delamination appearance of GOF(EDA) film on FSA surface as observed in the cross-section structure of FESEM image.

Table 4.8: Elemental composition, O/N ratio and degree of cross-linking of FSA and composite membranes

Membrane	Atomic concentration (%)					O/N Ratio	Degree of cross-linking (%)
	O1s	N1s	C1s	Al2s	Al2p		
FSA	47.44	-	11.62	16.14	24.80	-	-
5GOF(EDA)/FSA	22.71	4.58	55.09	7.53	10.09	4.96	99.30
10GOF(EDA)/FSA	15.69	3.83	73.71	2.50	4.27	4.10	82.27
15GOF(EDA)/FSA	10.32	4.01	83.40	0.91	1.36	2.57	32.10

4.5.4 Performance of 5GOF(EDA)/FSA composite membrane

Due to the highest PWF and degree of cross-linking, 5GOF(EDA)/FSA composite membrane, which contains the lowest GO concentration was chosen for the further measurement of flux stability, protein recovery performance and pore size distribution test. The stability and durability of selective layer are important criteria for evaluating their long-term application. As shown in Figure 4.32, thin 5GOF(EDA) film had a high flux of 312 L/m^2.h at the beginning of the permeation test at 3 bar of operation pressure. However, the flux showed a rapid decrease over time and reached a low steady state flux at 100 min of ~30 L/m^2.h. Similar declining trend in water flux for GO membrane is reported by Jeng et. al (2018), and they concluded that the decline of water flux due to compaction phenomenon during filtration (Chong, Wang, Mattevi, & Li, 2018). This trend also was comparable with the flux of FSA support membrane for a 5-hour duration as explained in section 4.3.3.1. The difference in flux trend was due to the addition of selective layer of GOF(EDA) film on the FSA membrane.

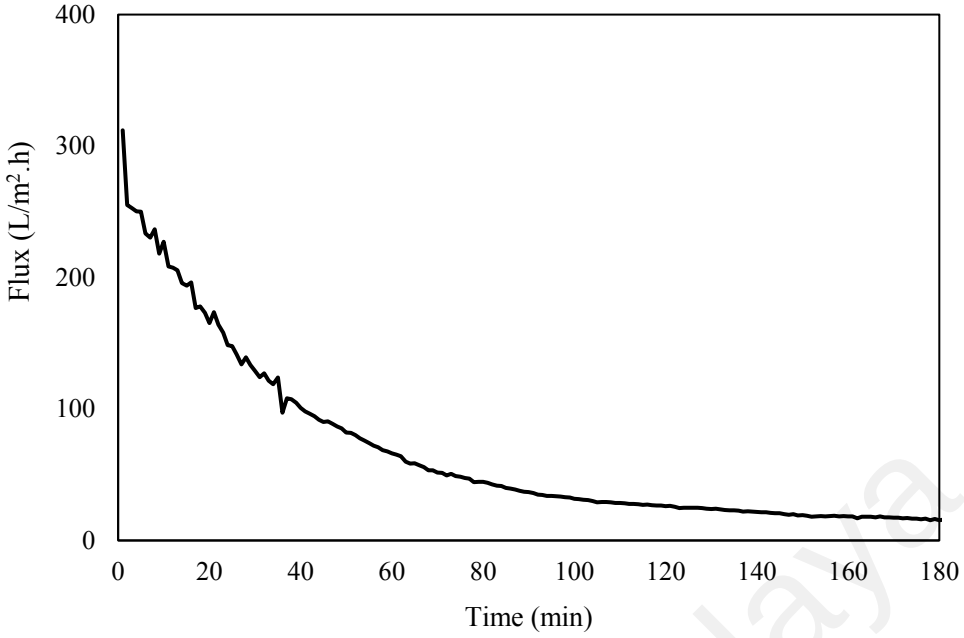

Figure 4.32: Flux stability of 5GOF(EDA)/FSA composite membrane for 180 min of duration time

In addition, the flux for first pure water (PWF-1), BSA and second pure water (PWF-2) and also the rate for BSA recovery and flux recovery (FRR) were determined for 5GOF(EDA)/FSA composite membrane due to its high stability of selective layer. These results were compared with the FSA support which is an unmodified membrane, as shown in Figure 4.33 and 4.34. From the Figure 4.34, the PWF-1 of FSA support showed the highest value of 1716 ± 51 L/m^2.h and had decreased to 825 ± 35 L/m^2.h and 436 ± 19 L/m^2.h for BSA flux and PWF-2, respectively. Meanwhile, for the 5GOF(EDA)/FSA composite membrane exhibited the PWF-1 of 41 ± 5 L/m^2.h and then decreased to 23 ± 8 L/m^2.h and 19 ± 4 L/m^2.h for BSA flux and PWF-2, respectively. Thus, the figure showed that both the unmodified and modified membrane had the same trend for these three cycles of filtration (PWF-1, BSA and PWF-2). Furthermore, after the addition of 5GOF(EDA) film on the FSA support, the PWF-1 reduced almost ~98% due to the increment of mass diffusion as mentioned before.

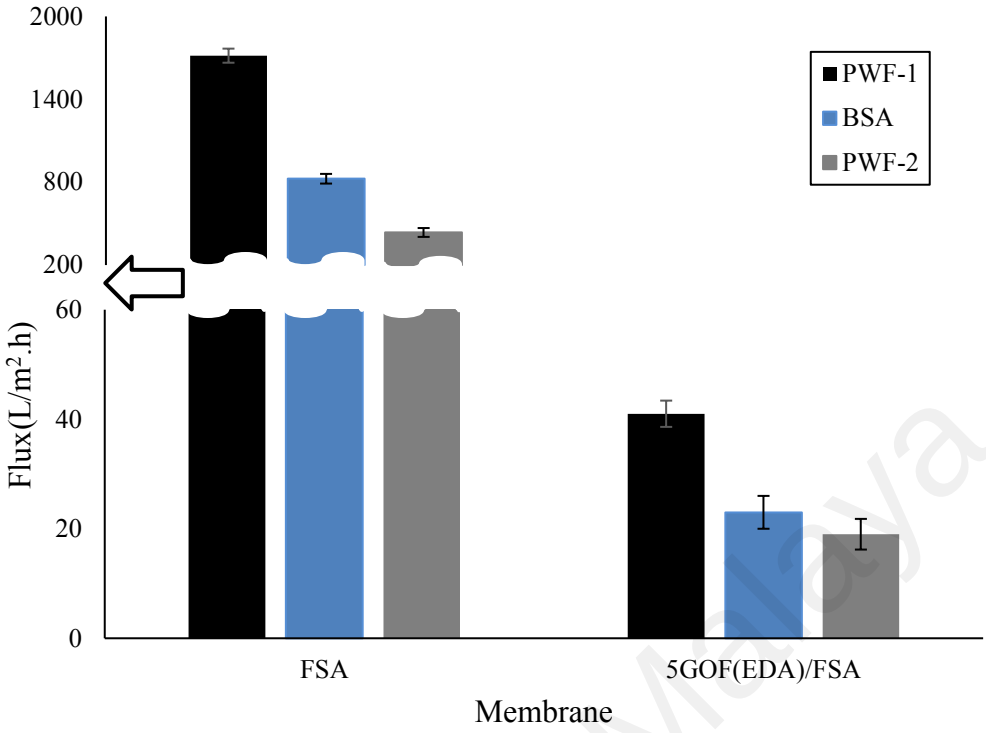

Figure 4.33: Flux of PWF-1, BSA and PWF-2 for FSA support and 5GOF(EDA)/FSA composite membrane

Figure 4.34 illustrated the rate of BSA recovery and FRR for FSA support and 5GOF(EDA)/FSA composite membrane. For the FSA support, the obtained results showed that the BSA recovery was 35 ± 5% at a low FRR of 25 ± 2%. Meanwhile, the 5GOF(EDA)/FSA composite membrane had a slight improvement of BSA recovery and FRR of 55 ± 6% and 46 ± 3% respectively. Whereas, the 5GOF(EDA)/FSA composite membrane had an improved 57% of BSA recovery at a highly-enhanced FRR at 84%. Overall, the addition of 5GOF(EDA) film on the FSA support had more improvement of FRR as compared to the BSA recovery. This improvement is due to the hydroxyl and carbonyl groups on the GOF(EDA) film which could form hydrogen bonds during water permeation and result in BSA solute not depositing onto the composite surface (Lou et al., 2014). Thus, the flux recovery was higher at a low deposition of BSA solute on the composite surface. However, the BSA recovery was low due to lower reduction of pore

size distribution of 5GOF(EDA)/FSA composite membrane, as presented in Figure 4.34.

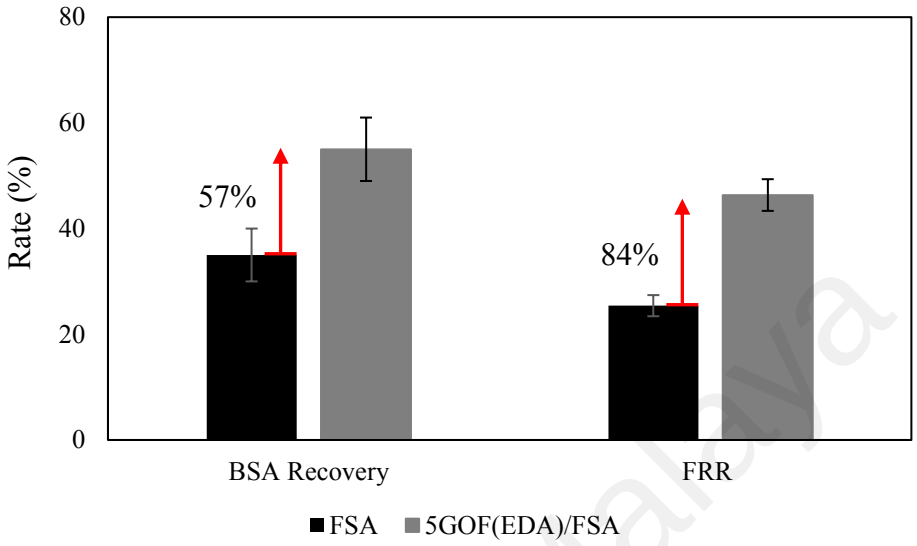

Figure 4.34: BSA recovery and FRR rate for FSA support and 5GOF(EDA)/FSA composite membrane

Figure 4.35 revealed the pore size distribution of FSA support and 5GOF(EDA)/FSA composite membrane at a diameter peak of 0.14 µm and 0.12 µm, respectively. The pore size distribution did not change significantly after the 5GOF(EDA) film was incorporated on FSA support, indicating that no significant change in pore size occurred. It can be observed that only ~14% of diameter reduction achieved for the addition of 5GOF(EDA) film on the FSA support. It was also reported that the pore size distribution had a significant influence on the separation of solutes (S. Lee, 2013). Both FSA support and 5GOF(EDA)/FSA composite membrane were in the range of MF, thus their BSA recovery was low due to larger membrane pore size. This result was in agreement with GO deposition on the membrane surface which was reported to be able to reduce the surface pore size diameter (Goh et al., 2015).

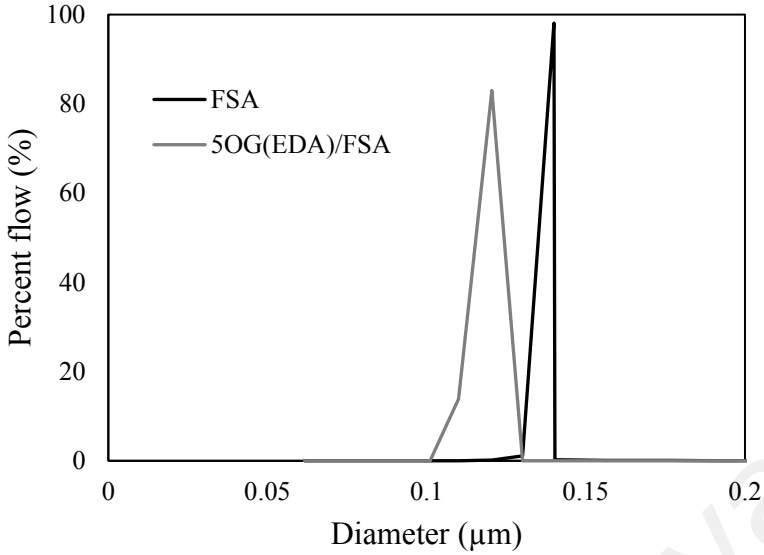

Figure 4.35: Pore size distribution of FSA support and 5GOF(EDA)/FSA composite membrane

The incorporated GOF(EDA) film was also able to withstand a long-term filtration for 180 min at a high operation pressure of 3 barg. Overall, the proposed simple GOF(EDA) deposition via PDD method yields results demonstrating an improvement in BSA recovery and FRR. The cross-linking of GO-EDA to form GOF film as a selective layer using smaller amount of GO (5ppm), had improved the selective layer stability at a PWF of 38.6 ± 1.1 L/m^2.h. However, it had least improved the BSA recovery of 55 ± 6% at a FRR of 46 ± 3%. Overall, this GOF incorporated with FSA membrane has shown some improvement even if it is not the highest BSA recovery and FRR value. Therefore, the introduction of selective layer using GOF further incorporated with HFA membrane at the next subchapter. Also, the improvement of GOF stability was introduced using different diamine monomers.

4.6 GOFs/HFA composite membrane

In this study, three GOF films were prepared with different diamine monomers which are EDA, BDA and PDA in order to prepare GOF(EDA), GOF(BDA) and GOF(PDA) films, respectively. Meanwhile, the bare GO sheet was also prepared to form GO film on the HFA membrane. In addition, the concentration of all GOFs and GO, and the deposition time using vacuum pump were fixed at 5 ppm and 1h, respectively.

4.6.1 Morphology structure

In general, GO and GOF nanosheets were stacked on the outer layer of the HFA as a support membrane through a self-assembly process via a force from vacuum pump (J. Y. Chong, B. Wang, & K. Li, 2016), forming a GO and GOFs films with certain thickness. Figure 4.36 shows the surface morphology of modified membranes which consists of GO and GOFs film as a selective layer on the support membrane. After surface modification, the surface of support membrane was fully covered with selective layers which are GO, GOF(EDA), GOF(BDA) and GOF(PDA) films, as shown in Figure 4.36(a), (b), (c) and (d), respectively. Among the modified membranes, the GOF(PDA) film was formed with high agglomeration of GOF particles (yellow circled) on the surface when compared to others composite membranes. Meanwhile, the GOF(BDA) had an excellent surface morphology, which is fully covered with selective layer and no excess of GOF particles. Overall, the selective layers successfully covered on the support membrane through the VD method for duration of 1 h of deposition time.

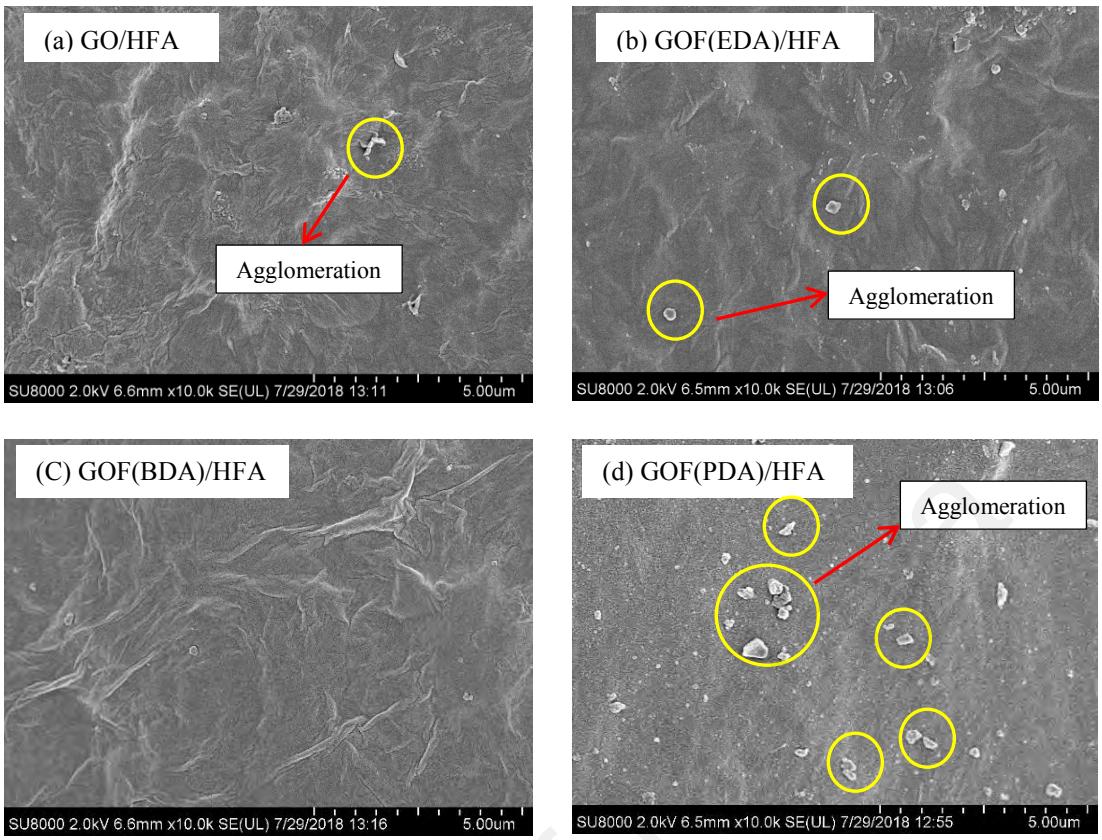

Figure 4.36: Outer surface morphology of FESEM for modified membranes of (a) GO/HFA, (b) GOF(EDA)/HFA, (c) GOF(BDA)/HFA and (d) GOF(PDA)/HFA composite membrane

In addition, Figure 4.37 shows the FESEM images of the cross-section for GO and GOFs composite membranes. The GO and GOF films were observed on the top of the support membranes. The thickness of GO film was ~363 nm, while the GOF films were ~234 nm, ~260 nm and 635 nm for GOF(EDA), GOF(BDA) and GOF(PDA), respectively. The GOF(EDA) film had the thinnest film as it has the shortest chain of diamine monomer. Different chain lengths of diamine offered different cross-linking reaction of GO-functionalization (Wan et al., 2014). Meanwhile, the GO/HFA composite membrane exhibited delamination which is due to the shrinking process of GO film. However, the GOF(PDA)/HFA composite membrane also formed some delamination. On the other hand, the GO(EDA)/HFA and GOF(BDA)/HFA composite membranes did not form delamination and had a better adhesion effect on the support

membrane. In conclusion, the absence of delamination between selective layer and support membrane significantly affected the performance of composite membranes, specifically their stability for long term application. This can be due to the lack of interfacial contact between the selective layer and the support (Jaggernauth et al., 2016).

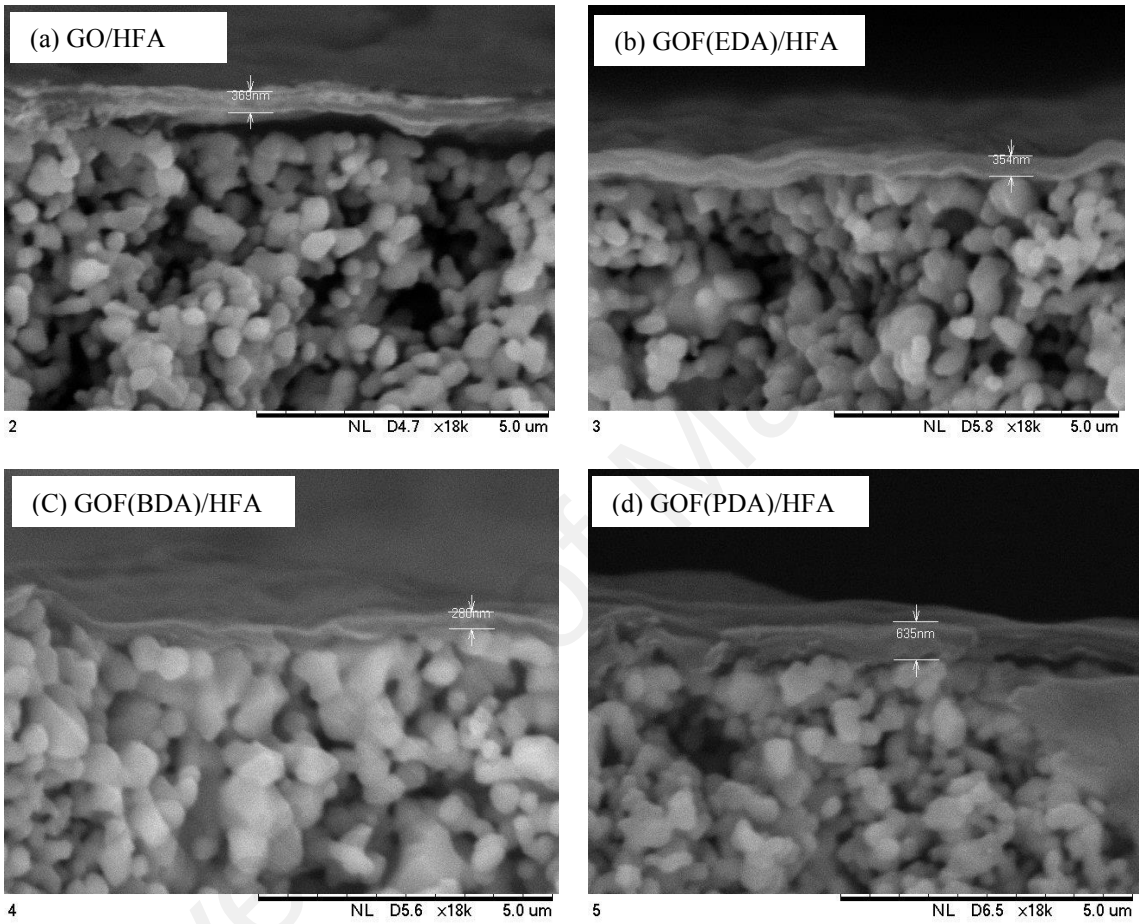

Figure 4.37: Cross-section of modified membranes for (a) GO/HFA, (b) GOF(EDA)/HFA, (c) GOF(BDA)/HFA and (d) GOF(PDA)/HFA using FESEM

4.6.2 Surface topology

Surface topology of the composite membranes was illustrated in Figure 4.38 using AFM. It can be clearly seen from the AFM images, the surface texture of the modified membranes developed are smoother manner than that of the support membrane. Thus, the surface roughness of all the modified membranes was relatively lower than the

roughness of the support membrane. The GO and GOFs film on the support membrane was significantly smoothened by filling the valley regions of the rough support surface. In modified membranes, the valleys and peaks structure were spaced more closely together. Among the modified membrane, GOF(BDA)/HFA composite membrane had valleys and peaks on the surface which are almost uniform as illustrated in Figure 4.38(c). The spacing between adjacent valleys and peaks was too small, and therefore, protein molecules could not accumulate on the surface of the composite membrane. Thus, the performance of the composite membrane is expected to remain stable during the filtration time.

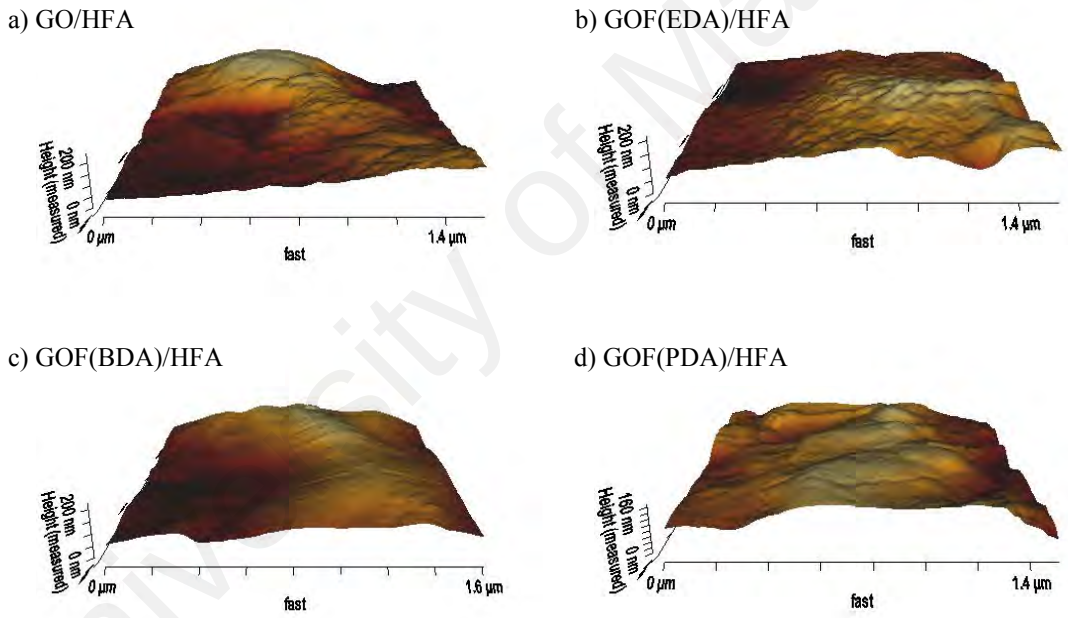

Figure 4.38: AFM images for (a) GO/HFA, (b) GOF(EDA)/HFA, (c) GOF(BDA)/HFA and (d) GOF(PDA)/HFA composite membranes

The AFM images were also used to measure the average roughness (Ra), mean square roughness (Rq) and maximum roughness (Rmax) for the support HFA and composite membranes, as shown in Table 4.9. From the table, all the composite membranes were having relatively lower of Ra value than the support HFA of 59.69

nm, where the Ra for the composite membranes are in the range of ~20 to ~45 nm. It was found that the highest surface roughness among the modified membranes is GO/HFA composite membrane due to the high level of GO film coverage on the support membrane. Meanwhile, GOF(BDA)/HFA exhibited the smoothest surface of ~20.76 nm, and this is due to hydrophilic whereby smoother membrane surface has higher hydrophilicity. The surface texture significantly avoids the membrane fouling due to high hydrophilic property and lower surface roughness (Fernandez-Gonzalez et al., 2017).

Table 4.9: Roughness measurement of support HFA and modified membranes.

Membrane	*Ra (nm)	*Rms (nm)	*Rmax (nm)
HFA	59.69	35.37	495.5
GO/HFA	45.71	54.60	226.9
GOF(EDA)/HFA	37.78	46.89	215.9
GOF(BDA)/HFA	20.76	25.12	164.10
GOF(PDA)/HFA	29.84	35.37	174.50

*Ra = average roughness
*Rms = mean square roughness
*Rmax = maximum roughness

4.6.3 Hydrophilicity and flexure strength

Hydrophilicity is an important surface property that is highly significant to the membrane performances especially antifouling properties. The presence of the antifouling is due to the strong hydration layer of the hydrophilic surface, which opposes the adsorption of any molecules and particles to the membrane surface (Tiraferri, Kang, Giannelis, & Elimelech, 2012). Figure 4.39 illustrated the contact angle and flexure strength of support HFA and composite membranes. The composite membranes exhibited a remarkably higher contact angle than the support HFA membrane ($\theta = 29 \pm 6$ °). The composite membranes which exhibited the GO and GOF films changed the wettability properties of the support membrane and reducing its

hydrophilicity, possibly due to less pore size distribution on these films. Among the composite membranes, the GOF(BDA)/alumina composite membrane has the lowest value for contact angle of ~57.84 ± 2 °. This is an advantage for water permeation to enhance the pathway of water molecules through the composite membrane.

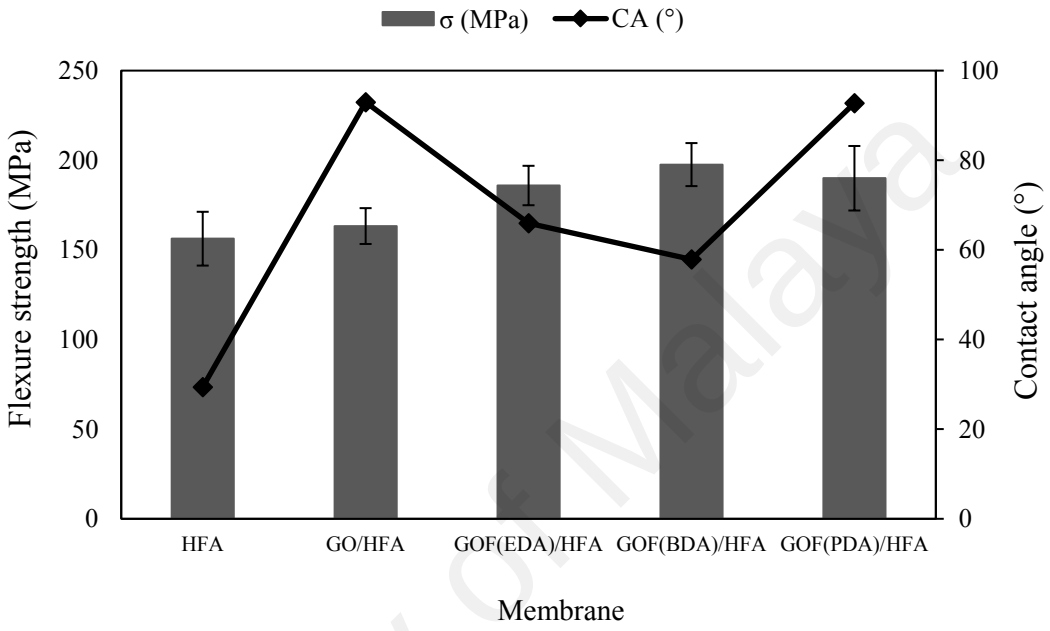

Figure 4.39: Flexure strength (σ) and contact angle (CA) of HFA support and modified membranes

The figure also shows the flexure strength of all the modified membranes. The flexure strength of the modified membranes was higher compared to the support membrane, which was 153 ± 25 MPa. The modified membranes exhibited a higher value of flexure strength due to the formation of selective layer to strengthen the composite membranes with the percentage of increment in the range of 5 – 26 %. Among the composite membrane, the GOF(BDA)/HFA has the highest value of flexure strength of 197.58 ± 12 MPa, which was at the highest percentage increment of 26% from the support membrane. As a conclusion from the overall characterization of the composite membrane, GOF(BDA)/HFA composite membrane has an excellent

morphology structure with better properties as an effective selective layer compared to other films. More hydrophilic and smoother surface of the GOF(BDA)/HFA composite membrane is expected to have better antifouling property for protein recovery process.

4.6.4 Performance of GOFs/HFA composite membrane

4.6.4.1 The PWF

Figure 4.40 presents the PWF of the support and modified membranes. The PWF value of support HFA membrane drastically dropped from 242.63 ± 24 L/m^2.h to the range of 3.10 ± 0.14 to 10.00 ± 0.6 L/m^2.h for composite membranes. As mentioned earlier, the introduction of a selective layer on the support membrane, definitely reduces the PWF due to the increment in mass diffusion. This phenomenon occurred due to the addition of extra thickness of overall composite membranes as observed at the cross-section image of FESEM structure for GO and GOFs composite membranes. The GO and GOF films decreased the PWF by increasing hydrodynamic resistance and also by reducing the effective contact area resulting from the smoothened surface (W. Choi, J. Choi, J. Bang, & J. H. Lee, 2013). This result contradicted with the statement of GO, which offered frictionless and ultrafast water flow through the stacked GO nanosheets. This phenomenon was attributed presumably to the surface hydrophilicity of GO and GOFs layer that increased the water flux but possibly overcome the flux loss by hydrodynamic resistance. In this matter, the observation in our study suggests that increasing the surface hydrophilicity and reducing the surface roughness via diamine functionalization of GO to form GOFs, possibly reduced the flux loss by hydrodynamic resistance.

Among composite membranes, the GOF(BDA)/HFA composite membrane had the highest PWF, while the lowest PWF is the GOF(PDA)/HFA composite membrane. The highest PWF of the composite membrane is due to its excellent surface properties at the

smoothest surface and high hydrophilicity as mentioned previously. Meanwhile, the lowest PWF of composite membrane is due to its poor stability of GOF(PDA) film as a selective layer as observed at a cross-section FESEM image with air gap formation. In addition, GO and GO(EDA) films exhibited almost same value for the PWF, which might be due to their surface properties (hydrophilicity and roughness) being almost the same. Overall, the morphology and surface character of membrane have strongly affected the PWF.

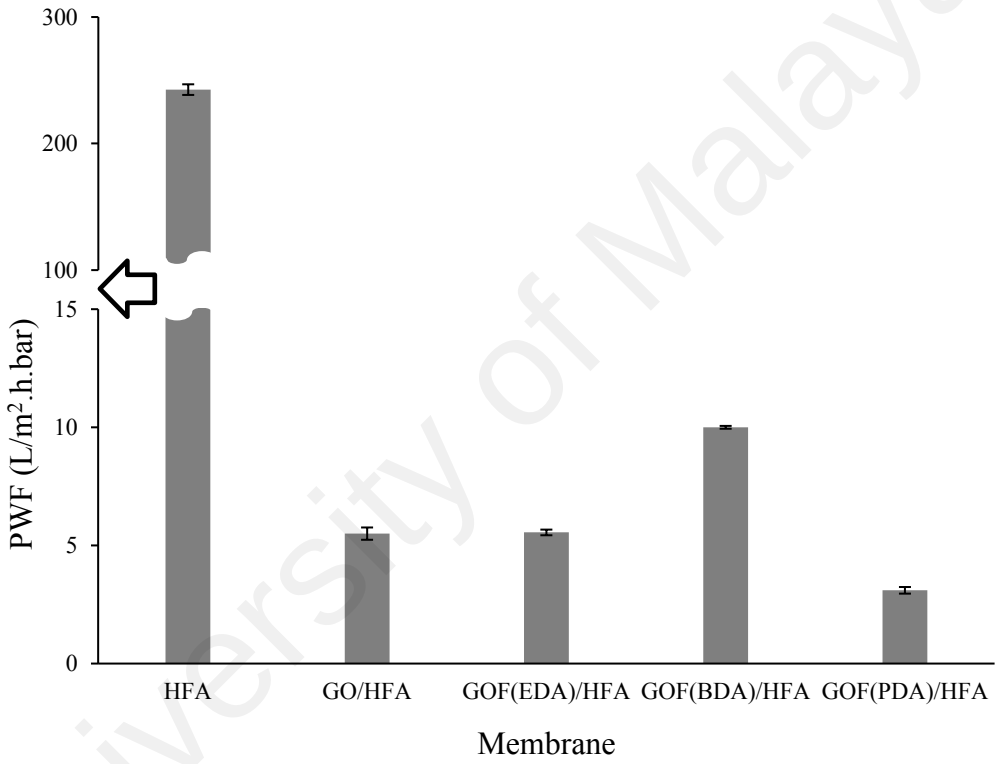

Figure 4.40: The PWF of HFA support and composite membranes

4.6.4.2 Proteins recovery

Protein recovery using support HFA and composite membranes was evaluated, as illustrated in Figure 4.41. The figure shows that all these protein recovery had less than 5% error bar value for three reading measurement. The support membrane exhibited lower protein recovery for BSA, EA, TR and LSZ, which were recorded to be 63.58, 53.99, 40.91 and 29.56 %, respectively. Interestingly, it was found that the PWF for composite membranes of GO and GOFs films decreased almost 80 % due to decreasing

pore size on composite membrane's surface. The decrement in pores size significantly enhanced the selectivity of the composite membrane by increasing proteins recovery. For example, the PWF of the GO/HFA composite membrane was 5.50 ± 0.26 L/m^2.h and exhibited protein recovery at 85.15, 75.34, 66.55 and 60.38 % for BSA, EA, TR and LSZ, respectively and was comparable to the support membrane.

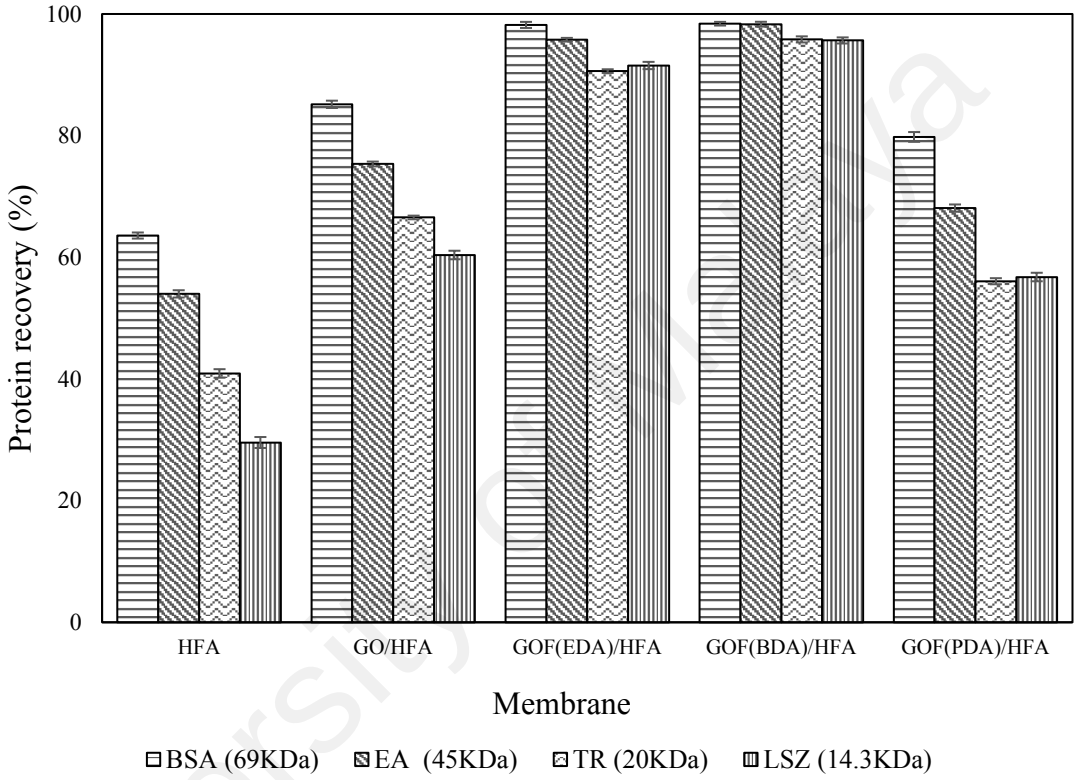

Figure 4.41: Proteins recovery for support HFA and composite membranes which are GO/HFA, GOF(EDA)/HFA, GOF(BDA)/HFA and GOF(PDA)/HFA

Generally, the decrease in pore size leads to the decrease in water permeability and an increase in recovery. The support HFA membrane had a higher PWF compared to all the composite membranes, which has a selective layer at lower PWF. Thus, the support membrane could recover less molecules as compared to the composite membranes, which is less than 65% for all the selected model protein at a high value of PWF. In addition, the water permeation enhancement of GO film was due to the GO nanosized that formed a mesh-like structure. Naturally, GO is an amphiphilic nanomaterial

whereby initially water molecules are adsorbed at the hydrophilic terminal (hydroxides),and then quickly diffused among the hydrophobic carbon core by developing a water channel that improves water permeation (Hegab & Zou, 2015). Once water molecules infiltrate the GO film, they create a single-layer configuration that drives the consecutive layers apart, resulting in the increase of interlayer spacing. Meanwhile, by introducing diamine monomers as a linker agent on GO structure, it could probably affect the interlayer spacing which acts as molecules pathway. Different diamine monomer structure offers different interlayer spacing of GOF which highly affected by pore size, elastic modulus and swelling degree (Jia et al., 2016).

As a conclusion, different diamine monomers at different structure could produce different GOF film with specific thickness and structure. Among the modified membranes, the GOF(BDA)/HFA composite membrane had highest protein recovery for all proteins, which are 98.40, 98.32, 95.82 and 95.65 % for BSA, EA, TR and LSZ, respectively. This is possibly because of the GOF(BDA) film, as selective layer, having more well-ordered structure which not only showed higher PWF, but also exhibited better protein recovery. This higher water permeation is due to the low friction flow in the well-order of the GOF interlayer space structure (J. Chong, B. Wang, & K. Li, 2016).

4.6.4.3 Antifouling properties

Antifouling study was performed using the long-term filtration for 3 cycles, which are first PWF, LSZ protein (1 mg/mL) and second PWF, as shown in Figure 4.42. Every cycle was run for 24 h at the room temperature using the cross-flow system. For the support membrane, the first PWF decreased rapidly in the early period of the filtration, and then decreased monotonically (almost linearly) with increasing time up to 24 h. Thus, the flux decline at the first PWF was ~35 % for 24 h operating time. In contrast,

at the LSZ, the flux reading decreased gradually and then reached a plateau for overall 24 h operation time by recording only ~6% of flux decline. Then, second PFW exhibited almost the same trend to the first PWF with ~10% of flux decline due to unstable flux measurement at constant pressure.

Meanwhile, for the composite membranes, it was noted that the GOF(BDA)/HFA composite membrane exhibited the lowest flux decline at first PWF of ~ 16% after filtration for 24 h and the GO/HFA composite membrane had the highest flux decline of ~25%. This demonstrated that the GOF film had improved stability performance as selective layer on support membrane. For the LSZ flux, the GOF(BDA)/HFA composite membrane had decreased slightly (almost linearly) along the filtration time of 24 h and at only ~11% of flux decline. In contrast, for second PWF, water flux decreased gradually to the end of filtration, which had the same trend to the first PWF. It was observed that this composite membrane also exhibited the lowest flux decline of ~15 % after filtration for 24 h compared to other modified membranes. The LSZ flux for 24h duration revealed the fouling behavior of the support and composite membranes. Overall, the trend of flux decline at LSZ flux was more stable compared to the first and second PWF. When the flux is constant, the transmission is the highest for protein recovery, due to its self-rejecting effect occurring between the protein in the bulk and the fouled membrane covered by adsorbed proteins (Rabiller-Baudry et al., 2001).

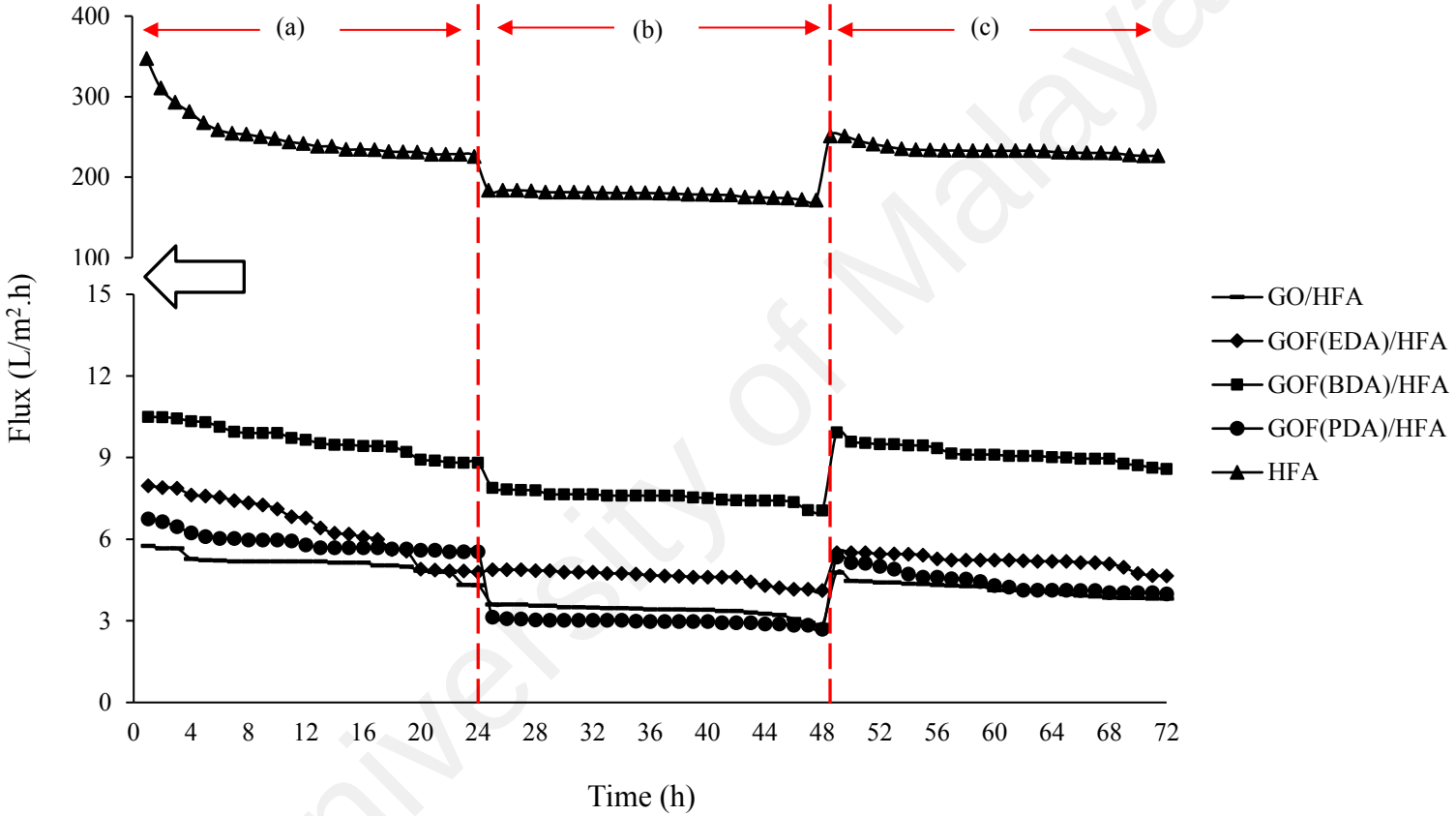

Figure 4.42: Long-term filtration of support HFA and composite membranes for three cycle (a) first PWF, (b) Lysozyme and (c) second PWF

However, it can be seen that the support membrane has less flux decline for LSZ protein than all the composite membranes. In general, during the cross-flow process the LSZ proteins were absorbed on the membrane surface and consequently formed a fouling layer and completely covered the membrane surface. Thus, this phenomenon happened to all the composite membranes except for support membrane due to less recovery of LSZ protein and the lowest flux decline. Moreover, among the modified membrane, the GOF(BDA)/HFA composite membrane had lower flux decline due to high hydrophilicity character on its surface. It was widely accepted that higher hydrophilicity results in the formation of a water molecule layer and steric hindrance on the membrane surface and in the pores, which greatly reduced the adsorption of protein molecules, and consequently decreases the flux decline (Alam et al., 2018). Consequently, membranes that are less fouled led to a lower flux decline.

On the other hand, the flux decline was measured in terms of Rt, Rr and Rir. The composite membranes observed higher flux decline compared to support membrane due to higher recovery rate. Moreover, the FRR and recovery rate also were used to measure the antifouling properties of membranes. The Figure 4.43 shows the antifouling properties, which are LSZ protein recovery, FRR, Rt, Rr and Rir for the support and composite membranes. From the Figure 4.43, the LSZ protein recovery was at the lowest value of 25.41% for the support membrane. For the composite membranes, the LSZ protein recovery was at 88.80, 95.40, 98.90 and 70.30 % for GO/alumina, GOF(EDA)/alumina, GOF(BDA)/alumina and GOF(PDA)/alumina composite membranes, respectively. Thus, it can be concluded that the GOF(BDA)/alumina composite membrane had the highest LSZ protein recovery with the lowest flux decline rate among other modified membranes.

In addition, the FRR was obtained to evaluate the extent of flux recovery after protein fouling. From the figure, the FRR of the support HFA membrane at 63.37% while the composite membranes regained the FRR, at 81.45, 80.32, 94.86 and 75.24 % for GO/HFA, GOF(EDA)/HFA, GOF(BDA)/HFA and GOF(PDA)/HFA composite membranes, respectively. It could be deduced that all composite membranes had a better FRR compared to the support membrane. These results suggested that composite membranes displayed better antifouling properties than the support membrane during LSZ protein fouling test, it was due to the adhesion of LSZ protein fouling layers on the composite membrane surface were weaker so the fouling layer was more reversible.

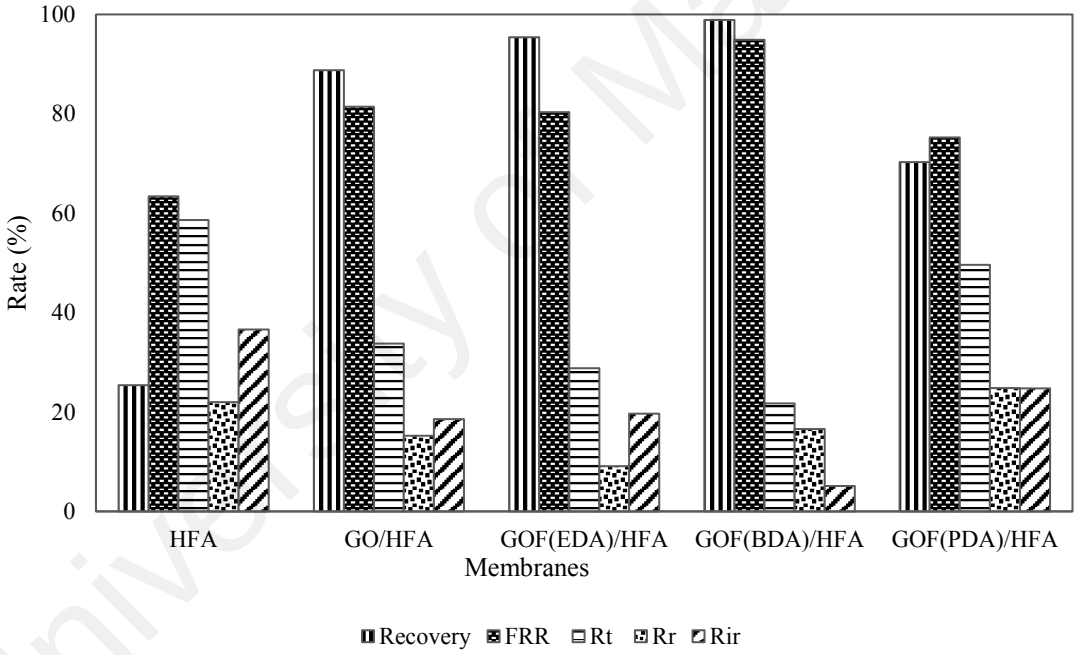

Figure 4.43: Antifouling properties of HFA support and composite membranes for long-term filtration of LSZ recovery, FRR, Rt, Rr and Rir

On the other hand, pore size of the membranes is also related to the membrane fouling phenomena, where protein sizes smaller than the pore size of the membrane, which could cause pore narrowing. When the protein and the membrane pore are of the same size, it leads to pore blocking. Whereas, when proteins are larger than the membrane pore, it will cause cake layer formation on the membrane surface (Siskens,

1996). The lowest LSZ protein recovery and the FRR value for the support membrane are probably due to its higher pore size properties that could not totally reject LSZ protein which has the smallest size of solute protein (14.3 KDa). However, the adsorption of proteins still occurred on its surface due to less antifouling properties. Antifouling properties of membranes could be evaluated using the ratio of LSZ flux and first PWF, which refers to the Rt value.

As shown in Figure 4.43, for the support HFA membrane, the Rt value was at ~59% while the other composite membranes exhibited less than ~50 % of Rt value. The other series resistance ratios investigated were Rr and Rir. When comparing antifouling properties of the prepared membranes, the highest FRR value and the lowest Rt were required in order to perform a better protein recovery application. Thus, the composite membrane of the GOF(BDA)/HFA was performed with better antifouling properties with higher FRR and lower Rt, which are almost ~95 and ~22 %, respectively.

The GOF(BDA)/HFA composite membrane exhibited the highest FRR of 94.86%, which indicated that the increase of hydrophilicity made the composite membrane more fouling resistant. Instead, the antifouling properties of the composite membranes can be attributed to the reduced surface roughness imparted by the GOF(BDA) film that could minimize the preferential attraction between the hydrophobic proteins molecule and the membrane surface and the possibility of the proteins molecule being stuck in the rough surface (Wansuk Choi et al., 2013). The molecules of organic foulant were likely attached to the hydrophobic surface, leading to the reduction in interfacial energy, while water molecules were easier to be adsorbed by the hydrophilic surface due to its low interfacial energy, which minimizes the adsorption of organic foulant like protein (Hegab et al., 2015).

Overall, the HFA membrane incorporated with GOFs film through VD method was successful as produce the GOFs/HFA composite membrane in term of significantly improved their antifouling properties that comparable with GO/HFA composite membrane. The improvement of GOFs/HFA composite membrane was combined effects of hydrophilicity, surface roughness, and membrane morphology with favorable thickness of selective layer form. Thus, among the GOFs/HFA composite membrane, the GOF(BDA) film was the desirable selective layer to support HFA membrane due high PWF, proteins recovery, FRR and less Rt.

CHAPTER 5: CONCLUSIONS AND RECOMMENDATIONS

5.1 Conclusions

The fabrication of alumina membrane via phase-inversion and sintering method was prepared by using the optimized alumina dope. The alumina dope was optimized by adjusting the alumina loading from 56 wt.% to 60 wt.% using three different particle size of alumina powder (1μm, 40-50nm and 10nm). It was found that the alumina dope at 57 wt.% of alumina loading shows the desirable dope with the viscosity value of ~17 Pa.s at the sheer rate of 30 s^{-1}. This dope also produced alumina membrane without any defect and had flexure strength of 17.01 MPa, porosity of 40.11 %, shrinkage of 12.42 % and highest BET surface area of 17.27 m^2/g.

The alumina dope at 57 wt.% were used for the fabrication of two different configuration of alumina membrane which are FSA and HFA membrane. The fabrication of FSA membrane was prepared by optimizing its fabrication parameter which are blade gap and sintering temperature using statistic tool of CCD method. The obtained optimum condition at the blade gap of 1.0 mm and the sintering temperature of 1500 °C, exhibits the highest flexure strength of 697 MPa and pure water flux of 1716 $L/m^2.h$ as well as the desired shrinkage and porosity values of 13.86% and 45.18%, respectively. This optimum FSA membrane has the narrowest pore size distribution with peak diameter at 0.14 μm. On the other hand, HFA membrane was fabricated by fixing the spinning parameter and sintering temperature. The obtained HFA membrane had the outer and inner diameter of ~1.3 and ~0.9 mm, respectively, and a wall thickness of ~0.2 mm. The HFA membrane had PWF of 242.63 ± 24 $L/m^2.h$, flexure strength of 153 ± 25 MPa, contact angle of 29 ± 6 ° and pore size distribution with peak

diameter at 0.182 μm. As conclusion, both FSA and HFA membrane had different properties even by using the same alumina dope.

However, both membranes had almost the same pore size diameter which is in the range of MF process. In term of BSA recovery, FSA and HFA membrane has low value of 35 ± 5% and 63.58 ± 0.5%, respectively. In contrast, for the FRR value, FSA and HFA membrane had 25.32% for BSA recovery and 63.37% for LSZ recovery respectively. In order to improved their protein recovery and FRR value for both FSA and HFA membrane, the GOF was introduced to form a selective layer on alumina membrane. Both FSA and HFA membranes were incorporated with GOFs via PDD and VD method, respectively to form composite alumina membranes. For the FSA membrane, three different GOF(EDA) film were prepared using different GO concentration. The results revealed that the lowest GO concentration of 5ppm was used to produce 5GOF(EDA)/FSA composite membrane had the highest PWF of 38.6 ± 1.1 $L/m^2.h$. However, it had least improved the BSA recovery of 55 ± 6% at FRR of 46 ± 3% due to the slight reduction of pore size distribution at a peak diameter of 0.12 μm. In contrast, the HFA membrane had three composite membranes with different diamine monomers. Among the composite membranes, the GOF(BDA)/HFA exhibited excellent morphology structure with highest hydrophilicity and flexure strength of ~57.84 ± 2° and 197.58 ± 12 MPa, respectively.

For the protein recovery, this composite membrane also exhibited the highest recovery rate among other modified membranes which are 98.40, 98.32, 95.82 and 95.65 % for BSA, EA, TR and LSZ protein, respectively. Furthermore, the FRR and Rt results also suggested that GOF(BDA)/HFA composite membrane had better antifouling properties due the highest FRR and lowest Rt of 94.86 % and 21.70 %, respectively for a total of 72 hr filtration time. As a conclusion, the performance of composite

membranes was affected not only by the variation in the GOFs structure but also by the surface properties of the composite membrane that altered their hydrophilicity and surface roughness. This improvement was enhancing the antifouling properties towards protein recovery application in downstream of biotechnology industries.

5.2 Recommendations

Based on the present work done in this study, several recommendations were provided for future work as stated below:

1. It is suggested that the work should be carried out using other proteins especially from industrial wastewater such at downstream in pharmaceutical factory for better characterize the behavior of these composite membranes.
2. Evaluation of GOF/alumina composite membranes in other application such gas permeation also could be performing in order to use in multi-application industry.
3. New development of GO framework such metal ion should be made in order to form a new selective layer on alumina membrane such as Zeolitic Imidazolate Framework (ZIF).

REFERENCES

Abdullah, N., Rahman, M. A., Dzarfan Othman, M. H., Jaafar, J., & Aziz, A. A. (2018). Preparation, characterizations and performance evaluations of alumina hollow fiber membrane incorporated with UiO-66 particles for humic acid removal. *Journal of Membrane Science, 563*, 162-174.

Abdullah, N., Rahman, M. A., Othman, M. H. D., Ismail, A. F., Jaafar, J., & Aziz, A. A. (2016). Preparation and characterization of self-cleaning alumina hollow fiber membrane using the phase inversion and sintering technique. *Ceramics International, 42*(10), 12312-12322.

Adams, M. (2012). Examination of methods to reduce membrane fouling during dairy microfiltration and ultrafiltration.

Afonso, M. D., Ferrer, J., & Bórquez, R. (2004). An economic assessment of proteins recovery from fish meal effluents by ultrafiltration. *Trends in food science & technology, 15*(10), 506-512.

Ahmad, A. L., Idrus, N. F., & Othman, M. R. (2005). Preparation of perovskite alumina ceramic membrane using sol–gel method. *Journal of Membrane Science, 262*(1-2), 129-137.

Ahmad, A. L., Low, S. C., Shukor, S. R. A., & Ismail, A. (2009). Optimization of membrane performance by thermal-mechanical stretching process using responses surface methodology (RSM). *Separation and Purification Technology, 66*(1), 177-186.

Alam, J., Shukla, A. K., Alhoshan, M., Arockiasamy Dass, L., Muthumareeswaran, M. R., Khan, A., . . . Abdulraqeb, F. (2018). Graphene oxide, an effective nanoadditive for a development of hollow fiber nanocomposite membrane with antifouling properties. *Advances in Polymer Technology*.

Albano, M. a. P., & Garrido, L. B. (2005). Influence of the slip composition on the properties of tape-cast alumina substrates. *Ceramics International, 31*(1), 57-66.

Albano, M. P., & Garrido, L. B. (2008). Influence of the aging time of yttria stabilized zirconia slips on the cracking behavior during drying and green properties of cast tapes. *Ceramics International, 34*(5), 1279-1284.

Allahbakhsh, A., Sharif, F., Mazinani, S., & Kalaee, M. (2014). Synthesis and characterization of graphene oxide in suspension and powder forms by chemical exfoliation method. *International Journal of Nano Dimension, 5*(1), 11.

Álvarez, J., Sola, L., Cretich, M., Swann, M. J., Gylfason, K. B., Volden, T., . . . Hill, D. (2014). Real time optical immunosensing with flow-through porous alumina membranes. *Sensors and Actuators B: Chemical, 202*, 834-839.

Alventosa-deLara, E., Barredo-Damas, S., Alcaina-Miranda, M. I., & Iborra-Clar, M. I. (2014). Study and optimization of the ultrasound-enhanced cleaning of an ultrafiltration ceramic membrane through a combined experimental–statistical approach. *Ultrasonics Sonochemistry, 21*(3), 1222-1234.

An, D., Yang, L., Wang, T.-J., & Liu, B. (2016). Separation Performance of Graphene Oxide Membrane in Aqueous Solution. *Industrial & Engineering Chemistry Research, 55*(17), 4803-4810.

Ananthakumar, S., Raja, V., & Warrier, K. G. K. (2000). Effect of nanoparticulate boehmite sol as a dispersant for slurry compaction of alumina ceramics. *Materials Letters, 43*(4), 174-179.

Arvanitoyannis, I. S., & Kassaveti, A. (2008). Fish industry waste: treatments, environmental impacts, current and potential uses. *International Journal of Food Science & Technology, 43*(4), 726-745.

Athanasekou, C. P., Morales-Torres, S., Likodimos, V., Romanos, G. E., Pastrana-Martinez, L. M., Falaras, P., . . . Silva, A. M. T. (2014). Prototype composite membranes of partially reduced graphene oxide/TiO2 for photocatalytic ultrafiltration water treatment under visible light. *Applied Catalysis B: Environmental, 158-159*, 361-372.

Auerkari, P. (1996). *Mechanical and physical properties of engineering alumina ceramics*: Technical Research Centre of Finland Finland.

Awanis Hashim, N., Liu, F., Moghareh Abed, M. R., & Li, K. (2012). Chemistry in spinning solutions: Surface modification of PVDF membranes during phase inversion. *Journal of Membrane Science, 415-416*, 399-411.

Bai, L., Zhang, L., He, H. Q., Rasheed, R. K. S. O. A., Zhang, C. Z., Ding, O. L., & Chan, S. H. (2014). Fabrication of phosphotungstic acid functionalized mesoporous silica composite membrane by alternative tape-casting incorporating phase inversion technique. *Journal of Power Sources, 246*, 522-530.

Bakhtiari, O., Samei, M., Taghikarimi, H., & Mohammadi, T. (2011). Preparation and characterization of mullite tubular membranes. *Desalination and Water Treatment, 36*(1-3), 210-218.

Barma, S., & Mandal, B. (2014). Effects of sintering temperature and initial compaction load on alpha-alumina membrane support quality. *Ceramics International, 40*(7), 11299-11309.

Barredo-Damas, S., Alcaina-Miranda, M. I., Iborra-Clar, M. I., & Mendoza-Roca, J. A. (2012). Application of tubular ceramic ultrafiltration membranes for the treatment of integrated textile wastewaters. *Chemical Engineering Journal, 192*, 211-218.

Benhabiles, M., Abdi, N., Drouiche, N., Lounici, H., Pauss, A., Goosen, M., & Mameri, N. (2013). Protein recovery by ultrafiltration during isolation of chitin from shrimp shells Parapenaeus longirostris. *Food Hydrocolloids, 32*(1), 28-34.

Biron, D. d. S., Bortoluz, J., Zeni, M., Bergmann, C. P., & Santos, V. d. (2016). Characterization of Mullite Ceramic Membranes and their Application in the Removal Escherichia Coli. *Materials Research, 19*(3), 513-519.

Bose, S., & Das, C. (2013). Preparation and characterization of low cost tubular ceramic support membranes using sawdust as a pore-former. *Materials Letters, 110*, 152-155. doi:10.1016/j.matlet.2013.08.019

Brahim, A., Lounis, A., Condom, S., & Taibi, K. (2013). Synthesis and Characterization of ZnAPSO-34 Membrane on Porous α- Al₂O₃ Support. *Applied Mechanics and Materials, 291-294*, 2758-2764.

Brahim, A., Lounis, A., Condom, S., & Taibi, K. (2013). Synthesis and Characterization of ZnAPSO-34 Membrane on Porous α-Al2O3 Support. *Applied Mechanics and Materials, 291*, 2758-2764.

Breite, D., Went, M., Prager, A., & Schulze, A. (2015). Tailoring Membrane Surface Charges: A Novel Study on Electrostatic Interactions during Membrane Fouling. *Polymers, 7*(10), 2017-2030.

Burress, J. W., Gadipelli, S., Ford, J., Simmons, J. M., Zhou, W., & Yildirim, T. (2010). Graphene Oxide Framework Materials: Theoretical Predictions and Experimental Results. *Angewandte Chemie International Edition, 49*(47), 8902-8904.

Cao, X., Zhang, T., Nguyen, Q. T., Zhang, Y., & Ping, Z. (2008). A novel hydrophilic polymer-ceramic composite membrane 1: Acrylic acid grafting membrane. *Journal of Membrane Science, 312*(1–2), 15-22.

Çelik, Y., Çelik, A., Flahaut, E., & Suvaci, E. (2016). Anisotropic mechanical and functional properties of graphene-based alumina matrix nanocomposites. *Journal of the European Ceramic Society, 36*(8), 2075-2086.

Centeno, A., Rocha, V. G., Alonso, B., Fernandez, A., Gutierrez-Gonzalez, C. F., Torrecillas, R., & Zurutuza, A. (2013). Graphene for tough and electroconductive alumina ceramics. *Journal of the European Ceramic Society, 33*(15-16), 3201-3210.

Chang, C.-S., & Suen, S.-Y. (2006). Modification of porous alumina membranes with n-alkanoic acids and their application in protein adsorption. *Journal of Membrane Science, 275*(1-2), 70-81.

Chang, Q., Zhou, J.-e., Wang, Y., Liang, J., Zhang, X., Cerneaux, S., . . . Dong, Y. (2014). Application of ceramic microfiltration membrane modified by nano-TiO2 coating in separation of a stable oil-in-water emulsion. *Journal of Membrane Science, 456*, 128-133.

Chang, Q., Zhou, J.-e., Wang, Y., Wang, J., & Meng, G. (2010). Hydrophilic modification of Al2O3 microfiltration membrane with nano-sized γ-Al2O3 coating. *Desalination, 262*(1-3), 110-114.

Chen, B., Liu, X., Zhao, X., Wang, Z., Wang, L., Jiang, W., & Li, J. (2014). Preparation and properties of reduced graphene oxide/fused silica composites. *Carbon, 77*, 66-75.

Chen, Y.-F., Bi, J.-Q., Yin, C.-L., & You, G.-L. (2014). Microstructure and fracture toughness of graphene nanosheets/alumina composites. *Ceramics International, 40*(9), 13883-13889.

Cheow, P.-S., Ting, E. Z. C., Tan, M. Q., & Toh, C.-S. (2008). Transport and separation of proteins across platinum-coated nanoporous alumina membranes. *Electrochimica Acta, 53*(14), 4669-4673.

Chew, C. M., Aroua, M., & Hussain, M. (2017). A practical hybrid modelling approach for the prediction of potential fouling parameters in ultrafiltration membrane water treatment plant. *Journal of Industrial and Engineering Chemistry, 45*, 145-155.

Chew, C. M., Aroua, M. K., Hussain, M. A., & Ismail, W. M. Z. W. (2016). Evaluation of ultrafiltration and conventional water treatment systems for sustainable development: an industrial scale case study. *Journal of Cleaner Production, 112*, 3152-3163.

Choi, W., Choi, J., Bang, J., & Lee, J.-H. (2013). Layer-by-layer assembly of graphene oxide nanosheets on polyamide membranes for durable reverse-osmosis applications. *ACS applied materials & interfaces, 5*(23), 12510-12519.

Choi, W., Choi, J., Bang, J., & Lee, J. H. (2013). Layer-by-layer assembly of graphene oxide nanosheets on polyamide membranes for durable reverse-osmosis applications. *ACS Appl Mater Interfaces, 5*(23), 12510-12519.

Chong, J., Wang, B., & Li, K. (2016). Graphene oxide membranes in fluid separations. *Current Opinion in Chemical Engineering, 12*, 98-105.

Chong, J. Y., Wang, B., & Li, K. (2016). Graphene oxide membranes in fluid separations. *Current Opinion in Chemical Engineering, 12*, 98-105.

Chong, J. Y., Wang, B., Mattevi, C., & Li, K. (2018). Dynamic microstructure of graphene oxide membranes and the permeation flux. *Journal of Membrane Science, 549*, 385-392.

Chu, L.-Y., Wang, S., & Chen, W.-M. (2005). Surface Modification of Ceramic-Supported Polyethersulfone Membranes by Interfacial Polymerization for Reduced Membrane Fouling. *Macromolecular Chemistry and Physics, 206*(19), 1934-1940.

Compton, O. C., & Nguyen, S. T. (2010). Graphene Oxide, Highly Reduced Graphene Oxide, and Graphene: Versatile Building Blocks for Carbon-Based Materials. *Small, 6*(6), 711-723.

Curtis, R. A., & Lue, L. (2006). A molecular approach to bioseparations: Protein–protein and protein–salt interactions. *Chemical Engineering Science, 61*(3), 907-923.

D'Souza, N. M., & Mawson, A. J. (2005). Membrane cleaning in the dairy industry: a review. *Crit Rev Food Sci Nutr, 45*(2), 125-134.

da Silva, A. L., Bernardin, A. M., & Hotza, D. (2014). Forming of thin porcelain tiles: A comparison between tape casting and dry pressing. *Ceramics International, 40*(2), 3761-3767.

Darcovich, K., Toll, F., Hontanx, P., Roux, V., & Shinagawa, K. (2003). An experimental and numerical study of particle size distribution effects on the sintering of porous ceramics. *Materials Science and Engineering: A, 348*(1-2), 76-83.

Das, B., Chakrabarty, B., & Barkakati, P. (2016). Preparation and characterization of novel ceramic membranes for micro-filtration applications. *Ceramics International, 42*(13), 14326-14333.

Das, B., Sarkar, S., Sarkar, A., Bhattacharjee, S., & Bhattacharjee, C. (2016). Recovery of whey proteins and lactose from dairy waste: A step towards green waste management. *Process Safety and Environmental Protection, 101*, 27-33.

Das, N., & Maiti, H. S. (2009). Ceramic membrane by tape casting and sol–gel coating for microfiltration and ultrafiltration application. *Journal of Physics and Chemistry of Solids, 70*(11), 1395-1400.

De Angelis, L., & de Cortalezzi, M. M. F. (2013). Ceramic membrane filtration of organic compounds: Effect of concentration, pH, and mixtures interactions on fouling. *Separation and Purification Technology, 118*, 762-775.

de F. Souza, L. P., & Mansur, H. S. (2004). Production and characterization of ceramic pieces obtained by slip casting using powder wastes. *Journal of Materials Processing Technology, 145*(1), 14-20.

DeFriend, K. A., Wiesner, M. R., & Barron, A. R. (2003). Alumina and aluminate ultrafiltration membranes derived from alumina nanoparticles. *Journal of Membrane Science, 224*(1-2), 11-28.

Di Girolamo, G., Brentari, A., Blasi, C., & Serra, E. (2014). Microstructure and mechanical properties of plasma sprayed alumina-based coatings. *Ceramics International, 40*(8), 12861-12867.

Dong, Y., Lin, B., Zhou, J.-e., Zhang, X., Ling, Y., Liu, X., . . . Hampshire, S. (2011). Corrosion resistance characterization of porous alumina membrane supports. *Materials Characterization, 62*(4), 409-418.

Dreyer, D. R., Park, S., Bielawski, C. W., & Ruoff, R. S. (2010). The chemistry of graphene oxide. *Chemical Society Reviews, 39*(1), 228-240.

Duran, C., Sato, K., Hotta, Y., & Watari, K. (2007). Covalently Connected Particles in Green Bodies Fabricated by Tape Casting. *Journal of the American Ceramic Society, 90*(1), 279-282.

Elaine Fung, Y.-L., & Wang, H. (2013). Investigation of reinforcement of porous alumina by nickel aluminate spinel for its use as ceramic membrane. *Journal of Membrane Science, 444*, 252-258.

Elam, J., Routkevitch, D., Mardilovich, P., & George, S. (2003). Conformal coating on ultrahigh-aspect-ratio nanopores of anodic alumina by atomic layer deposition. *Chemistry of Materials, 15*(18), 3507-3517.

Eom, J.-H., Kim, Y.-W., & Raju, S. (2013). Processing and properties of macroporous silicon carbide ceramics: A review. *Journal of Asian Ceramic Societies, 1*(3), 220-242.

Eskandari, A., Aminzare, M., Razavi hesabi, Z., Aboutalebi, S. H., & Sadrnezhaad, S. K. (2012). Effect of high energy ball milling on compressibility and sintering behavior of alumina nanoparticles. *Ceramics International, 38*(4), 2627-2632.

Falamaki, C., Naimi, M., & Aghaie, A. (2006). Dip-coating technique for the manufacture of alumina microfilters using PVA and Na-CMC as binders: a comparative study. *Journal of the European Ceramic Society, 26*(6), 949-956.

Fan, Y., Estili, M., Igarashi, G., Jiang, W., & Kawasaki, A. (2014). The effect of homogeneously dispersed few-layer graphene on microstructure and mechanical properties of Al2O3 nanocomposites. *Journal of the European Ceramic Society, 34*(2), 443-451.

Fang, H., Gao, J. F., Wang, H. T., & Chen, C. S. (2012). Hydrophobic porous alumina hollow fiber for water desalination via membrane distillation process. *Journal of Membrane Science, 403-404*, 41-46.

Fang, H., Ren, C., Liu, Y., Lu, D., Winnubst, L., & Chen, C. (2013). Phase-inversion tape casting and synchrotron-radiation computed tomography analysis of porous alumina. *Journal of the European Ceramic Society, 33*(10), 2049-2051.

Fernandez-Gonzalez, C., Zhang, B., Dominguez-Ramos, A., Ibañez, R., Irabien, A., & Chen, Y. (2017). Enhancing fouling resistance of polyethylene anion exchange membranes using carbon nanotubes and iron oxide nanoparticles. *Desalination, 411*, 19-27.

Galanakis, C. M., Chasiotis, S., Botsaris, G., & Gekas, V. (2014). Separation and recovery of proteins and sugars from Halloumi cheese whey. *Food Research International*.

Galusek, D., Ghillányová, K., Sedláček, J., Kozánková, J., & Šajgalík, P. (2012). The influence of additives on microstrucutre of sub-micron alumina ceramics prepared by two-stage sintering. *Journal of the European Ceramic Society, 32*(9), 1965-1970.

Gao, N., Ke, W., Fan, Y., & Xu, N. (2013). Evaluation of the oleophilicity of different alkoxysilane modified ceramic membranes through wetting dynamic measurements. *Applied Surface Science, 283*, 863-870.

Garcia-Ivars, J., Alcaina-Miranda, M.-I., Iborra-Clar, M.-I., Mendoza-Roca, J.-A., & Pastor-Alcañiz, L. (2014). Enhancement in hydrophilicity of different polymer phase-inversion ultrafiltration membranes by introducing PEG/Al2O3 nanoparticles. *Separation and Purification Technology, 128*, 45-57.

Gaucher, C., Jaouen, P., Legentilhomme, P., & Comiti, J. (2003). Influence of Fluid Distribution on the Ultrafiltration Performance of a Ceramic Flat Sheet Membrane. *Separation Science and Technology, 38*(9), 1949-1962.

Ghosh, R. (2003). Protein bioseparation: an overview. *Protein Bioseparation Using Ultrafiltration: Theory, Applications and New Developments*.

Ghosh, R., Wan, Y., Cui, Z., & Hale, G. (2003). Parameter scanning ultrafiltration: Rapid optimisation of protein separation. *Biotechnology and Bioengineering, 81*(6), 673-682.

Ghouil, B., Harabi, A., Bouzerara, F., Boudaira, B., Guechi, A., Demir, M. M., & Figoli, A. (2015). Development and characterization of tubular composite ceramic membranes using natural alumino-silicates for microfiltration applications. *Materials Characterization, 103*, 18-27.

Goh, K., Setiawan, L., Wei, L., Si, R., Fane, A. G., Wang, R., & Chen, Y. (2015). Graphene oxide as effective selective barriers on a hollow fiber membrane for water treatment process. *Journal of Membrane Science, 474*, 244-253.

Hassan, I. B., Ennouri, M., Lafforgue, C., Schmitz, P., & Ayadi, A. (2013). Experimental Study of Membrane Fouling during Crossflow Microfiltration of Yeast and Bacteria Suspensions: Towards an Analysis at the Microscopic Level. *Membranes (Basel), 3*(2), 44-68.

He, T., Li, J., Wang, L., Zhu, J., & Jiang, W. (2009). Preparation and consolidation of alumina/graphene composite powders. *Mater Trans, 50*(4), 749-751.

He, W., Huang, H., Gao, J.-f., Winnubst, L., & Chen, C.-s. (2014). Phase-inversion tape casting and oxygen permeation properties of supported ceramic membranes. *Journal of Membrane Science, 452*, 294-299.

Hegab, H. M., Wimalasiri, Y., Ginic-Markovic, M., & Zou, L. (2015). Improving the fouling resistance of brackish water membranes via surface modification with graphene oxide functionalized chitosan. *Desalination, 365*(Supplement C), 99-107.

Hegab, H. M., & Zou, L. (2015). Graphene oxide-assisted membranes: Fabrication and potential applications in desalination and water purification. *Journal of Membrane Science, 484*, 95-106.

Hendren, Z. D., Brant, J., & Wiesner, M. R. (2009). Surface modification of nanostructured ceramic membranes for direct contact membrane distillation. *Journal of Membrane Science, 331*(1-2), 1-10.

Heunisch, A., Dellert, A., & Roosen, A. (2010). Effect of powder, binder and process parameters on anisotropic shrinkage in tape cast ceramic products. *Journal of the European Ceramic Society, 30*(16), 3397-3406.

Hu, M., & Mi, B. (2013). Enabling graphene oxide nanosheets as water separation membranes. *Environ Sci Technol, 47*(8), 3715-3723.

Huang, H., Ying, Y., & Peng, X. (2014). Graphene oxide nanosheet: an emerging star material for novel separation membranes. *Journal of Materials Chemistry A, 2*(34), 13772-13782.

Huang, N. M., Lim, H., Chia, C., Yarmo, M., & Muhamad, M. (2011). Simple room-temperature preparation of high-yield large-area graphene oxide. *International journal of nanomedicine, 6*, 3443.

Huang, Y., Li, H., Wang, L., Qiao, Y., Tang, C., Jung, C., . . . Yu, M. (2015). Ultrafiltration Membranes with Structure-Optimized Graphene-Oxide Coatings for Antifouling Oil/Water Separation. *Advanced Materials Interfaces, 2*(2).

Hung, W.-S., Tsou, C.-H., De Guzman, M., An, Q.-F., Liu, Y.-L., Zhang, Y.-M., . . . Lai, J.-Y. (2014). Cross-linking with diamine monomers to prepare composite graphene oxide-framework membranes with varying d-spacing. *Chemistry of Materials, 26*(9), 2983-2990.

Inagaki, M., & Kang, F. (2014). Graphene derivatives: graphane, fluorographene, graphene oxide, graphyne and graphdiyne. *Journal of Materials Chemistry A, 2*(33), 13193-13206.

Inam, F., Vo, T., & Bhat, B. R. (2014). Structural stability studies of graphene in sintered ceramic nanocomposites. *Ceramics International*.

Issaoui, M., Bouaziz, J., & Fourati, M. (2013). Elaboration of membrane ceramic supports using aluminum powder. *Desalination and Water Treatment*, 1-8.

Jabbari, A., Ghasemzadeh, K., Khajavi, P., Assa, F., Abdi, M. A., Babaluo, A. A., & Basile, A. (2014). Surface modification of α-alumina support in synthesis of silica membrane for hydrogen purification. *International Journal of Hydrogen Energy*.

Jaggernauth, A., Silva, R. M., Neto, M. A., Hortigüela, M. J., Gonçalves, G., Singh, M. K., . . . Vila, M. (2016). Nanographene Oxide Functionalization with Organic and Hybrid Organic–Inorganic Polymers by Molecular Layer Deposition. *The Journal of Physical Chemistry C, 120*(42), 24176-24186.

Jamal, S., Chang, S., & Zhou, H. (2014). Filtration behaviour and fouling mechanisms of polysaccharides. *Membranes (Basel), 4*(3), 319-332.

Jana, S., Purkait, M. K., & Mohanty, K. (2010). Preparation and Characterizations of Ceramic Microfiltration Membrane: Effect of Inorganic Precursors on Membrane Morphology. *Separation Science and Technology, 46*(1), 33-45.

Jana, S., Purkait, M. K., & Mohanty, K. (2011). Clay supported polyvinyl acetate coated composite membrane by modified dip coating method: Application for the purification of lysozyme from chicken egg white. *Journal of Membrane Science, 382*(1-2), 243-251.

Jannatduost, E., Babaluo, A. A., Abbasi, F., Ardestani, M. A., & Peyravi, M. (2010). Surface modification of nanocomposite ceramic membranes by PDMS for condensable hydrocarbons separation. *Desalination, 250*(3), 1136-1139.

Jia, Z., Wang, Y., Shi, W., & Wang, J. (2016). Diamines cross-linked graphene oxide free-standing membranes for ion dialysis separation. *Journal of Membrane Science, 520*, 139-144.

Jing Dong, Zhaahui Yao, Tianzhang Yang, Lili Jiang, & Shen, C. (April 2013). Control of superhydrophilic and superhydrophobic graphene interface. *scientific reports, 3*(1733), 1-6.

Jingxian, Z., Dongliang, J., Weisensel, L., & Greil, P. (2004). Deflocculants for tape casting of TiO2 slurries. *Journal of the European Ceramic Society, 24*(8), 2259-2265.

Joshi, R. K., Carbone, P., Wang, F. C., Kravets, V. G., Su, Y., Grigorieva, I. V., . . . Nair, R. R. (2014). Precise and ultrafast molecular sieving through graphene oxide membranes. *Science, 343*(6172), 752-754.

Kang, C., Lu, H., Yuan, S., Hong, D., Yan, K., & Liang, B. (2012). Superhydrophilicity/superhydrophobicity of nickel micro-arrays fabricated by electroless deposition on an etched porous aluminum template. *Chemical Engineering Journal, 203*, 1-8.

Kashyap, S., Mishra, S., & Behera, S. K. (2014). Aqueous Colloidal Stability of Graphene Oxide and Chemically Converted Graphene. *Journal of Nanoparticles, 2014*, 1-6.

Kasperski, A., Weibel, A., Estournès, C., Laurent, C., & Peigney, A. (2013). Preparation-microstructure-property relationships in double-walled carbon nanotubes/alumina composites. *Carbon, 53*, 62-72.

Kattula, M., Ponnuru, K., Zhu, L., Jia, W., Lin, H., & Furlani, E. P. (2015). Designing ultrathin film composite membranes: the impact of a gutter layer. *Scientific reports, 5*.

Ke, X., Huang, Y., Dargaville, T. R., Fan, Y., Cui, Z., & Zhu, H. (2013). Modified alumina nanofiber membranes for protein separation. *Separation and Purification Technology, 120*, 239-244.

Khayet, M., Cojocaru, C., & García-Payo, M. C. (2010). Experimental design and optimization of asymmetric flat-sheet membranes prepared for direct contact membrane distillation. *Journal of Membrane Science, 351*(1-2), 234-245.

Kheirollahi, I., Abdellahi, M., Emamalizadeh, M., & Sharifi, H. (2015). Preparation and characterization of multilayer mesoporous alumina nano membrane via sol–gel method using new precursors. *Ceramics International, 41*(10), 15083-15088.

Khemakhem, M., Khemakhem, S., & Amar, R. B. (2013). Surface modification of microfiltration ceramic membrane by fluoroalkylsilane. *Desalination and Water Treatment*, 1-6.

Khemakhem, S., & Amara, R. B. (2012). Purification of industrial effluent by microfiltration and ultrafiltration ceramic membranes: comparative study between commercial and elaborated Tunisian clay membranes. *Desalination and Water Treatment, 39*(1-3), 182-189.

Kikkinides, E. S., Stoitsas, K. A., Zaspalis, V. T., & Burganos, V. N. (2004). Simulation of structural and permeation properties of multi-layer ceramic membranes. *Journal of Membrane Science, 243*(1-2), 133-141.

Kim, J., & Van der Bruggen, B. (2010). The use of nanoparticles in polymeric and ceramic membrane structures: Review of manufacturing procedures and performance improvement for water treatment. *Environ Pollut, 158*(7), 2335-2349.

Kim, Y. S., Kang, J. H., Kim, T., Jung, Y., Lee, K., Oh, J. Y., . . . Park, C. R. (2014). Easy Preparation of Readily Self-Assembled High-Performance Graphene Oxide Fibers. *Chemistry of Materials, 26*(19), 5549-5555.

Kingsbury, B. F., & Li, K. (2009). A morphological study of ceramic hollow fibre membranes. *Journal of Membrane Science, 328*(1), 134-140.

Kingsbury, B. F. K., & Li, K. (2009). A morphological study of ceramic hollow fibre membranes. *Journal of Membrane Science, 328*(1-2), 134-140.

Kujawa, J., Kujawski, W., Koter, S., Rozicka, A., Cerneaux, S., Persin, M., & Larbot, A. (2013). Efficiency of grafting of Al2O3, TiO2 and ZrO2 powders by perfluoroalkylsilanes. *Colloids and Surfaces A: Physicochemical and Engineering Aspects, 420*, 64-73.

Kumar, P., Sharma, N., Ranjan, R., Kumar, S., Bhat, Z. F., & Jeong, D. K. (2013). Perspective of Membrane Technology in Dairy Industry: A Review. *Asian-Australasian Journal of Animal Sciences, 26*(9), 1347-1358.

Kumar, P. V., Bardhan, N. M., Tongay, S., Wu, J., Belcher, A. M., & Grossman, J. C. (2014). Scalable enhancement of graphene oxide properties by thermally driven phase transformation. *Nature chemistry, 6*(2), 151-158.

La Flamme, K. E., Popat, K. C., Leoni, L., Markiewicz, E., La Tempa, T. J., Roman, B. B., . . . Desai, T. A. (2007). Biocompatibility of nanoporous alumina membranes for immunoisolation. *Biomaterials, 28*(16), 2638-2645.

Lai, G., Lau, W., Goh, P., Tan, Y., Ng, B., & Ismail, A. (2017). A novel interfacial polymerization approach towards synthesis of graphene oxide-incorporated thin film nanocomposite membrane with improved surface properties. *Arabian Journal of Chemistry*.

Le, T. T., Cabaltica, A. D., & Bui, V. M. (2014). Membrane separations in dairy processing. *Journal of food research and technology, 2*(1), 1-14.

Lee, B., Koo, M. Y., Jin, S. H., Kim, K. T., & Hong, S. H. (2014a). Simultaneous strengthening and toughening of reduced graphene oxide/alumina composites fabricated by molecular-level mixing process. *Carbon, 78*, 212-219.

Lee, B., Koo, M. Y., Jin, S. H., Kim, K. T., & Hong, S. H. (2014b). Simultaneous strengthening and toughening of reduced graphene oxide/alumina composites fabricated by molecular-level mixing process. *Carbon*.

Lee, J., Chae, H.-R., Won, Y. J., Lee, K., Lee, C.-H., Lee, H. H., . . . Lee, J.-m. (2013). Graphene oxide nanoplatelets composite membrane with hydrophilic and antifouling properties for wastewater treatment. *Journal of Membrane Science, 448*, 223-230.

Lee, K.-H., Youn, M.-Y., & Sea, B. (2006). Preparation of hydrophilic ceramic membranes for a dehydration membrane reactor. *Desalination, 191*(1-3), 296-302.

Lee, M., Wang, B., & Li, K. (2016). New designs of ceramic hollow fibres toward broadened applications. *Journal of Membrane Science, 503*, 48-58.

Lee, M., Wang, B., Wu, Z., & Li, K. (2015). Formation of micro-channels in ceramic membranes – Spatial structure, simulation, and potential use in water treatment. *Journal of Membrane Science, 483*(Supplement C), 1-14.

Lee, M., Wu, Z., Wang, R., & Li, K. (2014). Micro-structured alumina hollow fibre membranes – Potential applications in wastewater treatment. *Journal of Membrane Science, 461*(Supplement C), 39-48.

Lee, S. (2013). *Fouling characteristics of ceramic microfiltration and ultrafiltration membranes during surface water treatment.* Georgia Institute of Technology.

Levanen, E., & Mantyla, T. (2002). Effect of sintering temperature on functional properties of alumina membranes. *Journal of the European Ceramic Society, 22*(5), 613-623.

Li, B., Huang, M., Fu, T., Pan, L., Yao, W., & Guo, L. (2012). Microfiltration process by inorganic membranes for clarification of TongBi liquor. *Molecules, 17*(2), 1319-1334.

Li, F., Yang, Y., Fan, Y., Xing, W., & Wang, Y. (2012). Modification of ceramic membranes for pore structure tailoring: The atomic layer deposition route. *Journal of Membrane Science, 397-398*, 17-23.

Li, J., Zeng, X., Ren, T., & van der Heide, E. (2014). The Preparation of Graphene Oxide and Its Derivatives and Their Application in Bio-Tribological Systems. *Lubricants, 2*(3), 137-161.

Li, Q., Bi, Q.-y., Lin, H.-H., Bian, L.-X., & Wang, X.-L. (2013). A novel ultrafiltration (UF) membrane with controllable selectivity for protein separation. *Journal of Membrane Science, 427*, 155-167.

Lim, H. B., Cho, W.-S., & Kim, C. Y. (2012). Effect of particle size distribution of alumina on strength of glass-infiltrated alumina. *Ceramics International, 38*(4), 3069-3074.

Lim, M.-Y., Choi, Y.-S., Kim, J., Kim, K., Shin, H., Kim, J.-J., . . . Lee, J.-C. (2017). Cross-linked graphene oxide membrane having high ion selectivity and antibacterial activity prepared using tannic acid-functionalized graphene oxide and polyethyleneimine. *Journal of Membrane Science, 521*, 1-9.

Lim, Y. P., & Mohammad, A. W. (2010). Effect of solution chemistry on flux decline during high concentration protein ultrafiltration through a hydrophilic membrane. *Chemical Engineering Journal, 159*(1-3), 91-97.

Liu, J., Yan, H., & Jiang, K. (2013). Mechanical properties of graphene platelet-reinforced alumina ceramic composites. *Ceramics International, 39*(6), 6215-6221.

Liu, J., Yan, H., Reece, M. J., & Jiang, K. (2012). Toughening of zirconia/alumina composites by the addition of graphene platelets. *Journal of the European Ceramic Society, 32*(16), 4185-4193.

Liu, S., Li, K., & Hughes, R. (2003). Preparation of porous aluminium oxide (Al2O3) hollow fibre membranes by a combined phase-inversion and sintering method. *Ceramics International, 29*(8), 875-881.

Lo, Y. M., Cao, D., Argin-Soysal, S., Wang, J., & Hahm, T.-S. (2005). Recovery of protein from poultry processing wastewater using membrane ultrafiltration. *Bioresour Technol, 96*(6), 687-698.

Lou, Y., Liu, G., Liu, S., Shen, J., & Jin, W. (2014). A facile way to prepare ceramic-supported graphene oxide composite membrane via silane-graft modification. *Applied Surface Science, 307*, 631-637.

Maguire-Boyle, S. J., & Barron, A. R. (2011). A new functionalization strategy for oil/water separation membranes. *Journal of Membrane Science, 382*(1-2), 107-115.

Mahesh Kumar, S., & Roy, S. (2008). Filtration characteristics in dead-end microfiltration of living Saccharomyces cerevisiae cells by alumina membranes. *Desalination, 229*(1-3), 348-361.

Malaisamy, R., Lepak, L., Spencer, M., & Jones, K. L. (2013). Surface modification of porous alumina membranes by collagen layers: Performance and characterization. *Separation and Purification Technology, 115*, 114-122.

Manjumol, K. A., Shajesh, P., Baiju, K. V., & Warrier, K. G. K. (2011). An 'Eco-friendly' all aqueous sol gel process for multi functional ultrafiltration membrane on porous tubular alumina substrate. *Journal of Membrane Science, 375*(1-2), 134-140.

Meille, S., Lombardi, M., Chevalier, J., & Montanaro, L. (2012). Mechanical properties of porous ceramics in compression: On the transition between elastic, brittle, and cellular behavior. *Journal of the European Ceramic Society, 32*(15), 3959-3967.

Mendret, J., Hatat-Fraile, M., Rivallin, M., & Brosillon, S. (2013). Hydrophilic composite membranes for simultaneous separation and photocatalytic degradation of organic pollutants. *Separation and Purification Technology, 111*, 9-19.

Mittal, P., Jana, S., & Mohanty, K. (2011). Synthesis of low-cost hydrophilic ceramic–polymeric composite membrane for treatment of oily wastewater. *Desalination, 282*, 54-62.

Mukherjee, A., Maiti, B., Das Sharma, A., Basu, R. N., & Maiti, H. S. (2001). Correlation between slurry rheology, green density and sintered density of tape cast yttria stabilised zirconia. *Ceramics International, 27*(7), 731-739.

Mustafa, G., Wyns, K., Vandezande, P., Buekenhoudt, A., & Meynen, V. (2014). Novel grafting method efficiently decreases irreversible fouling of ceramic nanofiltration membranes. *Journal of Membrane Science, 470*, 369-377. doi:10.1016/j.memsci.2014.07.050

Nataraj, S. K., Roy, S., Patil, M. B., Nadagouda, M. N., Rudzinski, W. E., & Aminabhavi, T. M. (2011). Cellulose acetate-coated α-alumina ceramic composite tubular membranes for wastewater treatment. *Desalination, 281*, 348-353.

Ng, L. Y., Mohammad, A. W., Leo, C. P., & Hilal, N. (2013). Polymeric membranes incorporated with metal/metal oxide nanoparticles: A comprehensive review. *Desalination, 308*, 15-33.

Ohji, T. (2013). Chapter 11.2.2 - Porous Ceramic Materials. In S. Somiya (Ed.), *Handbook of Advanced Ceramics (Second Edition)* (pp. 1131-1148). Oxford: Academic Press.

Orr, V., Zhong, L., Moo-Young, M., & Chou, C. P. (2013). Recent advances in bioprocessing application of membrane chromatography. *Biotechnol Adv, 31*(4), 450-465.

Özgür, C., & Şan, O. (2011). Fabrication of superhydrophilic membrane filters using spherical glass particles obtained by ultrasonic spray pyrolysis. *Ceramics International, 37*(3), 965-970.

Patel, F., Baig, M. A., & Laoui, T. (2011). Processing of porous alumina substrate for multilayered ceramic filter. *Desalination and Water Treatment, 35*(1-3), 33-38.

Pećanac, G., Foghmoes, S., Lipińska-Chwałek, M., Baumann, S., Beck, T., & Malzbender, J. (2013). Strength degradation and failure limits of dense and porous ceramic membrane materials. *Journal of the European Ceramic Society, 33*(13-14), 2689-2698.

Pei, S., & Cheng, H.-M. (2012). The reduction of graphene oxide. *Carbon, 50*(9), 3210-3228.

Peng Lee, K., & Mattia, D. (2013). Monolithic nanoporous alumina membranes for ultrafiltration applications: Characterization, selectivity–permeability analysis and fouling studies. *Journal of Membrane Science, 435*, 52-61.

Poletto, P., da Silva Biron, D., Zeni, M., Bergmann, C. P., & dos Santos, V. (2013). Preparation and characterization of composite membranes ceramic/PSf and ceramic/PA 66. *Desalination and Water Treatment, 51*(13-15), 2666-2671.

Popović, S., Djurić, M., Milanović, S., Tekić, M. N., & Lukić, N. (2010). Application of an ultrasound field in chemical cleaning of ceramic tubular membrane fouled with whey proteins. *Journal of Food Engineering, 101*(3), 296-302.

Porwal, H., Tatarko, P., Grasso, S., Khaliq, J., Dlouhý, I., & Reece, M. J. (2013). Graphene reinforced alumina nano-composites. *Carbon, 64*, 359-369.

Prabhakaran, K., Ojha, P. K., Gokhale, N. M., & Sharma, S. C. (2009). Effect of polymer concentration on porosity and pore size characteristics of alumina membrane substrates prepared by gelcasting. *Ceramics International, 35*(5), 2083-2085.

Prabhakaran, K., Priya, S., Gokhale, N. M., & Sharma, S. C. (2007). Microporous alumina substrate with porosity >70% by gelcasting. *Ceramics International, 33*(4), 515-520.

Qi, H., Fan, Y., Xing, W., & Winnubst, L. (2010). Effect of TiO2 doping on the characteristics of macroporous Al2O3/TiO2 membrane supports. *Journal of the European Ceramic Society, 30*(6), 1317-1325.

Qin, W., Peng, C., Lv, M., & Wu, J. (2014). Preparation and properties of high-purity porous alumina support at low sintering temperature. *Ceramics International, 40*(8), 13741-13746.

Rabiller-Baudry, M., Chaufer, B., Lucas, D., & Michel, F. (2001). Ultrafiltration of mixed protein solutions of lysozyme and lactoferrin: role of modified inorganic membranes and ionic strength on the selectivity. *Journal of Membrane Science, 184*(1), 137-148.

Rahman, I. A., & Padavettan, V. (2012). Synthesis of Silica Nanoparticles by Sol-Gel: Size-Dependent Properties, Surface Modification, and Applications in Silica-Polymer Nanocomposites—A Review. *Journal of Nanomaterials, 2012*, 1-15.

Ramirez, C., & Osendi, M. I. (2014). Toughening in ceramics containing graphene fillers. *Ceramics International, 40*(7), 11187-11192.

Ramon, G. Z., & Hoek, E. M. V. (2013). Transport through composite membranes, part 2: Impacts of roughness on permeability and fouling. *Journal of Membrane Science, 425-426*, 141-148.

Rashidi, H., GhaffarianHoseini, A., GhaffarianHoseini, A., Nik Sulaiman, N. M., Tookey, J., & Hashim, N. A. (2015). Application of wastewater treatment in sustainable design of green built environments: A review. *Renewable and Sustainable Energy Reviews, 49*, 845-856.

Ravindran, R., & Jaiswal, A. K. (2016). Exploitation of food industry waste for high-value products. *Trends Biotechnol, 34*(1), 58-69.

Rezaei Hosseinabadi, S., Wyns, K., Meynen, V., Carleer, R., Adriaensens, P., Buekenhoudt, A., & Van der Bruggen, B. (2014). Organic solvent nanofiltration with Grignard functionalised ceramic nanofiltration membranes. *Journal of Membrane Science, 454*, 496-504.

Rincón, A., Chinelatto, A. S. a., & Moreno, R. (2014). Tape casting of alumina/zirconia suspensions containing graphene oxide. *Journal of the European Ceramic Society, 34*(7), 1819-1827.

Rincon, A., Moreno, R., Chinelatto, A. S. A., Gutierrez, C. F., Rayon, E., Salvador, M. D., & Borrell, A. (2014). Al2O3-3YTZP-Graphene multilayers produced by tape casting and spark plasma sintering. *Journal of the European Ceramic Society, 34*(10), 2427-2434.

Sahnoun, R. D., & Baklouti, S. (2013). Characterization of flat ceramic membrane supports prepared with kaolin-phosphoric acid-starch. *Applied Clay Science, 83-84*, 399-404.

Salehi, F. (2014). Current and future applications for nanofiltration technology in the food processing. *Food and Bioproducts Processing, 92*(2), 161-177.

Salgın, S., Takaç, S., & Özdamar, T. H. (2005). A Parametric Study on Protein-Membrane-Ionic Environment Interactions for Membrane Fouling. *Separation Science and Technology, 40*(6), 1191-1212.

Samaei, S. M., Gato-Trinidad, S., & Altaee, A. (2018). The application of pressure-driven ceramic membrane technology for the treatment of industrial wastewaters – A review. *Separation and Purification Technology, 200*, 198-220.

Samei, M., Mohammadi, T., & Asadi, A. A. (2013). Tubular composite PVA ceramic supported membrane for bio-ethanol production. *Chemical Engineering Research and Design, 91*(12), 2703-2712.

Sarkar, S., Bandyopadhyay, S., Larbot, A., & Cerneaux, S. (2012). New clay–alumina porous capillary supports for filtration application. *Journal of Membrane Science, 392-393*, 130-136.

Saxena, A., Kumar, M., Tripathi, B. P., & Shahi, V. K. (2010). Organic–inorganic hybrid charged membranes for proteins separation: Isoelectric separation of proteins under coupled driving forces. *Separation and Purification Technology, 70*(3), 280-290.

Saxena, A., Tripathi, B. P., Kumar, M., & Shahi, V. K. (2009). Membrane-based techniques for the separation and purification of proteins: An overview. *Advances in Colloid and Interface Science, 145*(1–2), 1-22.

Saxena, A., Tripathi, B. P., Kumar, M., & Shahi, V. K. (2009). Membrane-based techniques for the separation and purification of proteins: an overview. *Adv Colloid Interface Sci, 145*(1-2), 1-22.

Saxena, A., Tripathi, B. P., & Shahi, V. K. (2008). An improved process for separation of proteins using modified chitosan–silica cross-linked charged ultrafilter membranes under coupled driving forces: Isoelectric separation of proteins. *Journal of Colloid and Interface Science, 319*(1), 252-262.

Seal, A., Chattopadhyay, D., Das Sharma, A., Sen, A., & Maiti, H. S. (2004). Influence of ambient temperature on the rheological properties of alumina tape casting slurry. *Journal of the European Ceramic Society, 24*(8), 2275-2283.

Shao, F., Dong, L., Dong, H., Zhang, Q., Zhao, M., Yu, L., . . . Chen, Y. (2016). Graphene Oxide Modified Polyamide Reverse Osmosis Membranes with Enhanced Chlorine Resistance. *Journal of Membrane Science*.

Shi, G. M., & Chung, T.-S. (2013). Thin film composite membranes on ceramic for pervaporation dehydration of isopropanol. *Journal of Membrane Science, 448*, 34-43.

Shi, X., Tal, G., Hankins, N. P., & Gitis, V. (2014). Fouling and cleaning of ultrafiltration membranes: A review. *Journal of Water Process Engineering, 1*, 121-138.

Silva, K. K. O. S., Paskocimas, C. A., Oliveira, F. R., Nascimento, J. H. O., & Zille, A. (2015). Development of porous alumina membranes for treatment of textile effluent. *Desalination and Water Treatment, 57*(6), 2640-2648.

Siskens, C. (1996). Applications of ceramic membranes in liquid filtration. *Membrane Science and Technology, 4*, 619-639.

Smith, Z. P., & Freeman, B. D. (2014). Graphene Oxide: A New Platform for High-Performance Gas- and Liquid-Separation Membranes. *Angewandte Chemie International Edition, 53*(39), 10286-10288.

Snijkers, F., de Wilde, A., Mullens, S., & Luyten, J. (2004). Aqueous tape casting of yttria stabilised zirconia using natural product binder. *Journal of the European Ceramic Society, 24*(6), 1107-1110.

Song, Z., Fathizadeh, M., Huang, Y., Chu, K. H., Yoon, Y., Wang, L., . . . Yu, M. (2016). TiO 2 nanofiltration membranes prepared by molecular layer deposition for water purification. *Journal of Membrane Science, 510*, 72-78.

Su, T., Lu, J., Cui, Z., & Thomas, R. (2000). Fouling of ceramic membranes by albumins under dynamic filtration conditions. *Journal of Membrane Science, 173*(2), 167-178.

Sun, W., Chen, T., Chen, C., & Li, J. (2007). A study on membrane morphology by digital image processing. *Journal of Membrane Science, 305*(1–2), 93-102.

Suresh, K., Srinu, T., Ghoshal, A. K., & Pugazhenthi, G. (2016). Preparation and characterization of TiO 2 and γ-Al 2 O 3 composite membranes for the separation of oil-in-water emulsions. *RSC Advances, 6*(6), 4877-4888.

Tang, C.-M., & Li, X.-L. (2013). Separative capability of γ-Al2O3 porous ceramic membrane modified by ZIF-8. *Korean Journal of Chemical Engineering, 30*(5), 1119-1124.

Tavolaro, A., & Drioli, E. (1999). Zeolite membranes. *Advanced materials, 11*(12), 975-996.

Tiraferri, A., Kang, Y., Giannelis, E. P., & Elimelech, M. (2012). Superhydrophilic Thin-Film Composite Forward Osmosis Membranes for Organic Fouling Control: Fouling Behavior and Antifouling Mechanisms. *Environmental Science & Technology, 46*(20), 11135-11144.

Treccani, L., Yvonne Klein, T., Meder, F., Pardun, K., & Rezwan, K. (2013). Functionalized ceramics for biomedical, biotechnological and environmental applications. *Acta biomaterialia, 9*(7), 7115-7150.

Tseng, H.-H., Wang, C.-T., Zhuang, G.-L., Uchytil, P., Reznickova, J., & Setnickova, K. (2016). Enhanced H2/CH4 and H2/CO2 separation by carbon molecular sieve membrane coated on titania modified alumina support: Effects of TiO2 intermediate layer preparation variables on interfacial adhesion. *Journal of Membrane Science, 510*, 391-404.

Van Heetvelde, P., Beyers, E., Wyns, K., Adriaensens, P., Maes, B. U. W., Mullens, S., . . . Meynen, V. (2013). A new method to graft titania using Grignard reagents. *Chemical communications (Cambridge, England), 49*(62), 6998-7000.

van Reis, R., & Zydney, A. (2007). Bioprocess membrane technology. *Journal of Membrane Science, 297*(1-2), 16-50.

Vargas-Garcia, A., Torrestiana-Sanchez, B., Garcia-Borquez, A., & Aguilar-Uscanga, G. (2011). Effect of grafting on microstructure, composition and surface and transport properties of ceramic membranes for osmotic evaporation. *Separation and Purification Technology, 80*(3), 473-481.

Vasanth, D., Uppaluri, R., & Pugazhenthi, G. (2011). Influence of Sintering Temperature on the Properties of Porous Ceramic Support Prepared by Uniaxial Dry Compaction Method Using Low-Cost Raw Materials for Membrane Applications. *Separation Science and Technology, 46*(8), 1241-1249.

Wan, W., Li, L., Zhao, Z., Hu, H., Hao, X., Winkler, D. A., . . . Qiu, J. (2014). Ultrafast Fabrication of Covalently Cross-linked Multifunctional Graphene Oxide Monoliths. *Advanced Functional Materials, 24*(31), 4915-4921.

Wang, B., Wu, Z., Livingston, A. G., & Li, K. (2009). A novel phase transition technique for fabrication of mesopore sized ceramic membranes. *Journal of Membrane Science, 339*(1-2), 5-9.

Wang, C., Yang, F., & Zhang, H. (2010). Fabrication of non-woven composite membrane by chitosan coating for resisting the adsorption of proteins and the adhesion of bacteria. *Separation and Purification Technology, 75*(3), 358-365.

Wang, J., Zhang, J., Luo, D., Yang, H., Tang, D., & Kong, L. B. (2015). Densification and microstructural evolution of yttria transparent ceramics: The effect of ball milling conditions. *Journal of the European Ceramic Society, 35*(3), 1011-1019.

Wang, K., Wang, Y., Fan, Z., Yan, J., & Wei, T. (2011). Preparation of graphene nanosheet/alumina composites by spark plasma sintering. *Materials Research Bulletin, 46*(2), 315-318.

Wang, L., Mah, K. Z., & Ghosh, R. (2009). Purification of human IgG using membrane based hybrid bioseparation technique and its variants: A comparative study. *Separation and Purification Technology, 66*(2), 242-247.

Wang, L., Sun, Y. Y., Lee, K., West, D., Chen, Z. F., Zhao, J. J., & Zhang, S. B. (2010). Stability of graphene oxide phases from first-principles calculations. *Physical Review B, 82*(16), 161406. Retrieved from

Wang, P., Tan, K. L., Kang, E. T., & Neoh, K. G. (2002). Antifouling poly(vinylidene fluoride) microporous membranes prepared via plasma-induced surface grafting of poly(ethylene glycol). *Journal of Adhesion Science and Technology, 16*(2), 111-127.

Wang, Q., Li, Y., Luo, M., Sang, S., Zhu, T., & Zhao, L. (2014). Strengthening mechanism of graphene oxide nanosheets for Al2O3–C refractories. *Ceramics International, 40*(1), 163-172.

Wang, W.-N., Jiang, Y., & Biswas, P. (2012). Evaporation-induced crumpling of graphene oxide nanosheets in aerosolized droplets: confinement force relationship. *The journal of physical chemistry letters, 3*(21), 3228-3233.

Wee, S. L., Tye, C. T., & Bhatia, S. (2010). Process optimization studies for the dehydration of alcohol–water system by inorganic membrane based pervaporation separation using design of experiments (DOE). *Separation and Purification Technology, 71*(2), 192-199.

Wei, C. C., Chen, O. Y., Liu, Y., & Li, K. (2008). Ceramic asymmetric hollow fibre membranes—One step fabrication process. *Journal of Membrane Science, 320*(1-2), 191-197.

Wei, N., Peng, X., & Xu, Z. (2014). Understanding water permeation in graphene oxide membranes. *ACS Appl Mater Interfaces, 6*(8), 5877-5883.

Xie, Z.-P., Ma, C.-L., & Huang, Y. (2003). Effects of additives on alumina sheets forming by a novel gel-tape-casting. *Materials & Design, 24*(4), 287-291.

Yalamaç, E., Trapani, A., & Akkurt, S. (2014). Sintering and microstructural investigation of gamma–alpha alumina powders. *Engineering Science and Technology, an International Journal, 17*(1), 2-7.

Yang, G. C. C., & Yen, C.-H. (2013). The use of different materials to form the intermediate layers of tubular carbon nanofibers/carbon/alumina composite membranes for removing pharmaceuticals from aqueous solutions. *Journal of Membrane Science, 425-426*, 121-130.

Yeu, S., Lunn, J. D., Rangel, H. M., & Shantz, D. F. (2009). The effect of surface modifications on protein microfiltration properties of Anopore™ membranes. *Journal of Membrane Science, 327*(1-2), 108-117.

Yu, D., McLean, M., Hall, J., & Ghosh, R. (2008). Purification of monoclonal antibody from tobacco extract using membrane-based bioseparation techniques. *Journal of Membrane Science, 323*(1), 159-166.

Yuan, J., & Liew, K. M. (2014). Effects of grafted carboxyl groups on structural stability and elastic properties of graphene. *Materials Chemistry and Physics, 145*(3), 313-319.

Zawrah, M., Khattab, R., Girgis, L. G., El Shereefy, E., & Sawan, S. A. (2014). Effect of CTAB as a foaming agent on the properties of alumina ceramic membranes. *Ceramics International, 40*(4), 5299-5305.

Zawrah, M. F., Khattab, R. M., Girgis, L. G., El Shereefy, E. E., & Abo Sawan, S. E. (2014). Effect of CTAB as a foaming agent on the properties of alumina ceramic membranes. *Ceramics International, 40*(4), 5299-5305.

Zhang, H., Zhong, Z., & Xing, W. (2013). Application of ceramic membranes in the treatment of oilfield-produced water: Effects of polyacrylamide and inorganic salts. *Desalination, 309*, 84-90.

Zhang, M., Gao, B., Vanegas, D. C., McLamore, E. S., Fang, J., Liu, L., . . . Chen, H. (2014). Simple approach for large-scale production of reduced graphene oxide films. *Chemical Engineering Journal, 243*, 340-346.

Zhao, C., Xu, X., Chen, J., & Yang, F. (2013). Effect of graphene oxide concentration on the morphologies and antifouling properties of PVDF ultrafiltration membranes. *Journal of Environmental Chemical Engineering, 1*(3), 349-354.

Zhou, J.-e., Chang, Q., Wang, Y., Wang, J., & Meng, G. (2010). Separation of stable oil–water emulsion by the hydrophilic nano-sized ZrO2 modified Al2O3 microfiltration membrane. *Separation and Purification Technology, 75*(3), 243-248.

Zhou, S., Xue, A., Zhang, Y., Li, M., Wang, J., Zhao, Y., & Xing, W. (2014). Fabrication of temperature-responsive ZrO2 tubular membranes, grafted with poly (N-isopropylacrylamide) brush chains, for protein removal and easy cleaning. *Journal of Membrane Science, 450*, 351-361.

Zhou, S., Xue, A., Zhao, Y., Li, M., Wang, H., & Xing, W. (2013). Grafting polyacrylic acid brushes onto zirconia membranes: Fouling reduction and easy-cleaning properties. *Separation and Purification Technology, 114*, 53-63.

Zhu, Z., Xiao, J., He, W., Wang, T., Wei, Z., & Dong, Y. (2015). A phase-inversion casting process for preparation of tubular porous alumina ceramic membranes. *Journal of the European Ceramic Society, 35*(11), 3187-3194.

Zinadini, S., Zinatizadeh, A. A., Rahimi, M., Vatanpour, V., & Zangeneh, H. (2014). Preparation of a novel antifouling mixed matrix PES membrane by embedding graphene oxide nanoplates. *Journal of Membrane Science, 453*, 292-301.

LIST OF PUBLICATIONS

1. Ishak, N. F., Hashim, N. A., Othman, M. H. D., Monash, P., & Zuki, F. M. (2017). Recent progress in the hydrophilic modification of alumina membranes for protein separation and purification. ***Ceramics International,*** *43*(1), 915-925.

2. Ishak, N. F., Hashim, N. A., & Othman, M. H. D. (2020). Antifouling properties of hollow fibre alumina membrane incorporated with graphene oxide frameworks. ***Journal of Environmental Chemical Engineering***, 104059.